REPORT DOCUMENTATION PAGE

AFRL-SR-AR-TR-04-

0233

1. REPORT DATE *(DD-MM-YYYY)*	2. REPORT TYPE	3. DATES COVERED *(From - To)*
30-03-2004	Final Report	21-02-2001 - 21-02-2004

4. TITLE AND SUBTITLE

Performance Enhancement of High Speed Inlets Using MHD

5a. CONTRACT NUMBER
F49620-01-C-0022

5b. GRANT NUMBER

5c. PROGRAM ELEMENT NUMBER

6. AUTHOR(S)
Shashi Aithal, Ramakanth Munipalli, Vijaya Shankar

5d. PROJECT NUMBER

5e. TASK NUMBER

5f. WORK UNIT NUMBER

7. PERFORMING ORGANIZATION NAME(S) AND ADDRESS(ES)

HyPerComp Inc.,
31255 Cedar Valley Dr.,
Suite 327
Westlake Village, CA 91362

8. PERFORMING ORGANIZATION REPORT NUMBER

AFOSR-01-2004

9. SPONSORING / MONITORING AGENCY NAME(S) AND ADDRESS(ES)

Dr. Fariba Fahroo
Computational Mathematics
AFOSR/NM,
4015, Wilson Blvd, Rm 713
Arlington, VA 22203-1954

10. SPONSOR/MONITOR'S ACRONYM(S)

11. SPONSOR/MONITOR'S REPORT NUMBER(S)

12. DISTRIBUTION / AVAILABILITY STATEMENT
Approved for public release, distribution unlimited

20040426 059

13. SUPPLEMENTARY NOTES

14. ABSTRACT
In this report we summarize our recent accomplishments in the development of an unstructured mesh based parallel solver to model complex hypersonic MHD flows. An existing code environment using generalized mesh structure developed for Computational Electromagnetics, was adapted to model MHD with (a) Finite rate chemistry of ionizing air, (b) Thermal Non-equilibrium (Distribution of energy across various modes of storage), and (c) Electromagnetic effects. The effect of boundary conditions such as conducting/non-conducting walls, applied or extracted electric power and so forth, render this predictive capability invaluable in the study of MHD accelerators, power generators, turbulence control, and integrated analysis of fluid mechanics and electromagnetic fields. Motivation for this work stems from the need to assess recent designs of an MHD/plasma augmented hypersonic vehicle.

15. SUBJECT TERMS
Magnetohydrodynamics, thermochemical nonequilibrium, inlet flow control, hypersonic flow

16. SECURITY CLASSIFICATION OF:			17. LIMITATION OF ABSTRACT	18. NUMBER OF PAGES	19a. NAME OF RESPONSIBLE PERSON
a. REPORT	b. ABSTRACT	c. THIS PAGE			Ramakanth Munipalli
UNCLASSIFIED	UNCLASSIFIED	UNCLASSIFIED	SAR	83	19b. TELEPHONE NUMBER *(include area code)* (818) 865-3718

Performance enhancement of high speed inlets using MHD

AFOSR contract number: F49620-01-C-0022

Final Report, March 2004

Shashi Aithal, Ramakanth Munipalli, Vijaya Shankar
HyPerComp, Inc.,
31255 Cedar Valley Dr., Suite 327
Westlake Village, CA 91361

Table of Contents

1. Abstract

HyPerComp is developing advanced computational tools to model high speed flows with MHD effects. Unstructured, multi-dimensional hypersonic MHD codes have been developed at HyPerComp to study supersonic viscous flows in a self-consistent, fully coupled manner. Effects of thermal, chemical and internal mode dis-equilibrium with and without the presence of electro-magnetic fields have been included in these codes. An existing parallel code environment using generalized mesh structure (prisms, tetrahedra, etc.) developed for Computational Electromagnetics, was adapted to model MHD with (a) Finite rate chemistry of ionizing air, (b) Thermal Non-equilibrium (Distribution of energy across various modes of storage), and (c) Electromagnetic effects. The effect of boundary conditions such as conducting/non-conducting walls, applied or extracted electric power and so forth, render this predictive capability invaluable in the study of MHD accelerators, power generators, turbulence control, and integrated analysis of fluid mechanics and time-varying electromagnetic fields. The subject of inlet flow control for hypersonic vehicles with MHD has attracted attention due to the possibility of flow modifications without the need for moving parts. There are numerous proposed designs to reduce drag, decrease total pressure loss and enhance air mass capture using MHD. Additionally, proposed MHD based concepts can even serve as a source of auxiliary onboard power, and as means to increase thrust produced by nozzles in hypersonic vehicles. The code development activity at HyPerComp has resulted in a high performance toolkit by which these ideas can be tested computationally.

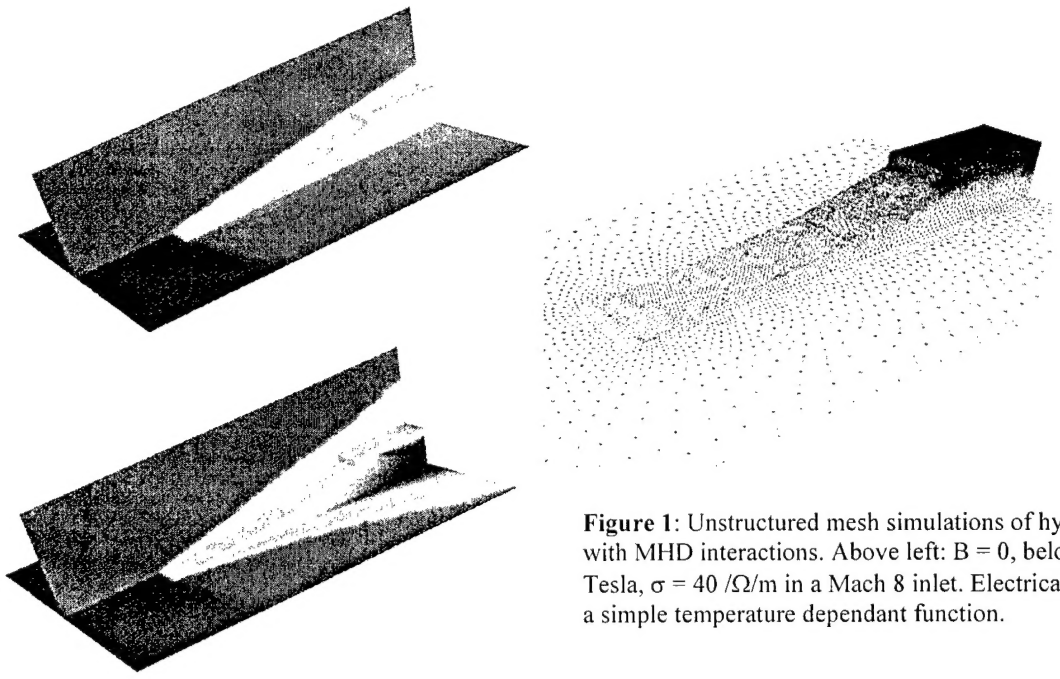

Figure 1: Unstructured mesh simulations of hypersonic inlet with MHD interactions. Above left: B = 0, below left: Bx = 1 Tesla, σ = 40 /Ω/m in a Mach 8 inlet. Electrical conductivity is a simple temperature dependant function.

2. Introduction

The application of plasma physics and MHD to aeronautics has recently captured public attention [1]. This represents a resurgence of interest from the initial studies in hypersonic MHD [2] and the pioneering work in the then Soviet Union ([3] among others,) which showed shock wave attenuation and dispersion in the presence of plasma. MHD has been known to produce numerous beneficial effects in hypersonic aerodynamics, starting from enhanced inlet mass capture, drag reduction, better combustion, to auxiliary power generation and flow acceleration. Many research groups have reproduced plasma-induced phenomena such as shock wave attenuation and dispersion, even though the mechanisms responsible for these effects are not clearly understood and are still being debated. The effect of cold plasma on a moving sphere in a ballistic range is shown in Fig. [2]. The Schlieren photographs here show gas without and with a glow discharge. The attenuation of the bow shock in the frame with the plasma turned on is one among numerous illustrations of this phenomenon. Current test activities within the United States (at AEDC, John Hopkins University) have produced drag comparison data for blunt body flows with and without plasma. These studies have repeatedly shown an increase in the shock stand-off distance and a decrease in drag in the presence of plasmas. Tests with wind tunnel scaled models of an F-15 with plasma jet nozzles in the nose cone have been conducted at IVTAN (Russia). A series of flight tests (as in Fig. [3]) have been proposed by Boeing and NASA-Dryden.

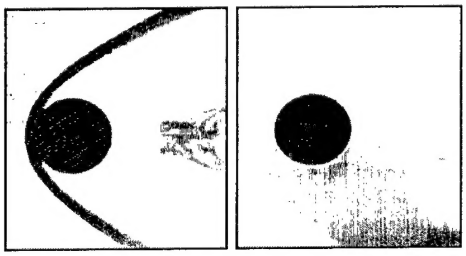

Figure 2: Flow past a sphere without and with a glow discharge plasma

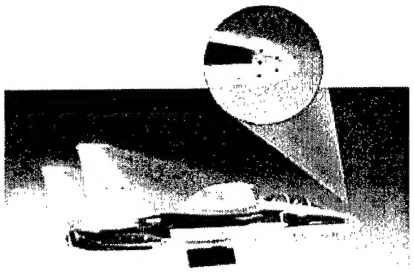

Figure 3: Illustration of F-15 equipped with plasma jet nozzles for flight test

A flurry of activity has also emerged in the area of hypersonic propulsion based on magnetohydrodynamic effects which has returned to vogue after several decades [2, 4]. Herein, a Russian vehicle concept, referred to as AJAX (discussed in [5]), will bypass a portion of the captured airflow and use it in MHD power generation and subsequent flow acceleration. The MHD generator-accelerator system essentially reduces the entropy rise of air diffusion and combustion which would be present in the unmodified engine flowpath. Enhancements to this vehicle such as drag reduction by injecting plasma at leading edges of the airframe, and increase in combustion efficiency by plasma interactions have been conceived and have firmly integrated the pursuit of the following two issues to one common goal:

(a) Plasma effects in subsonic and supersonic flows (vehicle drag, combustion efficiency, radar cross sections, etc.)
(b) The use of MHD in high enthalpy flows with sufficient electrical conductivity to improve inlet mass capture, shear layer mixing, auxiliary power generation and nozzle flow acceleration.

Thus, there is a strong need to understand the various physical phenomena and their impact on the success of the hypersonic propulsion program. However, the state of the art in modeling of engineering plasmas for the above applications is not adequate to comprehensively include all the relevant physical phenomena. Numerous simplifying models exist, which addresses some of the physics relevant to

hypersonic MHD/propulsion. Examples of such simplified approaches include the simulation of finite rate chemistry for multidimensional problems in complex geometries, solution of the integrated Navier-Stokes and Maxwell equations including the effects of finite electrical conductivity (for low Hartmann numbers at least,) and the validation of elaborate experimental data describing the relaxation processes taking place in high temperature air. More and more complex linkages between physical phenomena are continually being modeled: for example, coupling of discharge physics with surface effects of partially conducting objects [5, 6], e-beam interaction with vibrational energy modes of air [7], influence of thermal layers on shock propagation [8] and so forth. It would appear by all indications that the situation has arisen when the next generation of CFD codes based on sophisticated physical models is both urgently needed and within reach. Such a CFD code would be able to model supersonic, viscous flows in complex geometries with spatial and temporal variation of transport properties and include effects of finite-rate kinetics, thermal non-equilibrium and electromagnetic effects. Such a tool would be invaluable in the design/optimization of a hypersonic vehicle.

The objective of this research has been to develop a comprehensive design/optimization tool for hypersonic propulsion. A computational tool which includes state-of-the-art models describing the various physical phenomena (chemical/plasma kinetics, thermal non-equilibrium, energy transfer mechanisms and electromagnetic effects) was developed during the course of this research. The code was developed to study 3-D, unsteady flows on unstructured grids. A general purpose "pre-processor" was developed to generate the Jacobian and source terms for an arbitrary set of chemical reactions. This capability enables the study of various chemical kinetics models without any code modification. A Poisson solver generates the Lorentz force and Joule heating terms, which are used in the momentum and energy equations. Internal mode dis-equilibrium, which can be of great significance in gas-discharge phenomena, can also be modeled with this code. The general architecture of the code allows it to be extended easily to include models (transport properties, chemical kinetics etc.) with varying degrees of complexity. This capability enhances its utility as a research as well as a design tool.

3. Physical Phenomena of interest

Several physical phenomena are of importance in hypersonic MHD flows. Generation and sustenance of charged particles, interaction of these charged particles with magnetic fields, non-equilibrium energy transfer mechanisms, transport properties, viscous and turbulence effects and wall/electrode/sheath phenomena are some of the important physical effects of interest in such flows. The success of a hypersonic propulsion concept largely depends on the efficient generation and sustenance of charged particles. This is due to the fact that Lorentz forces generated by the applied magnetic field depends on the electrical conductivity of the flowing gas stream. All the above-mentioned effects such as chemical kinetics, non-equilibrium energy transfer mechanisms, wall/electrode/sheath effects, transport and viscous effects have an impact on the spatial and temporal variation of electrical conductivity. Hence a realistic assessment of a hypersonic propulsion design concept would require a thorough understanding of the above-mentioned phenomena and their interaction. Physical phenomena of importance in the study of hypersonic MHD are discussed next.

3.1 Mechanisms to create and sustain ionization:

A practical source of ionization to provide a large enough electrical conductivity is essential for the flow to exhibit MHD interactions. Hence, a key issue in hypersonic MHD applications is ionizing the incoming air stream. The requirements for producing this ionized air stream are very stringent. Large volumes (~ 1 m^3), low gas temperatures (1000 - 2000 K), high electron density (~ 10^{13} /cm^3), long residence times (≥ 10 msec), low power budget (1 – 10 MW/m^3), strong magnetic fields (~ 10 Tesla) are the main requirements for these air plasmas. Several techniques have been proposed in recent literature, to achieve these conditions. In the past, air seeded with an easily ionizable alkali salt [9] has been considered alongside the use of electron beams [10]. Additionally, high voltage nanosecond pulses, DC

& RF discharges, E-beams in vibrationally excited gases have also been proposed as possible means of efficient charge particle production. Seeded air and high energy E-beams are considered to be viable means of charged particle generation from an engineering standpoint, and hence were studied in detail in this research.

3.1.1 Seeded air: Seeded air flows may be well approximated by the local chemical equilibrium assumption, while the electron species may still be in thermal nonequilibrium, depending upon the incident power level and flow properties. Traditionally, MHD power generation concepts have involved seeding combustion effluents with some easily ionizable salt, such as Potassium Carbonate, Cesium, Sodium-Potassium solutions, and so forth. There are many practical issues involved in the seeding process, involving multi-phase flow, deposition of seed particles, conglomeration of seed particles near cold walls, and the resulting electrode shorting, to name a few. Nevertheless, well-seeded flows exhibit high electrical conductivity at a wide range of pressures and temperatures. The seed material ionizes essentially in an equilibrium manner. The electrons thus produced can still be in thermal non-equilibrium with the rest of the flow. Predicted values of electrical conductivity in the region of 100 – 200 mho/m can be derived at temperatures of 3000 K and flow pressures between 1 and 10 atm. Munipalli et al. [11] present a synthesis of a seeded air calculation procedure which uses the NASA-Lewis CEA code to obtain thermodynamic properties. Particle laden flow is simulated including the effects of gravity, and seed particle vaporization (sublimation) using a simple linear heat transfer analysis. Highly non-uniform seed distributions are common, greatly reducing effective conductivity of gas for a given mass of injected seed. Further, losses stem from relaxation processes resulting in heating and dissociation of seed material. Our present thinking is that seeded air flows are unusable in practical aerodynamics, except for ground based testing or power generation applications where it is convenient to regain some of the injected seed particles.

3.1.2 e-beams: The modeling of incident radiation and directed energy addition has been proposed at various levels of complexity in the recent past. This could also include the use of pulsed or steady RF (microwave) discharge, since the energy transfer mechanisms still involve the electron species predominantly. The set of transport equations for the charged particle number densities as proposed by Macheret [10] to evaluate the electrical conductivity σ for such situations are:

$$\frac{\partial n_e}{\partial t} + \bar{\nabla}\cdot\bar{\Gamma}_e = \alpha\left|\bar{\Gamma}_e\right| + q_i + k_d N n_- - \nu_a n_e - \beta n_+ n_e$$

$$\frac{\partial n_+}{\partial t} + \bar{\nabla}\cdot\bar{\Gamma}_+ = \alpha\left|\bar{\Gamma}_e\right| + q_i - \beta_{ii} n_- n_+ - \beta n_+ n_e$$

$$\frac{\partial n_-}{\partial t} + \bar{\nabla}\cdot\bar{\Gamma}_- = -k_d N n_- + \nu_a n_e - \beta_{ii} n_- n_+$$

where the fluxes $\bar{\Gamma}$ of the electrons, positive and negative ions are given by a product of their number densities n_i and their effective velocities. The gas is assumed to be locally neutral, thus implying $n_+ = n_e + n_-$. (An almost identical treatment has been successfully applied to model an RF discharge in [6]). The various quantities on the right hand side of this equation represent the ionization due to plasma electrons (α), e-beam induced ionization rate q_i, collisional detachment of electrons from negative ions (k), and electron-ion and ion-ion recombination (β and β_{ii}). N is the gas number density and ν_a is the electron-molecule collision frequency. The number densities may then be used in any model describing the electrical conductivity of partially ionized gas. The simple linear model proposed in [10] relates the number density computed above with the electron charge and the electron and ion Hall parameters to obtain the electrical conductivity as:

$$\sigma = \frac{e\mu_e n_e}{1 + \Omega_e \Omega_+}$$

It is desirable to use an expression of the following form (derived for a mixture of gases) when detailed species chemistry and collisional cross section data is available:

$$\sigma = \frac{\frac{n_e \varepsilon^2}{m_e c_e}}{\sum n_s \Delta_{se}^{(2)}(T_e) + 3.9 n_i \left(\frac{e}{8\pi\varepsilon_0 kT}\right)^2 \log\left(\frac{1.24\times10^7 T_e^{\frac{3}{2}}}{n_e^{1/2}}\right)}$$

The e-beam induced ionization term - q_i - is the critical parameter which must be evaluated to obtain the e-beam power balance correctly. This quantity is computed by assuming that the energy deposition profile (Q_b) is close to being Gaussian. The beam induced ionization rate is then given by:

$$q_i = \frac{Q_b}{eW_i}$$

where the denominator represents the energy cost of ionization by a high energy beam (in this case, low energy e-beams are known to be highly ineffective and lose almost all their energy to vibrational modes in the first few milliseconds upon incidence.) The following simple expression is currently being used in our codes to model the electrical conductivity from e-beams:

$$\sigma \cong \left[\frac{e^2}{mnk_c}\right]\sqrt{\frac{1}{w_i k_{dr}}\left(\frac{j_b \rho Y E_b}{e}\right)}$$

where e is the electron charge, m is the electron mass, n is the neutral species number density, k_c is an electron scattering rate constant, k_{dr} (= 1.5e-7 cm^3/s) is a dissociative recombination rate constant, w_i is the ionization constant (= 34 eV/electron-ion pair), j_b (about 0.1 A/cm^2) is the current density in the electron beam, E_b is the energy of the electrons, ρ is the flow density and Y is the electron stopping power. The energy of the e-beams can be varied in the range of 10 to 200 keV, to provide high enough electrical conductivity at moderate flow static pressures. The efficiency of electron beams diminishes with increasing pressure due to the inherent nature of the electrons to recombine with greater ease in such situations.

As a part of this research, an E-beam chemistry model proposed in [12] was implemented to study the electrical conductivity and MHD effects in an inlet geometry designed for Mach 8 operation [13]. It was concluded from this study that an E-beam strength of 1.5E24 m-3/s (based on a beam current density of 5 mA/cm2 and beam energy of 30 keV), yields an electrical conductivity of about 5 mho/m. This low value of electrical conductivity is inadequate for any appreciable MHD effect. The beam current would have to be increased by two orders of magnitude to get a four-fold increase in electrical conductivity [13], hence making it infeasible from an engineering standpoint.

3.2 Nonequilibrium energy transfer:

3.2.1 Thermal non-equilibrium: The preferential redistribution of internal energy in a gas to vibrational, rotational, electronic and translational modes may be modeled with the knowledge of relaxation laws, and the kinetics of dissociation and recombination. Literature is abundant with data pertaining to these phenomena. Agreement is gradually emerging in the relative importance and the dominant mechanisms which are responsible for global phenomena in nonequilibrium plasma physics. The code developed during the course of this research has multi-temperature capabilities, namely, the translational-rotation temperature (T), vibrational temperature (Tv) and electron temperature (Te). A two-temperature model [14] provides a fair representation of MHD physics in core flows for high temperature applications (4000 – 11000K), at which range, the e-V relaxation time is on the order of nanoseconds [15]. A three-temperature model is required for regions with lower temperatures or in regions close to the electrodes, where the e-V relaxation time can be on the order of milliseconds or higher.

3.2.2: Internal mode dis-equilibrium (State-Specific Kinetics): Under conditions of extreme dis-equilibrium, it might be necessary to study the internal modes of diatomic gases in hypersonic MHD. Under such situations, the internal modes (vibrational states, mostly) need to be modeled as individual species. Processes such as V-T (Vibration-Translation), V-V (Vibration-Vibration), Spontaneous Radiative Decay (SRD) and chemical kinetics must be included in the source term of these master equations to model the production-depletion of the internal modes. Recent studies have shown [16-18] that associative ionization mechanism in an optically pumped mixture can lead to significant increase in the ionization levels. Vibrational excitation of diatomic air species have a profound impact on the electron removal processes, namely, dissociative recombination and attachment of O2. Vibrationally induced detachment of electrons from O2- and vibrationally induced heating of free electrons lead to enhanced ionization levels by mitigating the effects of electron attachment and electron-ion recombination.

The MHD code architecture developed at HyPerComp has the framework to include internal mode dis-equilibrium (state-specific kinetics) coupled with flow, chemistry and EM fields. The vibrational levels of diatomic species would be modeled as individual species with the inclusion of V-T, V-V, SRD (spontaneous radiative decay) terms. Energy transfer into the higher vibrational manifolds of diatomic species required for associative ionization and mitigation of electron attachment/electron-ion recombination can be studied with this model. Such a study would elucidate methods to control the plasma density in various regions of the flow. Effects of diluent species on mitigating electron-attachment/recombination can also be investigated using this detailed state-specific kinetic model.

3.2.3 Non-Maxwellian Electron Energies – Boltzmann Solver for the Electron Energy Distribution Function (EEDF): Under discharge conditions, low-pressure molecular plasmas are characterized by several complex inelastic processes. Specifically, the energies of electrons in a molecular discharge couple very well with the vibrational states of tightly bound diatomic species via inelastic collisions. Consequently, in systems where V-V exchange collisions dominate V-T exchanges, the vibrational modes of molecular motion are out of equilibrium with the translational mode. This in turn causes the electron energies to also be out of equilibrium with the translational modes of the gas particles, and to be non-Boltzmann without a clearly definable average electron energy. Hence it is incorrect to describe the thermal state of the gas using an electron temperature (which assumes a Maxwellian energy distribution of electron energies, described by the electron temperature). The electron energy distribution and population of specific excited states govern the rate at which these inelastic collisional processes occur. Thus, the EEDF determines the chemistry and hence the characteristics of the plasma. The enhanced ionization levels reported in Ref. [12] is perhaps due to the high-energy tail of the EEDF. A deeper understanding of flowing plasmas in discharges can be obtained by a fully coupled approach which involves the flow, electromagnetics, heavy particle energy equation, master equations governing chemical kinetics and a Boltzmann equation describing the EEDF.

3.3 Electromagnetic Fields:

Electromagnetic fields play an important role in the study of hypersonic propulsion. The Lorentz body force and Ohmic heating terms in the momentum and energy equations are due to the presence of the electromagnetic fields. Several simplifying models have been used to compute the Lorentz force and Ohmic heating terms. Analytical and computational studies on MHD in the literature may be broadly divided on the basis of the magnetic Reynolds number (Re_m) which is an indication of the relative magnitude of the induced magnetic field to the applied field. For small values of Re_m ($<< 1$) the flow conservation laws may be decoupled from the Maxwell relations. This is sufficient for several situations of engineering interest (including seeded MHD generators, accelerators, wind tunnel equipment and so forth.) As Re_m increases, the induced field becomes progressively stronger and can have a significant impact on flow physics. Such a flow permits the formation of complex wave systems (Fast and slow

Magnteto-acoustic waves where the magnetic field and flow variables may jump across a discontinuity, Alfven waves where only the magnetic field rotates in a direction perpendicular to the flow and other complex interaction patterns). The capture of these wave systems places stringent requirements on the numerical methods employed. Other than dissipative and dispersive errors, these equations suffer from a singular eigenvalue structure. Powell [19] offered an empirical fix which was placed on firmer mathematical foundation by Vinokur [20] which has been used successfully in upwind schemes in recent times. Some of the approaches of coupling electromagnetic fields with the flow equations are discusses next.

3.3.1 Source term approach: The most straightforward method in which MHD effects may be introduced into an existing CFD code is by the addition of source terms corresponding to the Lorentz force in the momentum equation, and Joule heating in the energy equation with an initially prescribed distribution of electric and magnetic field. Such an approach is simple to implement in an existing fluid flow code. The applicability of this method is limited by the size of the magnetic field that is induced in the flow by virtue of the currents generated. For large values of induced fields, the magnetic field must be computed simultaneously at each time step. Pressure tends to be underpredicted by such a source term based implementation.

3.3.2 Constant B, with spatially varying electric field: The general Ohm's law including an electric field, is given by $\bar{J} = \sigma\left(\bar{E} + \bar{V} \times \bar{B}\right)$. For situations in which the electric field may be deduced from a potential (which always exists when the magnetic field is constant in time,) may be rewritten as:

$$\bar{J} = \sigma\left(-\bar{\nabla}\varphi + \bar{V} \times \bar{B}\right)$$

In order to determine this potential, the divergence of the above equation which is zero, by the law of conservation of charge, is taken, yielding the following equation:

$$\nabla^2\varphi = \nabla \cdot \left(\bar{V} \times \bar{B}\right)$$

Various simplifications may now be applied to this equation. If a space varying magnetic field acting in the z-direction is applied to a two-dimensional velocity field,

$$\nabla^2\varphi = \frac{\partial\left(vB_z\right)}{\partial x} - \frac{\partial\left(uB_z\right)}{\partial y}$$

When the electrical potential is computed, it is readily used to obtain the value of J and thus, the Lorentz force JxB may be deduced. This set of equations must be augmented by the appropriate boundary conditions described in the following section. These equations may be written out trivially for a general three-dimensional situation of current interest.

3.3.3 Induced magnetic field in one direction: Several authors [21,22] have studied situations in which the applied magnetic field is oriented along a fixed direction. This leads to a situation wherein the induced electric field is determined by Fleming's Left Hand Rule. Consider the case when the induced field Bx is in the x-direction and the applied field (0,By,Bz) is oriented in the y-z plane. The momentum equation may be rewritten in terms of the induced field, as opposed to the current as used earlier. This and the time advancement of the induced field, are governed by:

$$\frac{\partial \rho \boldsymbol{u}}{\partial t} + \frac{\partial\left(\rho \boldsymbol{u}^2 + \boldsymbol{P} - \boldsymbol{R}_b \boldsymbol{B}_x^2/\mu_m\right)}{\partial \boldsymbol{x}} - \boldsymbol{R}_b\left(\boldsymbol{B}_y \frac{\partial \boldsymbol{B}_x}{\partial \boldsymbol{y}} + \boldsymbol{B}_z \frac{\partial \boldsymbol{B}_x}{\partial \boldsymbol{z}}\right) = \frac{1}{\mathrm{Re}}\nabla^2 \boldsymbol{u}$$

$$\frac{\partial \boldsymbol{B}_x}{\partial t} - \boldsymbol{B}_y \frac{\partial \boldsymbol{u}}{\partial \boldsymbol{y}} + \boldsymbol{B}_z \frac{\partial \boldsymbol{u}}{\partial \boldsymbol{z}} = \frac{1}{\mathrm{Re}_\sigma\, \sigma\mu_m}\nabla^2 \boldsymbol{B}_x$$

This equation without the time derivatives and assuming a fully developed channel flow in the x-direction has been applied with insightful results in [21, 22]. The formulation for a general 3-D situation where all the components of the induced field exist has been presented in Ref. [23].

3.3.4 Integrated NS-Maxwell equations: A full complement of Navier-Stokes and Maxwell equation set has been solved at HyPerComp for problems of interest in compressible flow [24]. The principal difficulty in solving this set of equations is to maintain a divergence free magnetic field [25]. Characteristics based techniques exist in compressible flow solvers, designed to avoid this problem. In incompressible flows, one must post-process the magnetic field to remove the effects of non-zero divergence. This typically involves the solution to a Poisson-type equation and may be computationally expensive. However the equation using the electric potential also has this difficulty. The Maxwell equations are written in terms of the magnetic field components.

3.4 **Near wall phenomena:**

The effects of nonequilibrium in MHD are most pronounced near the electrode region. This is an important region from the standpoint of chemical kinetics, electromagnetics and thermal non-equilibrium.

3.4.1 Thermal Non-Equilibrium and Chemical Kinetics: As mentioned above, in the core of the flow, vibrational and electron modes are tightly coupled (for temperatures from 4000-11000K), and a two temperature model proposed by Park [14], as evidenced from the work of Lee [25] may be adequate. Near an electrode wall, the vibrationally temperature quickly cools to the boundary value, while the electron mode loses temperature much more gradually, well into the sheath region, in the vicinity of a few mean free paths from the wall. A three-temperature model is necessary to evaluate the electron temperatures correctly in these near-wall regions. Since the electron-induced reaction rates depend on the electron temperature, an accurate prediction of charged-species concentration depends on the correct prediction of electron temperatures. A three-temperature model along the lines of [26] has been developed during the course of this work.

3.4.2 Electromagnetic Effects: Sheaths exist in the near-electrode regions. Sheath physics in hypersonic MHD is not well understood. Sheath thickness is on the order of a few Debye lengths and can be varying from a few microns to a millimeter, depending on the electron number density and electron temperature. Sheath regions are characterized by high electric fields, which means, highly energetic electrons and hence high levels of ionization. The production of charged species in the sheath region has a profound impact on important engineering issues such as electrode erosion and electrode shorting. The electrical conductivity and hence Lorentz forces in the near-wall region impact the use of MHD forces in flow control, laminar to turbulence transition and flow-separation.

Wall regions also present a challenge in terms of correctly specifying the problem from a numerical standpoint. Boundary conditions have to be correctly specified to model the electromagnetic effects accurately. These boundary conditions depend on the choice of wall material. For a perfect conductor, the normal component of the magnetic field is zero and the jump in the electric field has no tangential component. For a perfect insulator, the gradient of the magnetic field is zero at the surface. The flow of a conducting medium in the presence of a magnetic field produces currents that must form closed loops or extend indefinitely, in the absence of charge sources. While the solid walls of the airframe are normally assumed to be insulating in CFD estimates of AJAX performance, even mildly conducting airframe materials cause currents to leak away from the flow (considering the very low achievable values of electrical conductivity of air in flight,) and may potentially cause major changes in flow compression and shock structures on this account. Hence the effect of conducting walls in hypersonic inlet flow computations must be considered carefully. Even small cracks in insulations (4-5 orders of magnitude smaller than the flow length scale) have large-scale effects on the flow, and the influence of MHD on flow control aspects. We have initiated studies in including conducting wall phenomena in our codes during the course of this research [27].

3.5 Chemical Kinetics: A chemical kinetics model provides critical reactions which are necessary to describe the state of a gas under a given set of thermodynamic conditions. Preference is usually given to simplified reaction mechanisms which involve as few species and as few reactions as possible which reproduce the correct global phenomena such as ionization fraction, mixture viscosity, thermal conductivity, vibrational energy absorption rate and so forth. This is in the interest of saving computational time for large problems. However, these simplified chemistry models must be capable of predicting the gas species composition correctly. These models must be capable of predicting the charged species concentration accurately, in order to get realistic estimates of the electrical conductivity. An important consideration in developing chemical kinetic mechanisms is to obtain the rate constants of individual elementary reactions. Also of equal importance is the ability to obtain thermodynamic data (specific heats and heats of formation) of the individual species under conditions of temperature and pressure, pertinent to the operating conditions for a particular problem. Obtaining reaction rate constants and thermodynamic data for high temperature low-pressure conditions (as in hypersonic MHD) is a daunting task. Many chemical kinetic models have emerged over the years. The Park model (21 reactions) and Dunn and Kang model (26 reactions) [26] have been found to provide satisfactory results for a wide range of flight conditions. Using ionization mechanisms such as e-beams adds further complications and demands appropriate kinetic mechanisms to accommodate them.

There are several numerical challenges in chemical kinetic modeling. Depending on the reaction rates, a model can be very stiff numerically, thus imposing very stringent constraints on the stability and computational time. An implicit solver provides greater stability and allows the use of large time-constants. A major impediment in the use of an implicit scheme involves the developing the Jacobian matrix for a given reaction set. This process can be considerably time-consuming and also very susceptible to errors. To alleviate this problem, a "pre-processor" was developed to automatically develop the Jacobian and source terms for a given set of elementary reactions. . This preprocessor reads in a text file consisting of the chemical reactions and generates the Jacobian and source terms. The Jacobian and source terms can be included in the solver without any code modification. This feature greatly simplifies the process of testing different chemistry models and is thus invaluable in obtaining reduced chemical kinetics model for a particular set of conditions.

3.6 Viscous Flow Features, Turbulence modeling

Appreciable electromagnetic effects will occur near the boundary layer, with the result that the temperature profile in the boundary layer will change. A survey of turbulence modeling techniques in MHD may be found in Ref. [28].

Turbulent flows comprise of vorticity components in all directions. A uniform magnetic field acting on a turbulent conducting fluid dampens the components of vorticity perpendicular to itself. A scale independent anisotropic damping of the velocity field is caused, which makes turbulent eddies essentially two-dimensional, which result in greatly reduced turbulence and are damped by viscous effects. This has been confirmed by direct numerical simulation. A magnetic field acting axially in a pipe with turbulent flow tends to damp the turbulence, reduce frictional drag for a given flow rate, and actually raise the critical Reynolds number for instability of laminar flow.

Enhancement of the vorticity in the flow due to MHD effect and modification of the velocity layer near the wall due to interplay between change in the temperature profile and velocity profile can be the primary source of change in the turbulence profile. A secondary effect may be the change due to electro-magnetic **jXB** term in the momentum equation, which will change the turbulent kinetic energy and turbulent dissipation equations when these last equations are obtained by taking higher moments of the momentum equations. While turbulence effects might be important in hypersonic MHD, these effects have not been included in our current development.

4. Governing Equations and Numerical Method

4.1 Problem Formulation:

The conservation equations governing the flow of weakly ionized gases may be written in the following form:

$$\frac{\partial U}{\partial t} + \vec{\nabla} \cdot (F_x, F_y, F_z) + \vec{\nabla} \cdot (H_x, H_y, H_z) = S$$

in which the fluxes F are inviscid or convective, while H are viscous or dissipative. The source term S comprises of the production of, and interaction between the various flow quantities. This equation may be expressed in the integral conservation form in a control volume Ω bounded by $\partial\Omega$, as follows:

$$\int_{\Omega} \frac{\partial U}{\partial t} d\Omega + \oint_{\partial \Omega} [F_n ds + H_n ds] = \int_{\Omega} S d\Omega$$

F_n and H_n in the above equation are face normal flux components. The vector used in this equation is expanded below. An index s is used for the various gaseous species that are considered. If one were to consider internal mode disequilibrium, ρ_s would comprise of various internal modes (vibration/electronic levels) of individual species. We show the three-temperature formulation along the lines of [26]. Energy addition by MHD at high temperatures can bring about a departure from equilibrium between the various energy modes. There are three energy equations, one for the total energy conservation and the other two describing the vibrational energy of the diatomic species and the electron energy. The following matrices describe the conservation laws:

$$U = \begin{bmatrix} \rho_s \\ \rho \vec{V}^T \\ \rho E \\ \rho e_v \\ \rho e_e \end{bmatrix}$$

$$\vec{V} = [u, v, w]$$

$$F_n = \begin{bmatrix} \rho_s U_n \\ \rho U_n \vec{V}^T + p\vec{n} \\ \rho U_n H \\ \rho U_n e_v \\ \rho U_n e_e \end{bmatrix},$$

$$H_n = \begin{bmatrix} -\rho D_s \vec{\nabla} y_s \cdot \vec{n} \\ -\vec{\tau}_n \\ -\vec{V} \cdot \vec{\tau}_n - \eta \vec{\nabla} T \cdot \vec{n} - \eta_v \vec{\nabla} T_v \cdot \vec{n} - \rho \sum_s h_s D_s \vec{\nabla} y_s \cdot \vec{n} \\ -\eta_v \vec{\nabla} T_v \cdot n - \rho \sum_s h_{v,s} D_s \vec{\nabla} y_s \cdot \vec{n} \\ -\eta_e \vec{\nabla} T_e \cdot n - \rho \sum_s h_{e,s} D_s \vec{\nabla} y_s \cdot \vec{n} \end{bmatrix}$$

$$S = \begin{bmatrix} \dot{\omega}_s \\ (\vec{j} \times \vec{B}) \\ \vec{J} \cdot \vec{E} + \dot{Q}_{rad} \\ \dot{\omega}_v \\ \vec{J}_e \cdot \vec{E}' + \dot{\omega}_e + p_e \vec{\nabla} u + \dot{Q}_{rad} \end{bmatrix}$$

The transfer of energy across the various energy levels is contained in the non-equilibrium energy production rate $\dot{\omega}_v$ and $\dot{\omega}_e$. The source term in the vibrational energy equation ($\dot{\omega}_v$) contains the energy transfer to the vibrational mode from the electronic and translational modes via collisions, and vibrational energy gained or lost due to molecular depletion (dissociation) or production (recombination). The source term in the electron energy ($\dot{\omega}_e$) equation contains terms due to the electric field (Joule heating) electron pressure gradient, energy exchange with the translational modes of heavy particles and the vibrational modes due to collisions. The source term also includes energy deposited due to external radiations and energy released due to formation/depletion of electrons. The expressions used to model these features may be found in [26]. The three-temperature formulation is explained in detail in appendix-A. In this work, the source terms in the electron energy equation do not include the net work done due to the electron pressure gradients. This is justified due to the low mass fraction of electrons. Electron velocity is assumed to be equal to ion velocity and hence there is no contribution due to charge separation effects. Radiative energy addition by means of microwave and other beams can possibly be used to cause an increase in the electron energy and ionization. This is modeled by the terms Q_{rad}. Fluxes F_n and H_n are written at the cell face in each control volume. Species mass fractions, velocities and temperature(s) can be obtained from the above set of equations. The electromagnetic effects (current density, electric fields and potential) are obtained by the solution of a Poisson-type equation solved iteratively at each time-step. The MHD model is discussed next.

MHD Model:

In this work, the magnetic Reynolds number is assumed to be small. This implies that the induced magnetic field is negligible and that the electric field may be derived from a scalar potential: $\vec{E} = -\vec{\nabla}\varphi$. Ohm's law may then be used to relate this potential to the current density:

$$\vec{J} = \sigma\left(-\vec{\nabla}\varphi + \vec{V} \times \vec{B}\right) - \frac{\omega\tau}{B}\left(\vec{J} \times \vec{B}\right)$$

Where σ denotes the electrical conductivity, $\omega\tau$/B is the Hall parameter, J is the electric current density and B is the applied magnetic field vector. Since the induced magnetic field is neglected, the only electromagnetic field quantity that needs to be computed numerically at each time step is the electric potential.

When the divergence of the above expression is set to zero and is re-written in terms of the electric potential, a Poisson type equation is obtained, which must be solved at each computational time step. In the results presented in this paper, the Hall-effect terms are neglected in the generalized Ohm's law given above. Setting the divergence of the current density (without the Hall terms) to zero leads to the following expression:

$$\nabla \cdot \left[\sigma\left(-\nabla\varphi + \vec{V} \times \vec{B}\right)\right] = 0$$

Solution of the above Poisson equation yields the electric potential φ and electric current density J. The joule heating term and Lorentz forces in the energy and momentum equations can thus be obtained.

4.2 Space/time integration: Numerical Scheme

A point-implicit finite volume scheme is used to solve the governing equations shown earlier. For a cell bearing the index i, volume Ω_i, the time advancement scheme is written as:

$$U_i^{t+\Delta t} = U_i^t + C_L^{-1} r_i^t$$

where,

$$C_L = \left[I + \frac{\delta t}{\Omega_i} M_L^{'} \right]$$

and

$$M_L^{'} = M_{inv}^{'} + M_{visc}^{'} - \Omega_i M_{src}^{'}$$

The right hand side vector r is the flux summation based on quantities at time level t. Inviscid fluxes are computed from a Roe-type procedure, in which a density based averaging is performed similar to the perfect gas equivalent. Viscous and dissipative fluxes are computed from central differences. Details of this implementation may be found in [15]. In the above equation, $\boldsymbol{I}$ is an n x n (n is the total number of dependent variables in the vector U) identity matrix and M_L' is the combined Jacobian including inviscid, viscous and source term contributions.

Reacting and plasma flow equations are characterized by widely varying spatial and time-scales. The point-implicit formulation is necessary in order to obtain stable solutions for a stiff system of governing equations. The formal order of accuracy of this numerical procedure can be enhanced using the TVD approach, as described by Barth [29], using local gradients computed from a Gaussian summation. Work is underway to develop this environment into a higher order multi-physics solver using the Discontinuous Galerkin technique.

5. Accomplishments

5.1 Thermochemical nonequilibrium

Primarily the Park two-temperature model, and a three-temperature model were developed in the course of this study. In the two temperature model, the two temperatures used were T: Translational and Rotational temperature, Tv: Vibrational, electronic and electron temperature. In the three temperature model, the three temperatures were T: (Translational and Rotational) as in the two-temperature model, vibrational temperature, Tv and an electron temperature, Te. In high temperature applications, the two-temperature model is known to be accurate. The energy transmitted to the electron species from the electromagnetic fields is quickly transferred to the vibrational modes and at a much slower rate, to the translational and rotational modes. The difficulty arises near electrode surfaces or situations wherein the temperatures are not high (as in E-beam applications), where the gas temperature might be less than 1000K. An example of the applicability of the two temperature model is a high temperature MHD accelerator. Figure [5] shows the axial variation of temperature for a two-temperature model in an accelerator channel. It is seen that the temperature difference between the vibrational and translational levels remains constant through the length of the channel. This difference may be evaluated from analytical relations as in Kerrebrock [30], thus validating the nonequilibrium model.

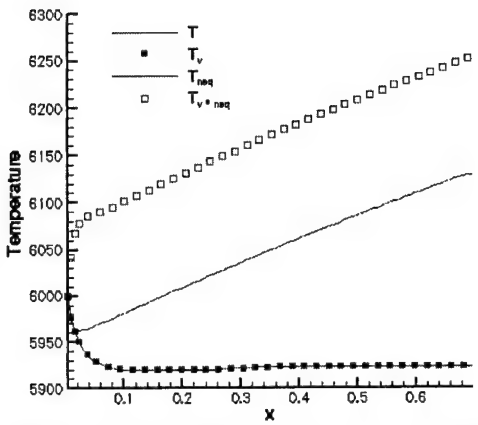

Figure 5 : Nonequilibrium Temperature variation along an unseeded air MHD accelerator with and without the MHD fields

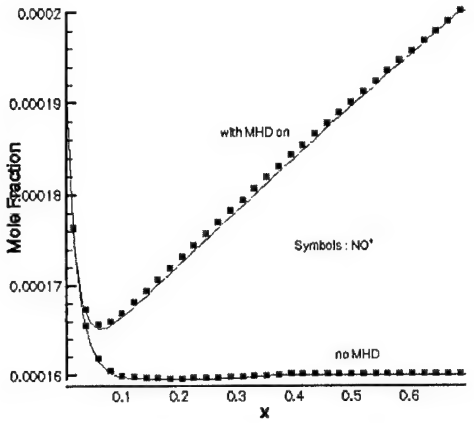

Figure 6: Variation of electron and NO+ mole fractions along a nonequilibrium unseeded air MHD accelerator

5.2 Equilibrium models, seeding

The NASA-Lewis CEA code has been interfaced with a Navier-Stokes solver. Ability now exists to model about 70 different reacting species, with about 1600 products, including multiple phases. As a simple illustration, the injection of liquid droplets of Potassium Carbonate solution in water has been studied. The effect of finite rate evaporation of these seed particles, and their settling due to gravity in an MHD channel have been modeled. The results from this study were originally presented in Ref. [11].

5.3 Integrated NS-Maxwell equation modeling

In cases where the Magnetic Reynolds number is large ($\mathrm{Re}_m = \sigma\mu_0 L U_\infty >> 1$,) the magnetic field induced in the flow by virtue of the currents generated will be large, and a system of combined Navier-Stokes and Maxwell equations must be solved. Recent years have witnessed a significantly enhanced understanding of the computation of such flows. The electrical conductivity values encountered in hypersonic aerodynamics are rather low, and a study was performed to study the need for the integrated NS-Maxwell modeling (ref. [22]). Three different numerical methods were developed: Roe's scheme, Xu's Kinetic Flux Vector Splitting scheme, and a simple central difference with artificial dissipation (Jameson-Schmidt-Turkel) scheme. With varying levels of difficulty each of these schemes has been seen to function appropriately, and complex MHD wave structures have been resolved.

5.4 Boundary conditions

Various boundary condition procedures have been developed for use in hypersonic MHD.

5.4.1 Effect of segmentation of electrodes: In applying current boundary conditions on a wall comprising of segmented electrodes, certain simplifications must be made. If the computational mesh can resolve each electrode sufficiently (which is extremely difficult to accomplish in real problems,) one would set the normal component of current to zero in the insulating region and the tangential gradient of the electric potential to zero on a conducting surface. However, if an infinitely segmented electrode arrangement is assumed, it is possible to deduce the following condition on the wall [22]:

$$\frac{\partial \varphi}{\partial y} = -\beta \frac{\partial \varphi}{\partial x}$$

where y denotes the direction normal to the wall and x along the wall, φ is the electric potential and β is the Hall parameter. This expression seems adequate for practical applications.

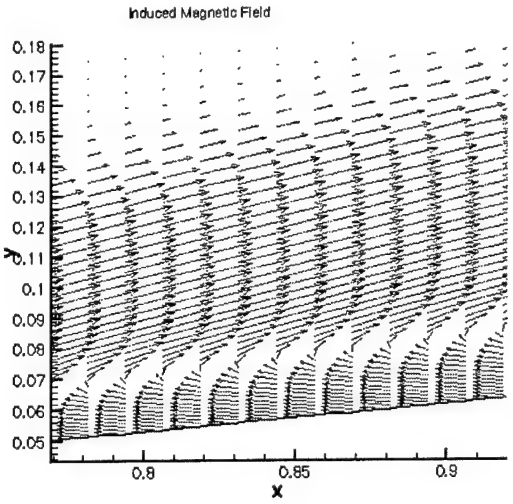

5.4.2 Magnetic Field: At a perfectly conducting wall, normal component of the magnetic induction H is continuous across the wall. Frequently in computations, the tangential component of this field is set to zero, which is an approximation for slender bodies. The magnetic field strength inside the solid body would be obtained by scaling the gas magnetic field strength by the ratio of the magnetic permeability in the two media. The induced magnetic field vectors in a supersonic conducting flow past a ramp is shown in Fig. [7]. Here, a vertical magnetic field is applied, which is nearly cancelled tangential to the wall by a tangential induced field in the opposite direction.

5.4.3 Various treatments of induced fields: In the recent past, we have studied in considerable depth, the application of various descriptions of MHD flow features. Of these, the main ones are: (a) The induced electrical field approach, (b) Induced B-field, (c) Induced current and (d) The integrated Navier-Stokes-Maxwell equations. A few sample results are shown here. Fig. [8] shows a channel flow situation in which the magnetic field is ramped up from 0 to 0.35 Tesla while the velocity profile flattens and develops an M-shape that is characteristic of such flows. Fig. [9] shows the effect of wall thickness and wall conductivity on the induced magnetic field contours in a fully developed channel flow in 3-D. The development of the 3-D M-shape is also apparent here.

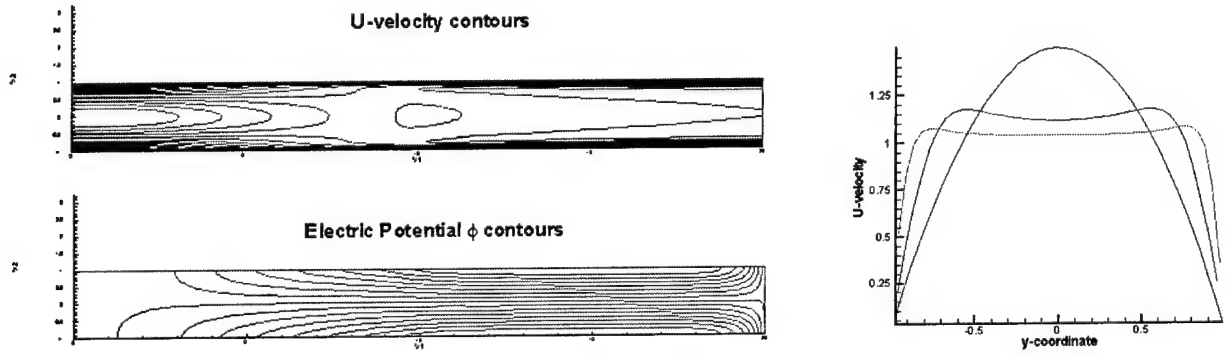

Figure 8 : 2-D channel flow using the induced electric field formulation. Bz is zero initially, ramped up to 0.35 Tesla and held fixed for the rest of the channel. U-profiles are shown with the developing M-shape.

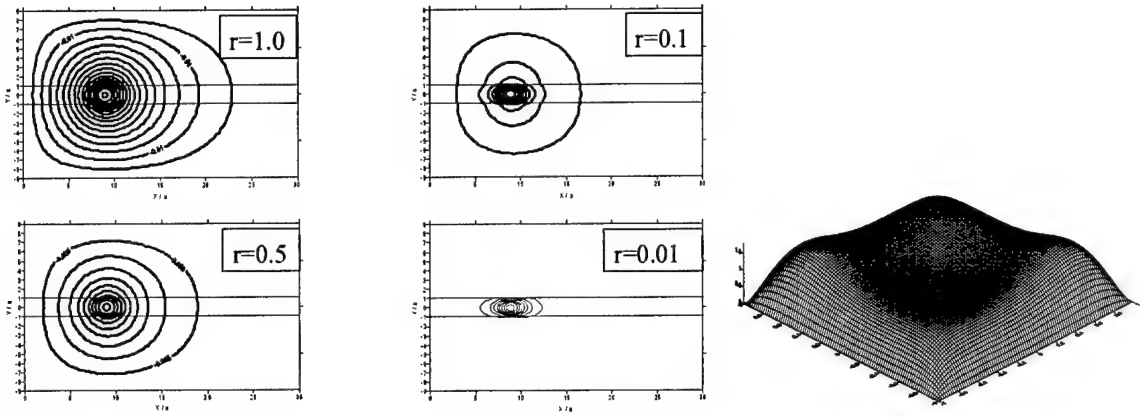

Figure 9: 3-D Channel flow using the induced B-field formulation. Magnetic field has a bell shaped peak at x = 10. "r" is the ratio of wall to fluid conductivities. Plotted alongside is the velocity profile along the cross section.

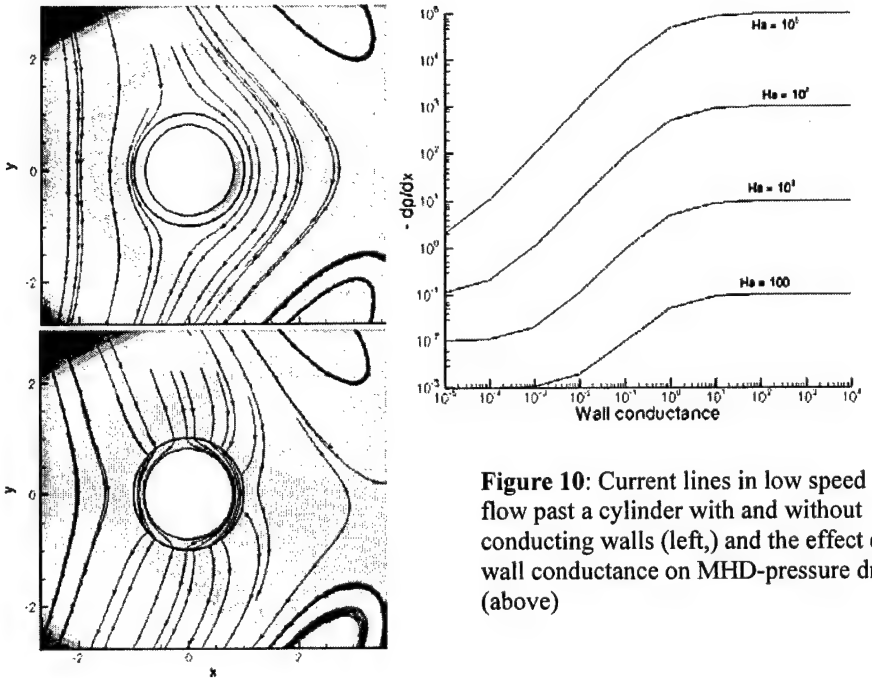

Figure 10: Current lines in low speed flow past a cylinder with and without conducting walls (left,) and the effect of wall conductance on MHD-pressure drop (above)

5.5 Wall conduction effects in Hypersonic MHD:

Existing literature in the area of hypersonic flows with MHD frequently relies on the assumption that the walls bounding ionized flows are insulating, or have some pre-set potential distribution that determines the current within the fluid medium. When the walls are fully conducting, or comprise of insulation in which imperfections may occur (albeit minute,) literature has shown numerous situations in which the computed pressure is vastly different (by more than an order of magnitude,) from the insulating wall assumption. In airframes, a metallic structure is more of a norm than an exception, and this seems to call for a major revision of MHD performance estimates obtained from insulating wall approximations. Hence a part of this research was focussed on understanding the impact of wall physics on MHD flows.

When the walls are thick, computations must be carried out within the wall region for electromagnetic and thermal quantities but not for fluid momentum and density. This involves blocking out of these regions from the flow solver. An index array denotes the material type in each cell. Boundary conditions are applied at this interface rather than the edges of the computational domain, for the flow solver. When the conducting wall surfaces are thick, the Boundary Element Method (BEM) may be used to model the flow of currents in these regions, which can then be approximated by semi-infinite boundaries. In the limit of thin conducting walls, a wall-tangential Poisson-type equation may be coupled with the flow solver, thus avoiding the need to generate a computational mesh inside the wall. All of these approaches are being presently considered, and a BEM routine is being developed for the compressible MHD code environment. Figure [10] shows sample computations involving conducting walls. Current lines in conducting and insulating wall situations is shown, and an estimate of pressure gradient with varying wall conductance ration is presented, for a range of Hartmann numbers (these estimates are based on the calculations of Tillack [35]).

5.6 Implementation of the E-beam chemistry model:

E-beams are considered to be the most efficient way of generating charged species concentrations required for MHD aerospace applications. A major thrust in this research was to develop a fully coupled model incorporating the effects of flow, finite-rate E-beam induced chemistry and electromagnetics. The goal was to compute the spatial variation of electrical conductivity, based on charged-species concentration and use it with the MHD model to obtain the Lorentz forces and Ohmic heating. This self-consistent modeling methodology is necessary to evaluate the potential of the proposed E-beam concept for several MHD based applications such as enhancement of inlet mass transfer, drag reduction and shock mitigation. While several groups have studied various aspects of this problem [31-33], none of these studies have attempted to do so in a fully-coupled, self-consistent manner. During the course of this research, self-consistent, fully coupled model was used to study a 3-D Mach 8 inlet geometry under realistic flight conditions. It was seen that for values of beam current and voltage obtained under current engineering constraints, the maximum electrical conductivity is too low to achieve MHD-based flow control. A detailed hypothetical analysis of the E-beam model (in terms of beam strength and extent of the E-beam) was conducted. This was done to obtain the range of conditions under which MHD-based control would be possible. Details of this work can be found in [13].

5.7 Implementation of the three-temperature model:

A simple three-temperature model (details given in Appendix) was also developed as a part of this study. The Jacobian matrix for the inviscid flux vector F, was derived along the lines described in [26]. A simplified 2-D geometry of M-8 geometry (as in Ref. [13]) was used to study the two-temperature and three-temperature models. The freestream conditions were as follows: T_∞ = 226.51K, P_∞ = 193.6 N/m2 corresponding to conditions at 30K feet (10K meters). Figure 11 show the variation of temperature along the surface of the ramp for the two-temperature and three-temperature model. It is seen that in the two-temperature model, the vibrational temperature is very close to the gas temperature, whereas for the three-temperature model, the electron temperature is very close to the gas temperature while the vibrational temperature is virtually unchanged. At low temperature and pressures, the VT relaxation time is very large (on the order of seconds) according to the Millikan-White formula [26], however, the T-E relaxation time is on the order of micro-seconds. In the two-temperature model, since the electron temperature is assumed to be equal to the vibrational temperature, the electrons equilibrate with the translational mode. In the three-temperature model, however it is clearly seen that the vibrational temperature is low (since the energy exchange between vibrational mode and heavy particles is on the order of seconds), whereas the electrons equilibrate with the translational temperature. This comparison shows that for low temperature/pressure cases a two-temperature model predicts an incorrect vibrational temperature.

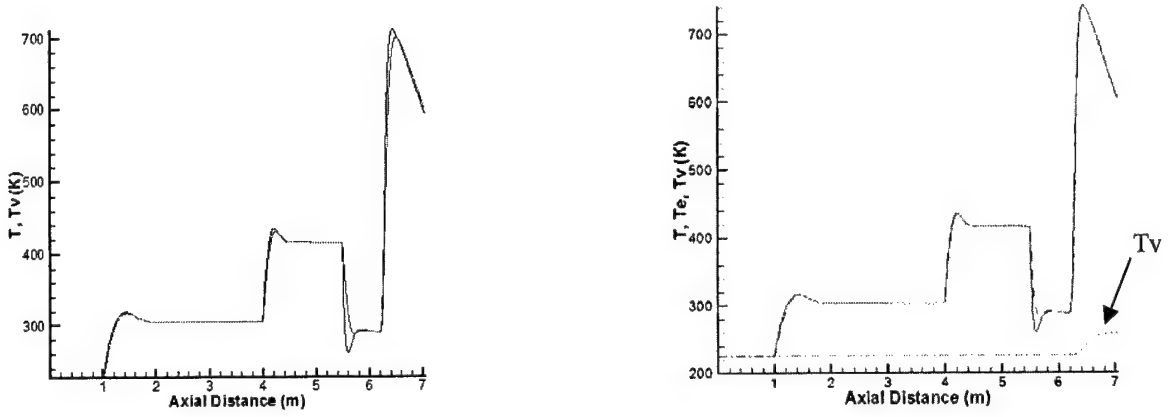

T, Tv for 2-temp model

T, Tv,Te, for 3-temp model

Figure 11: Two and three temperature models used in an inlet flow

6. Code Architecture and Attributes

The development of the HyPerComp CFD/MHD coupled solver is based on the code architecture of an existing unstructured grid-based CEM solver. This finite-element CEM algorithm has been implemented for massively parallel and scalar computer architectures. Along with the CEM solver, a complete suite of user interface utilities are provided in the computational environment to go from a CAD model to the final solution. These tools are shown in Figure [12], arranged as they are used in the simulation cycle.

The tools include:

- The Rockwell Science Center developed grid generator UNISG for performing unstructured grid generation.
- A 3-D GUI (graphical user interface) for pre and post-processing called UNSPREP. This tool aids the user in setting up grid-related solver parameters.
- A help sensitive run control parameter input page GUI.
- Domain decompositioning tools for parallel simulations.
- The solver, which has been ported to many parallel and scalar computer architectures.
- A collection of graphically driven post-processing tools for performing results visualization and solver performance analysis.

The software written by HyPerComp is implemented in a combination of C++, C, and Fortran and includes C++ class libraries for common re-usable functions. It should be noted that all of the software in the solver suite is either freely available or developed in-house.

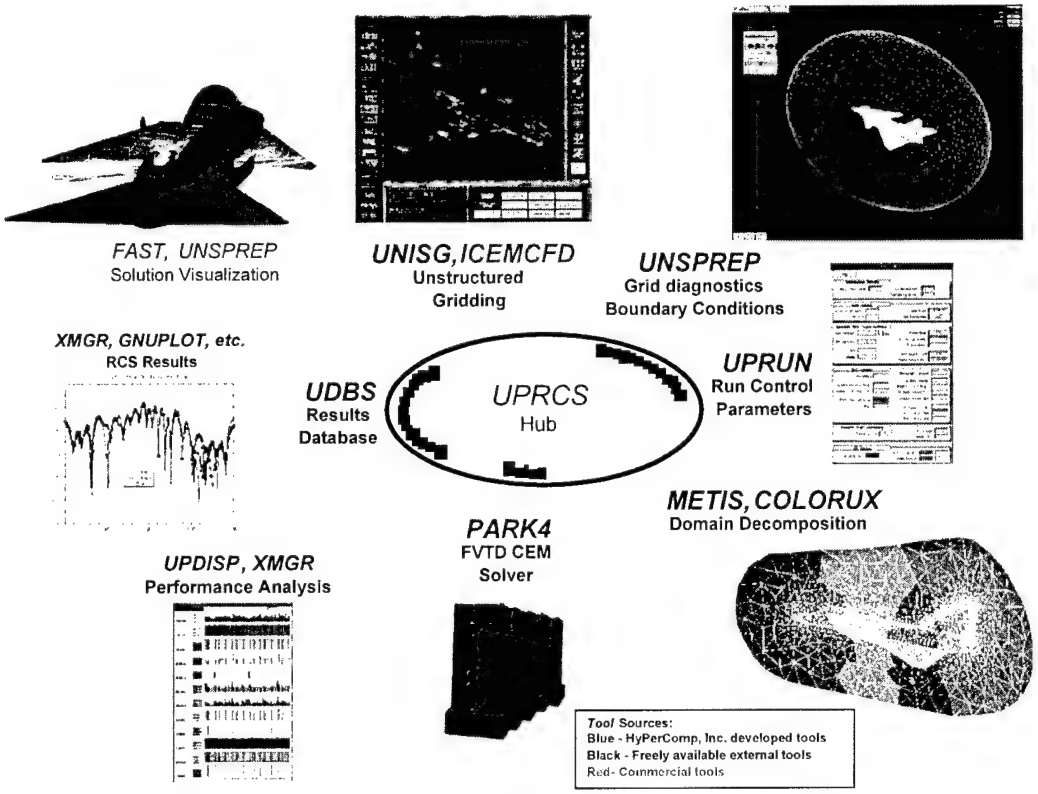

Figure 12: Integrated electromagnetics environment at HyPerComp, Inc.

7. Summary and Recommendations for future work

7.1. Summary of accomplishments:

A 3-D unstructured code capable of simulating compressible, supersonic viscous flows has been developed during the course of this research. Effects of thermal non-equilibrium (multi-temperature models) finite-rate chemical kinetics and electromagnetic effects have been coupled with the flow solver in a self-consistent manner. The architecture of the code, derived from an existing CEM solver, makes it amenable to be ported to many parallel and scalar computers. A separate preprocessor is used to generate the Jacobian and source terms for any set of chemical reactions. This preprocessor reads in a text file consisting of the chemical reactions and generates the Jacobian and source terms, which can then be included in the solver. This code framework allows the user to study any arbitrary set of chemical kinetics (species and chemical reactions) without the need for any code modification. Code development for studying internal mode dis-equilibrium (vibrational non-equilibrium) has been completed.

This research has resulted in the first study of a validated e-beam chemistry model in a 3-D Mach 8 inlet geometry under realistic operating conditions. Since the flow, chemistry and electromagnetic effects were coupled self-consistently, realistic estimates of electrical conductivity and MHD interactions could be obtained. Several important engineering/design issues such as maximum attainable electrical conductivity for a given beam-strength (beam current and beam energy (keV)), location and extent of the e-beam were investigated. Based on engineering constraints on achievable beam strengths and magnetic fields, it was concluded that no appreciable MHD interactions/flow modification could be achieved. The charged species generation by E-beams would have to be augmented by some other means for its successful application in hypersonic propulsion. Vibrational excitation of air by means of RF or laser

excitation has been proposed as a plausible solution. This research has also developed the first 3 temperature model coupled with electromagnetic effects and is likely to lead to a more detailed E-beam chemistry model with rate constants based on electron temperatures.

7.2 Recommendations for future research:
Developments to the code can be made in the following areas, namely (a) Physical models, (b) Numerical techniques,.

7.2.1 Physical models: While the current code addresses several physical phenomena relevant to hypersonic propulsion, the following additions is likely to enable a better understanding of the underlying physics

(a) Turbulence models: Hypersonic flowfields in the fore-body inlet regions of proposed NASP-type geometries tend to be dominated by turbulent effects. MHD has the effect of suppressing and laminarizing turbulent flows. Two equation models for incompressible MHD turbulence are used widely in literature, (see e.g., [34] for a description). An extension of these models to compressible flows has been undertaken by some researchers in recent times. However, this problem, like much of turbulence modeling, remains open-ended, particularly due to the lack of suitable test data. In an ongoing research effort funded by the Department of Energy, we are investigating closure models for incompressible MHD at the limit of large Hartmann numbers. We intend to extend this effort into compressible flows in due course.

(b) Sheath models: Treatment of sheaths in hypersonic MHD can be a daunting task. Since our formulation does not make an assumption of quasi-neutrality in the computation of charged species concentrations, it will be able to capture sheath effects. However, sheath-resolution can be a difficult problem. Sheath thickness can vary from a few microns to tens of microns or more, depending on several factors such as operating conditions, method of generating charged species and generation and application of electromagnetic fields. A series of parametric studies can help ascertain the sheath thickness for various operating conditions. It might be necessary to use some semi-empirical/analytical sheath models using results from the MHD code as inputs.

(c) Internal mode dis-equilibrium and EEDF: Code development for the inclusion of vibrational dis-equilibrium has been completed during the course of this research. Knowledge of this internal mode dis-equilibrium can be coupled to a Boltzmann-solver for the distribution of electron energies. The direct coupling between the electrons and internal modes can be studied with this formulation. The assumption of a common average temperature describing the electrons can thus be eliminated. Reaction rate constants for electron induced reactions can be computed on the basis of the EEDF instead of the Arrhenius rates. Important physics pertaining to reactions induced by the high-energy tail of the EEDF can be investigated by this approach.

(d) Issues related to relaxation time constants, transport properties and reaction rate constants: There are several crucial issues related to accurately predicting the electrical conductivity, relaxation times for VT, V-E and T-E processes, transport properties such as thermal conductivity of heavy particles and electrons, viscosity and diffusion co-efficients, reaction rate constants and thermodynamic properties. A detailed study of the range of applicability of these constants has to be ascertained. This is of particular significance if one is interested in pursuing low-temperature methods of producing ionization such as E-beams, RF excitation or lasers.

7.2.2: Numerical methods: HyPerComp is currently developing higher order numerical schemes to solve the coupled set of MHD equations using the induced magnetic field formulation. A suite of codes, tentatively christened as HOME (Higher Order Multiphysics Environment), is being developed based on the Discontinuous Galerkin approach to higher order numerics, to be used on arbitrary meshes, with parallel computers. Higher order schemes provide the ability to economically resolve complex physics occurring in ordinarily un-resolvable length scales, such as Hartmann layers, acoustic-type wave

propagation, and various types of flow instabilities. It is of imminent interest to transfer the work developed here to such an environment, to be able to perform full-airframe computations for practical geometries.

8. References

[1] "Plasma Magic," *New Scientist* Magazine, 28 October 2000

[2] Resler, E.L., Sears, W.R., "The prospects for Magneto-aerodynamics," *Journal of the aeronautical Sciences*, pg. 235, April 1958

[3] Klimov, A.I., Koblov, A.N., Mishin, G.I., Serov, Yu.L., Yavor, I.P., *Soviet Technical Physics Letters*, Vol. 8, pg. 192, 1982

[4] Grad, H., "Reducible problems in magneto-fluid dynamic steady flows," *Reviews of modern physics*, Vol. 32, no. 4, October 1960

[5] Bruno, C., Czysz, P.A., Murthy, S.N.B., "Electro-magnetic interactions in hypersonic propulsion systems," AIAA 97-3389, 33rd AIAA/ASME/SAE/ASEE Joint Propulsion Conference & Exhibit, Seattle, WA, July 1997

[6] Candler, G.V., Kelley, J.D., "Effect of internal energy excitation on supersonic air flow," AIAA 99-4964, presented at the 9th AIAA International Space Planes and Hypersonic Systems and Technologies Conference, Norfolk, VA, November 1999

[7] Macheret, S.O., Shneider, M.N., Miles, R.B., "Modeling of air plasma generation by electron beams and high voltage pulses," AIAA 2000-2569, presented at 31st AIAA Plasmadynamics and Lasers Conference, Denver, CO, June 2000

[8] Ionikh, Yu.Z., Chernysheva, N.V., Yalin, A.P., Macheret, S.O., Martinelli, L., Miles, R.B., "Shock wave propagation through glow discharge plasmas: evidence of thermal mechanism of shock dispersion," AIAA 2000-0714 38th AIAA Aerospace Sciences Meeting, Reno, NV, January 2000

[9] Baughman, J.A., Micheletti, D.A., Nelson, G.L., Simmons, G.A., "Magnetohydrodynamics Accelerator Research Into Advanced Hypersonics (MARIAH)," NASA-CR-97-206242 Oct. 1997

[10] Macheret, S.O., Shneider, M.N., Miles, R.B., "External supersonic flow and scramjet inlet control by MHD with electron beam ionization," AIAA 2001-0492, 39th AIAA Aerospace Sciences Meeting, Reno, NV, January 2001

[11] Munipalli R., Anderson, D. A., Wilson, D. R., "CFD evaluation of seeded and unseeded air MHD accelerators," AIAA 2000-0215, January 2000

[12] P. Palm, E. Ploenjes, I. V. Adamovich, J. W. Rich, 'E- Beam Sustained Low-power Budget Air Plasmas', AIAA Paper 2002-0637, 40th AIAA Aerospace Sciences Meeting & Exhibit 14-17 January 2002/ Reno, NV.

[13] S. M. Aithal, R. Munipalli, V. Shankar, "A Design Environment for Plasma and Magneto-Aerodynamics", AIAA Paper 2003-4167, AIAA Joint Propulsion Conference, Orlando, FL, June 2003.

[14] Park, Chul, "Assessment of two-temperature kinetic model for ionizing air," Journal of Thermophysics and Heat Transfer, Vol. 3, No. 3, July 1989

[15] R. Munipalli, "Ph.D. Thesis" University of Texas, Arlington, June 1998

[16] E. Ploenjes, P. Palm, J.W. Rich, and I.V. Adamovich, "Electron-Mediated Vibration-Electronic (V-E) Energy Transfer in Optically Pumped Plasmas", Chemical Physics, vol. 279, 2002, pp. 43-54

[17] I.V. Adamovich, "Control of Electron Recombination Rate and Electron Density in Optically Pumped Nonequilibrium Plasmas", Journal of Physics D: Applied Physics, vol. 34, 2001, pp.319-325

[18] P. Palm, E. Ploenjes, M. Buoni, V.V. Subramaniam, and I.V. Adamovich, "Electron Density and Recombination Rate Measurements in CO-Seeded Optically Pumped Plasmas", Journal of Applied Physics, vol. 89, No. 11, 2001, pp. 5903-5910

[19] Powell, K.G., "A Riemann solver for ideal MHD that works in more than one dimension," ICASE report 94-24, 1994

[20] Vinokur, M., "A rigorous derivation of the MHD equations based only on Faraday's and Ampere's laws," presentation at LANL workshop, 1996

[21] Shishko, A.Ya., "A theoretical investigation of steady-state film flows in a coplanar magnetic field," Magnetohydrodynamics, Vol. 28, pg. 170, 1992

[22] Munipalli R., Shankar V., "Development of computational capabilities in real gas MHD," AIAA 2001-0198, January 2001

[23] Munipalli R., Shankar V., Liu Z., Hadid A., "An unstructured grid parallel MHD solver for real gas simulations," AIAA 2001-2738, June 2001

[24] Brackbill, J.U., Barnes, D.C., "The effect of nonzero $\nabla.B = 0$ on the numerical solution of the magnetohydrodynamic equations," J. Comp. Phys., Vol. 35, pg. 426, 1980

[25] Lee, J.-H., "Electron-Impact vibrational excitation rates in the flowfield of Aeroassisted orbital transfer vehicles," Progress in Aeronautics and Astronautics: Thermophysical aspects of re-entry flows, Vol. 103, ed. J. N. Moss and C. D. Scott, pg. 197, AIAA, NY, 1986

[26] Gnoffo, P.A., Gupta, R.N., Shinn, J.L., "Conservation equations and physical models for hypersonic air flows in thermochemical nonequilibrium," NASA report, TP-2867, February 1989

[27] R. Munipalli, S. M. Aithal, V. Shankar, "Effect of wall conduction in proposed MHD enhanced hypersonic vehicles,", 11th AIAA International Space Planes and Hypersonics Conference, Norfolk, VA, December 2003

[28] Yoshizawa, A., "Hydrodynamic and Magnetohydrodynamic turbulent flows: Modeling and Statistical Theory," Kluwer Academic Publishers, 1998

[29] Barth, T.J., "Aspects of unstructured grids and finite volume solvers for the Euler and Navier-Stokes equations," VKI Lecture series, 1994-05

[30] Kerrebrock, J. L., "Nonequilibrium Ionization Due to Electron Heating (2 parts)," *AIAA Journal*, Vol. 2, No. 6, pg. 1072, June 1964

[31] S. O. Macheret, M. N. Shneider, R. B. Miles, "External Supersonic flow and scramjet inlet control by MHD with electron beam ionizer", AIAA paper, 2001-0492, 39th AIAA Aerospace Sciences Meeting and Exhibit, 8-11 January 2001, Reno, NV

[32] A. L. Kuranov, E. G. Sheikin, " MHD control on Hypersonic Aircraft under "AJAX" concept. Possibilities of MHD Generator", 40th AIAA Aerospace Sciences Meeting January 2002/ Reno, NV.

[33] Y. P. Golovachov, S. Yu. Sushchikh, D. M. Van Wie, "Numerical Simulation of MGD Flows in Supersonic Inlets", AIAA paper 2000-2666, 31st AIAA Plasmadynamics and Lasers Conference, 19-22 June 2000/Denver, CO.

[34] Kenjeres, S., Hanjalic, K., "On the implementation of effects of Lorentz force in turbulence closure models," Int. J. Heat Fluid flow, Vol. 21, pg. 329, 2000

[35] Tillack, M.S., "MHD flow in rectangular ducts," UCLA report, FNT-41, Department of Mechanical and Aerospace Engineering, UCLA, July 1990

8. Interactions/Transitions

Incompressible MHD: (Free Surface Liquids for Heat Removal) In this DOE funded investigation, HyPerComp is studying the potential for using electromagnetic control for heat extraction from the plasma core of advanced nuclear fusion concepts. Liquid metals (Lithium or Lithium salts) flowing along the walls of toroidal magnetic confinement fusion devices can minimize the harmful effects of continued exposure to neutron bombardment of static walls, and at the same time, will extract heat energy more effectively from the plasma. An added benefit is the formation of Tritium, which is used regeneratively as fuel. A critical element of this design is the need to predict correctly the flow of liquid metals under electromagnetic fields. Three dimensional incompressible flow calculations involving turbulent, radiative and conductive heat transfer at complex free surfaces (involving the liquid metal and an air/plasma exterior), will be the ultimate target of this effort, in the present phase and beyond. The fusion lab at UCLA is the immediate beneficiary of this research, which will add to their ongoing DOE funded APEX (Advanced Power Extraction) program. A code environment, tentatively named HIMAG (HyPerComp Incompressible MHD solver for Arbitrary Geometries), has been developed by HyPerComp under these contracts. HIMAG is already making significant contributions to the study of liquid metal flows of interest in the nuclear fusion community.

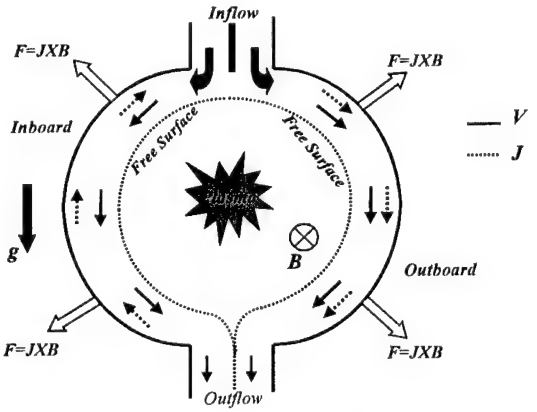

Figure 11 : Schematic of liquid wall cooled magnetically contained fusion device

Appendix-A: Three temperature formulation

Details of the three-temperature model used in our work are described below.

Definitions:
Translational and rotational modes of heavy particles (T)
Vibrational energy of diatomic/polyatomic molecules (T_v)
Translational energy of electrons (T_e)

Total energy equation/unit mass
E_T = sum of translational energies of heavy particles, kinetic energy due to flow, vibrational energy of all diatomics and electron energy

$$E_T = \sum_{s\neq e}^{n} c_s e_s + \frac{1}{2}u^2 + \Sigma c_s e_{s,v} + c_e c_{v,tr}^e T_e$$

(Curve fits for individual species account for the heats of formation)

Internal energy/mass

$$E = \sum_{s\neq e}^{n} c_s e_s + c_e c_{v,tr}^e T_e$$

Vibrational energy/mass

$$E_v = \Sigma c_s e_{s,v}$$

Electron energy/mass

$$E_e = c_e c_{v,tr}^e T$$

The total pressure:

$$P = \sum_{s\neq e}^{n} \frac{\rho_s}{M_s}\overline{R}T + \frac{\rho_e}{M_e}\overline{R}T_e$$

Based on the above definition for pressure, the total differential for pressure can be written as

$$dp = \overline{R}T\sum_{s\neq e}^{n}\frac{d\rho_s}{M_s} + \overline{R}dT\sum_{s\neq e}^{n}\frac{\rho_s}{M_s} + \overline{R}T_e\frac{d\rho_e}{M_e} + \overline{R}\frac{dT_e}{M_e}\rho_e$$

The total differential for pressure can be written in terms of partial differentials as follows:

$$dp = \frac{\partial p}{\partial \rho E}d\rho E + \frac{\partial p}{\partial \rho E_v}d\rho E_v + \frac{\partial p}{\partial \rho E_e}d\rho E_e + \frac{\partial p}{\partial \rho_s}d\rho_s$$

Based on the definition of internal, vibration and electron energies given above the differentials for the three temperatures can be written as

$$\frac{dE - dE_v - c_e dE_e - \sum_s^n (e_S - e_{v,S}) dc_S}{C_{v,tr}} = dT$$

$$\frac{dE_v - \sum_s^n (e_{v,S}) dc_S}{C_{v,v}} = dT_v$$

$$\frac{dE_e}{C^e_{v,tr}} = dT_e$$

The differentials for energies in terms of the primitive variables can then be written as

$$dE = \frac{(d\rho E - Ed\rho - (ud\rho u + vd\rho v + wd\rho w) + (u^2 + v^2 + w^2)d\rho)}{\rho}$$

$$dE_v = \frac{(d\rho E_v - E_v d\rho)}{\rho}$$

$$dE_e = \frac{(d\rho E_e - E_e d\rho)}{\rho}$$

$$dc_s = \frac{(d\rho_s - c_s d\rho)}{\rho} \Rightarrow \rho dc_s + c_s d\rho = d\rho_s$$

Substituting the above expressions for dT, dT_e, dE, dE_v, dE_e in the total differential for pressure, we have the following definitions.

$$\beta = \frac{dp}{d\rho E} = \frac{\overline{R}}{\rho C_{v,tr}} \sum_{s \neq e}^{n} \frac{\rho_r}{M_r}$$

$$\varphi = \frac{dp}{d\rho E_e} = \frac{\overline{R}\rho_e}{\rho C^e_{v,tr} M_e} - \beta c_e$$

$$-\beta = \frac{dp}{d\rho E_v}$$

$$\gamma_s = \frac{dp}{d\rho_s} = \frac{\overline{R} T_q}{M_s} + \beta \frac{\left(u^2 + v^2 + w^2\right)}{2} - \beta e_s + \beta e_{v,s} - \varphi e_e$$

Where, $T_q = T_e$ if $s = e$ and $T_q = T$ if $s \neq e$

Based on these definitions the Jacobian of the inviscid matrix F can be written as:

$$A=\begin{bmatrix} U(\delta_{sr}-c_s) & c_s n_x & c_s n_y & c_s n_z & 0 & 0 & 0 \\ \gamma_r n_x - Uu & un_x(1-\beta)+U & -\beta v n_x + u n_y & -\beta w n_x + u n_z & \beta n_x & \varphi n_x & \varphi n_x \\ \gamma_r n_y - Uv & -\beta u n_y + v n_x & v n_y(1-\beta)+U & -\beta w n_y + v n_z & \beta n_y & \varphi n_y & \varphi n_y \\ \gamma_r n_z - Uw & -\beta u n_z + w n_x & -\beta v n_z + w n_y & w n_z(1-\beta)+U & \beta n_z & \varphi n_z & \varphi n_z \\ \gamma_r U - UH & -\beta u U + H n_x & -\beta v U + H n_y & -\beta w U + H n_z & \beta U + U & \varphi U & \varphi U \\ -UE_v & E_v n_x & E_v n_y & E_v n_z & 0 & U & 0 \\ -UE_e & E_e n_x & E_e n_y & E_e n_y & 0 & 0 & U \end{bmatrix}$$

Source term for vibrational energy in a two-temperature model:

$$\dot{w}_v = \left\{ \sum_{s=mol} \dot{w}_S D_S - \sum_{r=elct.imp} \left(R_{f,r} - R_{b,r} \right) \hat{I}_r \right\} + \left\{ \sum_{s=mol} \rho_S \frac{\left(\overset{*}{E}_{v,s} - E_{v,s} \right)}{\langle \tau_S \rangle} + 3\rho_e R(T - T_v) \sum_{s \neq e} \frac{\nu_{es}}{M_S} \right\}$$

$$+ \left\{ Q_{rad} - p_e \vec{\nabla}.\vec{u} \right\}$$

Source terms for the vibrational and electron energies in the three-temperature model is given below.

$$\dot{w}_e = 3\rho_e R(T - T_e) \sum_{s \neq e} \frac{\nu_{es}}{M_S} - \sum_{s=mol} \rho_S \frac{\left(\overset{**}{E}_{v,s} - E_{v,s} \right)}{\langle \tau_{es} \rangle} - \sum_{r=elct.imp} \left(R_{f,r} - R_{b,r} \right) \hat{I}_r + \left\{ Q_{rad} - p_e \vec{\nabla}.\vec{u} \right\}$$

$$\dot{w}_v = \sum_{s=mol} \dot{w}_s D_s + \sum_{s=mol} \rho_s \frac{\left(E^{*}_{v,s} - E_{v,s}\right)}{\langle \tau_s \rangle} + \sum_{s=mol} \rho_s \frac{\left(E^{**}_{v,s} - E_{v,s}\right)}{\langle \tau_{es} \rangle}$$

The definition of various terms in the above equations is defined below.

$\sum_{s=mol} \dot{w}_s D_s \Rightarrow$ *Average vibrational energy per unit mass created or destroyed*

$\sum_{r=elct.imp} \left(R_{f,r} - R_{b,r}\right)\hat{I}_r \Rightarrow$ *Average energy per unit mass created or destroyed due to change in electron number density*

$\sum_{s=mol} \rho_s \frac{\left(E^{*}_{v,s} - E_{v,s}\right)}{\langle \tau_s \rangle} \Rightarrow$ *Energy exchange between Tand* T_v

$3\rho_e R(T - T_v)\sum_{s\neq e} \frac{\nu_{es}}{M_s} \Rightarrow$ *Energy exchange between heavy particles and electrons*

$Q_{rad} - p_e \vec{\nabla}.\vec{u} \Rightarrow$ *source terms due to external radiation and electron pressure gradient*

$\sum_{s=mol} \rho_s \frac{\left(E^{**}_{v,s} - E_{v,s}\right)}{\langle \tau_{es} \rangle} \Rightarrow$ *energy exchange between electrons and vibrational energy*

Appendix-B

Principal technical papers based on this research

Shock waves in hypersonic inlets with MHD

Ramakanth Munipalli[1], V. Shankar[1], and A. Hadid[2]

[1] HyPerComp, Inc., 31255 Cedar Valley Dr., #327, Westlake Village, CA 91362, USA
[2] Boeing-Rocketdyne Propulsion and Power, Canoga Park, CA 91309, USA

Abstract. We present here our recent studies in the computation of electrically conducting air flow in hypersonic inlets in the presence of electromagnetic fields. In numerical simulations, one has the opportunity to study such flows under various levels of abstraction. Models studied range from linear Lorentz force terms to induced field formulations using reduced as well as a full treatment of Maxwell equations. Real gas phenomena such as chemical and thermal nonequilibrium are considered. Electrical conductivity enhancement via seeding and the use of electron-beams for significant interactions to occur. A comparative study of numerical models and physical issues is presented.

1 Introduction

Interest in MHD applications to aeronautics dates back to the 1950s (e.g., Resler and Sears [9], following its active study in problems related to interstellar gasdynamics, and ground based power generation. The resurgence of interest in the present times is owed largely to the Russian AJAX concept in which a scramjet inlet flow field is bypassed through an auxiliary MHD power generator, reducing the net flow compression required. Benefits arise from lower drag, increased combustion efficiency via plasma injection, generation of additional power, flow control without the need for variable geometry in the inlet as well as the nozzle. Ref. [1] may be consulted for a recent account of these concepts.

Significant advances have been made in the development of numerical schemes for MHD in the recent past. Powell [8] developed a method which provides for the proper advancement of solenoidal magnetic fields in time, thereby enabling the development of effective Riemann solvers in MHD. DeStreck et al. [2], Linde [4], among others, have performed high accuracy computations and attempted to interface current numerical methods with classical characteristics based analysis of MHD. Direct applications to aerospace engineering problems have been taken up by several researchers (e.g., [3], [5]).

A hierarchy of gas models and MHD models have been considered in the present work. The intent is to develop a three dimensional, unstructured (hybrid) mesh code to run on parallel machines for general time accurate MHD problems. An existing code environment developed for use in computational electromagnetics is being modified for MHD. Refs. [6] and [7] may be consulted for further details on past activities. Recent results pertaining to inlet studies are presented here with a brief summary of physical models used.

2 Gas Models

An important distinguishing feature of magneto-aerodynamics as encountered in hypersonics is the low electrical conductivity and the perennial quest to increase its value. The choice of a gas model is closely related to the manner in which this electrical conductivity is enhanced or produced. Among the most popular options to increase the electrical conductivity are : (a) Seeding the flow with an easily ionizable salt, (b) Using electron beams or other forms of radiation to increase the concentration of mobile electrons in the flow.

(a) Perfect gas: The perfect gas assumption, while being physically inaccurate in general MHD flows of engineering interest, is preferred due to its simplicity and speed in numerical simulations. Parameters such as the ratio of specific heats (γ) and the gas constant can be varied, to suit the mean flow properties. Sutherland's law type of temperature dependence of viscosity and thermal conductivity is used.

(b) Chemical equilibrium: We have, in the past, (Ref. [6]) used the equilibrium air assumption in order to study high temperature air seeded with Potassium Carbonate particles. Seeding provides an effective mechanism to enhance flow conductivity at temperatures in the vicinity of 3000 K. Simple corrections for multiphase effects of heat transfer, phase change and particle settling due to gravity have been made in our equilibrium air simulations. A set of routines developed at NASA-Glen Research Center are being used to model the equilibrium composition and properties of high temperature air with and without seeding, when finite rate effects are not significant.

(c) Thermochemical nonequilibrium: Seed particles result in a weight penalty, contaminate the flow, and are rarely recoverable for cyclical usage. Currently, there is interest in ionizing air by means of electron-beams and other forms of radiation. Such methods of ionization tend to be dominated by nonequilibrium processes. Electron collision and recombination times are comparable to the flow time scales.

Hypersonic flows at high altitudes possess their own charge of nonequilibrium features. Energy distribution among the various modes, as well as chemical reactions among gaseous species take place at a finite rate. In our work, we have used the two-temperature model developed by Chul Park. In this mode, the translational and rotational temepratures are characterized by one temperature scale (say T,) and the vibrational and electronic modes are characterized by T_v. This model degenerates in accuracy near electrodes, where the electron temperature differs significantly from vibrational and translational temperatures.

Electrical conductivity from e-beams is frequently expressed as:

$$\sigma = \left[\frac{e^2}{mnk_c}\right]\sqrt{\frac{1}{w_i k_{dr}}\left(\frac{j_b \rho Y E_b}{e}\right)}$$

where e is the electronic charge, m is the electron mass, n is the neutral species number density, k_c is an electron scattering rate constant, k_{dr} (=1.5 e-7 cm^3/s) is a dissociative recombination rate constant, w_i is the ionization constant (=34

eV), j_b (about 0.1 A/cm^2) is the current density in the electron beam, E_b is the energy of the electrons, ρ is the flwo density and Y is the electron stopping power. The energy of the e-beams in the range of 10-200 keV is needed to provide high enough electrical conductivity at moderate flow static pressures.

3 MHD Models

When the magnetic Reynolds number ($Re_m = V_\infty L \sigma \mu_0$) in a flow is much greater than 1, sizeable magnetic fields are induced in the flow from the currents that are generated by virtue of its movement in a magnetic field. These fields are not significant in aerodynamics, where the electrical conductivity is often very low.

(a) Inductionless MHD: In the limit of low magnetic Reynolds number, the Navier Stokes and Maxwell equations are decoupled. A shock tube problem has been simulated with MHD included as source terms where a magnetic field is applied in the z-direction and no electric or magnetic field is induced. As remarked earlier, the magnetic field is seen to retard the shock waves and dissipate the discontinuities. A constant value of electrical conductivity (40 $/\Omega/m$) has been assumed. While the codes we have developed include Hall effect, consider for the present Ohm's law neglecting Hall effect and electron pressure gradient: $\boldsymbol{j} = \sigma\,(-\boldsymbol{\nabla}\phi + \boldsymbol{V} \times \boldsymbol{B})$

This current must be divergence free, as per Maxwell's equations. In order to satisfy this, it is customary to rewrite the above equation in terms of an electric potential ($\boldsymbol{E} = -\boldsymbol{\nabla}\phi$) and take the divergence of both sides. The following potential relation may then be obtained for the electric potential. Flows with and without this induced potential have been studied.

$$\boldsymbol{\nabla} \cdot \boldsymbol{j} = 0 \Rightarrow \nabla^2 \phi = \boldsymbol{\nabla}(\log \sigma) \cdot (-\boldsymbol{\nabla}\phi + \boldsymbol{V} \times \boldsymbol{B}) + \boldsymbol{\nabla} \cdot (\boldsymbol{V} \times \boldsymbol{B}) \qquad (1)$$

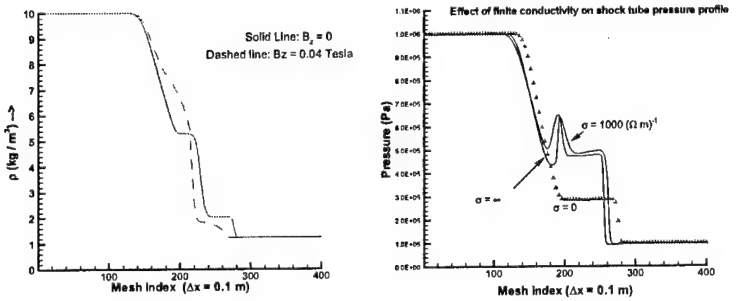

Fig. 1. Density profile in a shock tube flow with MHD as source terms (left) and Pressure profile showing the effect of finite σ

(b) The induced field formulation: In the general case of large electrical conductivity, induced magnetic fields are significant and present a wave structure that cannot be captured by the previous formulation. Fig. 1 shows a shock tube problem with σ set to zero, a finite value (1000 $/\Omega/m$) and ∞. The presence of additional waves due to MHD and their eventual damping due to finite σ is seen here.

4 Numerical Methods

In the case of the inductionless approximation, MHD terms are included as source terms in the Navier-Stokes (NS) equations, and as constant terms in the Jacobian matrix when an implicit scheme is used. The Poisson equation for electric potential is solved by relaxation. Heavy under-relaxation ($\omega = 0.01$) is sometimes necessary for strong shocks. Roe's scheme with MUSCL type evaluation of fluxes is used to obtain second order accuracy in spatial coordinates. Where time accuracy is desired, a second order Runge-Kutta time stepping was used.

To solve the coupled NS-Maxwell equations, the Powell [8] formulation is used, wherein a source term proportional to the divergence of $\boldsymbol{B}$ is introduced on the right hand side. Three different solution procedures were used: (1) Xu's Kinetic Flux Vector Splitting [10], (2) Roe's scheme as presented by Linde [4], and (3) a central difference scheme with artificial dissipation based on the magnetic pressure. Neumann stability of the finitely conducting MHD equations depends upon two parameters ν and r:

$$\nu = (u + c_f)\frac{\Delta t}{\Delta x}, r = \left(\frac{1}{\mu_0 \sigma}\right)\frac{\Delta t}{\Delta x^2}$$

where $u + c_f$ is the fastest wave speed at a cell interface. For stability of an explicit scheme:

$$\nu^2 \leq 2r, r \leq \frac{1}{2}$$

5 Results and Discussion

(a) Mach 10 inlet at off-design conditions: A two-ramp inlet designed for operation at Mach 10 is shown in Fig. 2 at $M = 10$ and 6. At a Mach number of 6, not only are the shock strengths too large for the compression obtained, but also the intake mass capture is greatly reduced. An equilibrium seeded flow study and a simulation using e-beams to enhance electrical conductivity of the flow are shown in Fig. 3. When a magnetic field of 5 Tesla is applied in the x-direction, the mass capture is enhanced by about 9%, and the total pressure loss is reduced by about 5%.

(b) Coupled NS-Maxwell simulations: Ideal MHD simulations of flow past a 5^o ramp at Mach 6 are shown in Fig. 4. A magnetic field (of different strengths) is applied in the y-direction. An insulating solid wall condition is imposed on the ramp wall, and a ratio of relative magnetic permeabilities between the flow

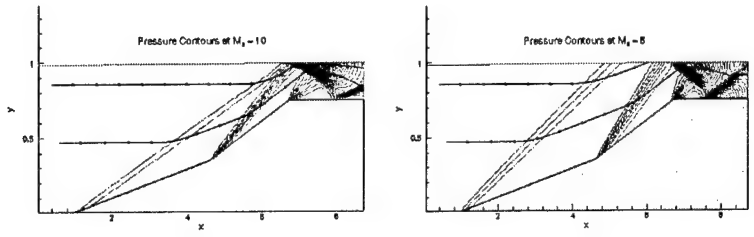

Fig. 2. 2D inlet at design condition M=10 (left) and off-design at M=6 (right)

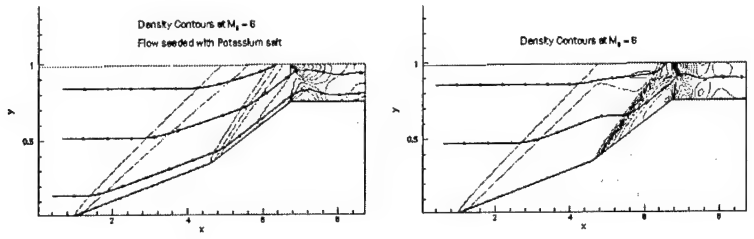

Fig. 3. Seeded flow with applied B_x (left) and Flow ionized by e-beams (right)

and the solid wall was taken as 14. The continuity of magnetic induction vector $\boldsymbol{H} = \mu_0 \boldsymbol{B}$ was imposed. The formation of fast and slow magnetosonic shock waves is seen in this illustration. The two-dimensional nature of this simulation does not permit the formation of an Alfven wave. At low values of σ, these discontinuities merge into seemingly a continuous (nearly linear) transition of pressure from free stream to the wall condition after the leading shock wave.

(c) Nonequilibrium simulations: A model of air involving 11 species: N, O, $N_2, O_2, NO, N^+, O^+, N_2^+, O_2^+, NO^+$ and e^- and two temperatures as described earlier is used in our CFD studies. 21 chemical reactions between these species including the ionization of NO (which is the significant source of electrons in hypersonic flows considered,) are studied. Refs. [6] and [7] present more details about the nonequilibrium studies. Here, we present a double ramp inlet designed for Mach 8, operating at low supersonic (M = 2.68) speed. A magnetic field projecting out of the plane of the paper is applied centered at $x = 4m$, spanning 1m. The upper and lower boundaries are assumed to be non-conducting walls. Current direction here will be tangential to the walls. Electrical conductivity was enhanced by introducing a source term in the electron continuity equation that is active in the region where the magnetic field is non-zero.

Fig. 5 shows the variation of temperature along the wall for cases with and without MHD. The vibrational temperature absorbs the Joule heating first, and rapidly equilibriates with the translational temperature. In this situation,

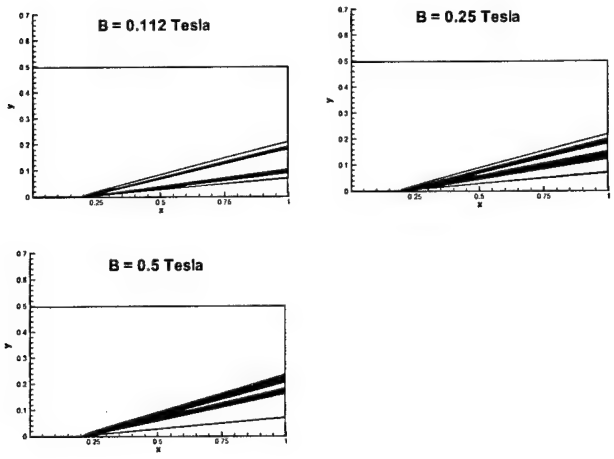

Fig. 4. Effect of magnetic field on magnetosonic shocks

nonequilibrium processes are not critical. Electric field is computed from the potential equation as discussed earlier. An interesting feature in this flow, is that if the electric field is not computed, the magnetic field makes the flow unstable, as in an inlet unstart. A strong shock is formed, down stream of which the flow is subsonic, and propagates upstream and "unstarts" the inlet. This is seen in figs. 6. The solution obtained with the electric field is stable and converges smoothly. When this field is neglected, it appears that no steady state solution is possible.

It is a tedious task to validate MHD flow features, due to their highly non-intuitive nature. A systematic study is underway to unite various research teams to set up test problems and analyze the effects of physics and numerics in numerical MHD. A study of this nature in ideal MHD seems to be already under progress, as described in Ref.[2]. Hypersonic MHD is dominated by additional physical issues whose synergy seems to be yet understood and exploited for engineering use.

Acknowledgement This work is being supported by the Air Force Office of Scientific Research, under the supervision of Maj. William Hilbun, and was initiated by Dr. Len Sakell.

References

1. Brichkin, D.I., Kuranov, A.L., Sheikin, E.G.: 'Scramjet with MHD control under "AJAX" concept. Physical Limitations,' AIAA paper 2001-0381 (2001)
2. De Streck, H., Csik, A., Abeele, D.V., Poedts, S., Deconinck, H.: J. Comp. Phys., **166**, 28, (2001)

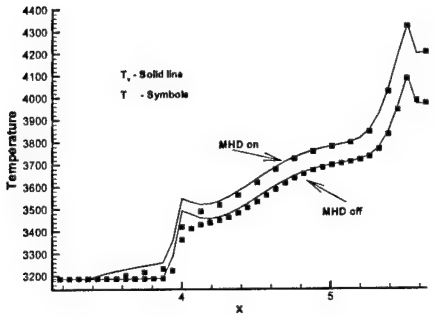

Fig. 5. T and T_v profiles for flow with and without MHD along lower wall

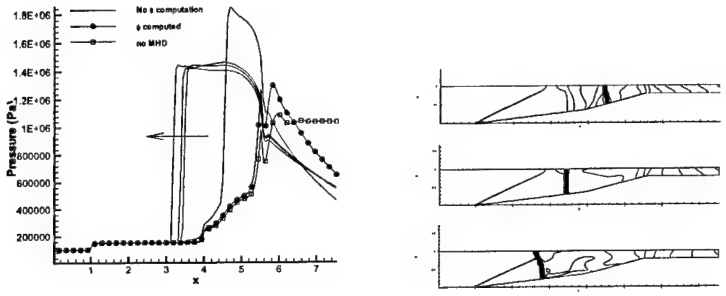

Fig. 6. Pressure profiles in Mach 8 inlet (left) Unstable shock generated from neglecting induced electric field (right)

3. Gaitonde, D.V.: 'Development of a solver for 3-D non-ideal magnetogasdynamics,' AIAA paper 99-3610 (1999)
4. Linde, T.J.: 'A Three-Dimensional Adaptive Multifluid MHD Model of the Heliosphere,' Ph.D. Dissertation, *Univ. of Michigan* (1998)
5. Macheret, S.O., Shneider, M.N., Miles, R.B.: 'Energy-efficient generation of nonequilibrium plasmas and their applications to hypersonic MHD systems,' AIAA paper 2001-2880 (2001)
6. Munipalli R., Anderson D.A., Wilson D.R.: 'CFD Evaluation of Seeded and Unseeded Air MHD Accelerators,' AIAA paper 2000-0215 (2000)
7. Munipalli R., Shankar V.: 'Development of Computational Capabilities in Real Gas MHD,' AIAA paper 2001-0198 (2001)
8. Powell, K.G.: *ICASE report 94-24,* Langley, VA (1994)
9. Resler, E.L., Sears, W.R.: J. of Aero. Sc., **25**, 235, (1958)
10. Xu, K.: *ICASE Report 98-53,* Langley, VA (1998)

AIAA 2001-0198

Development of Computational Capabilities in Real Gas MHD Simulations

Ramakanth Munipalli*, Vijaya Shankar†
HyPerComp, Inc., 31255, Cedar Valley Dr., Suite #327,
Westlake Village, CA 91361

Abstract

In this paper we describe the development of simulation capabilities to perform computations of magneto-hydrodynamic (MHD) flow in large complex domains. Numerical simulation tools available in the present time are heavily inadequate to realistically simulate the motion of conducting gases in the presence of electromagnetic fields. Realism, here refers to the inclusion of finite conductivity, thermal nonequilibrium, charge seperation, chemical reactions, dissipative effects and the ability to simulate large induced magnetic fields. Much understanding has been gained in the numerical study of ideal fluid MHD in recent times. Likewise, real gas computations involving thermochemical nonequilibrium and gas-kinetic modeling of transport properties are also plentiful in recent literature. This work attempts to combine these disciplines to develop a comprehensive numerical treatment of MHD. This paper is organized into two parts. The first deals with an assessment of physical models and available data in MHD modeling. The second presents CFD techniques used to model the integrated Navier-Stokes – Maxwell equation set in multiple dimensions.

Physical Phenomena in Real Gas MHD

Generation and sustenance of σ

The operation of any device based on MHD depends critically upon the level of electrical conductivity that may be attained. Electrical conductivity may be enhanced principally by the following mechanisms:

1. Increase in gas temperature: The bulk of the electric current in a conductor is carried by the electrons due to their low mass. Raising the temperature of a gas causes an increase in the degree of ionization, thereby increasing the electron number density. This form of ionization is frequently referred to as equilibrium ionization. The electron concentration results predominantly from the ionization of Nitric Oxide (NO) molecules, forming NO ions, until about 6000 K. The usable values in the vicinity of 100 mho/m are attained at prohibitively high values of gas temperature (over 7,000 K). The need is therefore felt for additional mechanisms to enhance electrical conductivity.
2. Nonequilibrium ionization by preferential elevation of electron energy: Diatomic Nitrogen remains the dominant diatomic species carrying the vibrational energy over much of this temperature range. Energy exchange mechanisms between Nitrogen and the electron species have been the subject of several investigations spanning over half a century. It is fairly certain at the present time that under moderate electromagnetic fields, the electron energy is in close equilibrium with the vibrational energy of air, when compared with other forms of energy storage, e.g., rotational and heavy particle translational modes. In air, energy can be added preferentially to the electron species by means of Joule heating. An electric current with a component parallel to an applied electric field heats the gas at a rate proportional to the magnitude of both of these quantities. This heat is added to the electron species directly and then passed on to the rest of the gas via collisional processes. The reason is that electrons carry most of the conduction current due to their low mass. In a steady state situation, a compressible gas undergoing Joule heating has an elevated electron temperature given by the following relation (Kerrebrock [4]):

$$\frac{T_e - T_g}{T_g} = \frac{\gamma}{3\delta'}(1-K)^2 M^2 \omega^2 \tau^2$$

where T_e and T_g are the electron and gas temperatures respectively. The quantity δ' denotes a mean fractional energy loss, and is about 44 at 6000 K in air. M is the flow Mach number, $\omega\tau$ denotes the hall parameter. $K = E/(uB)$ is the MHD interaction parameter, and γ is the ratio of specific heats of the working medium.
3. Electron beams: Electron beams produce directed ionization in gases. They provide convenient means to generate locally high electrical conductivity at relatively low flow temperatures. The electrical conductivity

* Member Technical Staff, Member AIAA; e-mail: mrk@hypercomp.net
† Fellow, AIAA; Vice-President, HyPerComp, Inc.

generated by an electron beam is usually obtained from the following expression:

$$\sigma \cong \left[\frac{e^2}{mnk_c}\right]\sqrt{\frac{1}{w_i k_{dr}}\left(\frac{j_b \rho Y E_b}{e}\right)}$$

where e is the electron charge, m is the electron mass, n is the neutral species number density, k_c is an electron scattering rate constant, k_{dr} (= 1.5e-7 cm^3/s) is a dissociative recombination rate constant, w_i is the ionization constant (= 34 eV), j_b (about 0.1 A/cm^2) is the current density in the electron beam, E_b is the energy of the electrons, ρ is the flow density and Y is the electron stopping power. The energy of the e-beams can be varied in the range of 10 to 200 keV, to provide high enough electrical conductivity at moderate flow static pressures. The efficiency of electron beams diminishes with increasing pressure due to the inherent nature of the electrons to recombine with greater ease in such situations.

4. Seeding with easily ionizable alkali salt: Traditionally, MHD power generation concepts have involved seeding combustion effluents with some easily ionizable salt, such as Potassium Carbonate, Cesium, Sodium-Potassium solutions, and so forth. There are many practical issues involved in the seeding process, involving multi-phase flow, deposition of seed particles, conglomeration of seed particles near cold walls, and the resulting electrode shorting and so forth. Nevertheless, well-seeded flows exhibit high electrical conductivity at a wide range of pressures and temperatures. The seed material ionizes essentially in an equilibrium manner. The electrons thus produced can still be thermally in nonequilibrium with the rest of the flow. Predicted values of electrical conductivity in the region of 100 – 200 mho/m can be derived at temperatures of 3000 K and flow pressures between 1 and 10 atm.

Vibrational-electronic nonequilibrium in MHD

Numerical illustrations of supersonic flow in thermochemical nonequilibrium are presented here with and without MHD effects. The thermal model used here is the Park two-temperature model (Ref. [11]). In this model, the vibrational-electron-electronic energies are described by one temperature, referred to as Tv. The translational-rotational temperatures are assigned the symbol T. The formal justification for this model may be found in Ref.[11]. This model is useful in MHD studies of air, since it provides a simple framework in which various modes of thermal nonequilibrium can be considered in a complex mixture of gases. The strong coupling between the electron and vibrational modes is valid in many types of MHD flows of importance. It is, however, invalid when detailed studies of the anode sheath is undertaken.

The first case studied, is that of a supersonic flow of air (3000 m/s at T = 3,000 K, p = 1 atm.). The geometry used is a ramp of slope ¼ over a length of 0.8 m. An 11 species model of air, including N, O, NO, N2, O2, N+, O+, NO+, N2+, O2+ and e- is used to model the dissociation phenomena. Specific heats are deduced from curve fits. Vibrational relaxation is assumed to obey the Landau-Teller theory. Cases in which the inflow temperatures T and Tv are both 3,000 K are compared with the situations when Tv is forced to be much higher at the inflow. This mimics a situation in which energy is deposited in the electronic mode by means of some suitable mechanism at the inflow of a supersonic inlet. Fig. [2] shows a plot of the thermal relaxation process across a leading shock wave. It is seen that rapid energy transfer takes place, bringing the two temperatures together in relatively short distance. At higher levels of Tv, the relaxation process is faster due to the increased frequency of collisions. The post-shock increase in the vibrational energy lags the translational energy. This is due to the fact that the vibrational mode experiences the shock discontinuity only through relaxation with the translational mode.

Fig. [3] shows an interesting aspect of these flows. In the nonequilibrium situation, the electron concentration has been artificially set to 3 orders of magnitude higher than the equilibrium value in this case. Clearly, the electron species does not respond very much to the presence of a shock wave. This is evident from the relatively small variation of the electron density across the shock wave, while the Nitric Oxide and other species exhibit much higher relative variations. This indicates that the electron species responds rather sluggishly to shock and contact discontinuities. In flows involving MHD based inlet design, this manifests as a loss mechanism, since the electron temperature will rise slowly across a shock wave, thereby making the conduction mechanisms also slower.

The second case studied is that of a channel with electric and magnetic fields applied to high temperature supersonic flow of air. Air flows into a constant width channel at 3000 m/s, 6000 K, 1 atm., and an electric field of strength 400 V/inch is applied along the y-axis using infinitely segmented electrodes. A Hall field of strength about 1200 V/m is

generated in the x-direction as a consequence. Constant magnetic field of strength 2.7 T is applied in the z-direction. Fig. [4] shows the variation of the temperatures T and Tv with and without the MHD fields. First, the lower two curves show the equilibrium behavior of T and Tv in the absence of MHD. There is a slight dip in their value at the inlet due to chemical relaxation of gas composition to the correct equilibrium value. When the MHD is turned on, both temperatures rise almost linearly across the length of the channel. They also maintain a uniform distance between them, which can be obtained from the closed form equation almost exactly. This serves as a validation of the CFD simulations. Fig. [4] shows the electron and NO+ mole fractions. It is seen that with or without MHD, there is not a significant chemical nonequilibrium generated at this pressure level. The electron species retains charge neutrality in the gas.

Numerical formulations and perspectives

Maxwell – Navier-Stokes coupled equation set

The conservation equations governing the present applications may be written in the following form:

$$\frac{\partial U}{\partial t}+\vec{\nabla}\cdot(Fx,Fy,Fz)+\vec{\nabla}\cdot(Hx,Hy,Hz)=S$$

in which the fluxes F are inviscid or convective, while H are viscous or dissipative. The source term S comprises of the production of, and interaction between the various flow quantities. This equation may be expressed in the integral conservation form in a control volume Ω bounded by $\partial\Omega$, as follows:

$$\int_{\Omega}\frac{\partial U}{\partial t}\quad d\quad \Omega+\oint_{\partial\Omega}[F_n\quad ds+H_n\quad ds]=\int_{\Omega}S\quad d\Omega$$

The fluxes F_n and H_n now corresponding to normal face fluxes. The various components in this equation are described below. An index s is used for the various gaseous species that are considered. The gas model is thought to comprise of the components: N, O, K, N_2, O_2, NO, N^+, O^+, NO^+, N_2^+, O_2^+, K^+, e^-. In this work we wish to consider a two temperature model of the flow. The reason is that energy addition by MHD at high temperatures can bring about a departure from equilibrium between the various energy modes. In cases where the gas is weakly ionized and is in equilibrium, small perturbations from the equilibrium state may be modeled based upon the Saha equation for electron number density. In the following equations, we will use the two temperature model of Park[11]. There are two energy equations, one for the total energy conservation and the other describing the vibrational-electronic energy. The following matrices describe the conservation laws:

$$U=\begin{bmatrix}\rho_s\\ \rho\vec{V}^T\\ \rho E\\ \rho e_v\\ \vec{B}^T\end{bmatrix},\quad \text{with } \rho_s=\begin{bmatrix}\rho_N\\ .\\ .\\ .\\ \rho_{e^-}\end{bmatrix},$$

$$\vec{V}=[u,v,w],\ \vec{B}=[B_x,B_y,B_z]$$

$$F_n=\begin{bmatrix}\rho_s U_n\\ \rho U_n\vec{V}^T+p\vec{n}\\ \rho U_n H\\ \rho U_n e_v\\ U_n\vec{B}^T-\vec{V}^T B_n\end{bmatrix},$$

$$H_n=\begin{bmatrix}-\rho D_s\vec{\nabla}y_s\cdot\vec{n}\\ -\vec{\tau}_n\\ -\vec{V}\cdot\vec{\tau}_n-\eta\vec{\nabla}T\cdot\vec{n}-\eta_v\vec{\nabla}T_v\cdot\vec{n}-\rho\sum_s h_s D_s\vec{\nabla}y_s\cdot\vec{n}\\ -\eta\vec{\nabla}T_v\cdot n-\rho\sum_s h_{v,s} D_s\vec{\nabla}y_s\cdot\vec{n}\\ -\frac{1}{\mu_0\sigma}\vec{\nabla}\vec{B}\cdot\vec{n}\end{bmatrix}$$

$$S=\begin{bmatrix}\dot{\omega}_s\\ -(\vec{\nabla}\cdot\vec{B})\frac{\vec{B}}{\mu_0}\\ -(\vec{\nabla}\cdot\vec{B})\frac{\vec{V}\cdot\vec{B}}{\mu_0}+\vec{J}\cdot\vec{E}+\dot{Q}_{rad}\\ \vec{J}_e\cdot\vec{E}'+\dot{\omega}_v+\dot{Q}_{e,rad}\\ -(\vec{\nabla}\cdot\vec{B})\quad\vec{V}\end{bmatrix}$$

The transfer of energy across the various energy levels is contained in the nonequilibrium energy production rate $\dot{\omega}_v$. This term contains the energy transfer to the electronic and vibrational modes via collisions, electron pressure gradient, Landau-Teller type of relaxation of these modes with the translational and rotational modes, and release in vibrational and electronic energy caused by ionization or the change in the number densities of polyatomic molecules. The expressions used to

model these features may be found in various references (e.g.: Munipalli [9,10]). Radiative energy addition by means of microwave and other beams can possibly be used to cause an increase in the electron energy and ionization. This is modeled by the terms Q_{rad}. Energy is distributed among various modes through transport processes. Several additional relations are required to complete the description of nonequilibrium MHD gas flow. The calculation of physical properties is described in the next sub-section. Fluxes F_n and H_n are written at the cell face in each control volume. The normal components of the velocity and the Magnetic field at the cell face are:

$$U_n = \vec{V} \cdot \vec{n},\ B_n = \vec{B} \cdot \vec{n}$$

The shear stress vector $\vec{\tau}_n$ is related to the flow velocity gradients and the coefficients of viscosity. Using Stokes' assumption and the tensor notation, we may write the shear stress as a flux vector of the following form:

$$\vec{\tau}_n = \left\{ \mu \left[\frac{\partial u_i}{\partial x_j} + \frac{\partial u_j}{\partial x_i} \right] - \frac{2}{3} \delta_{ij} \frac{\partial u_k}{\partial x_k} \right\} \cdot \vec{n}$$

The two temperature model used above may be formally justified in several ways. It is known that the electro-magnetic fields add energy directly to the "electron pool" of the flow. Therefore, it is essential to model the electron energy as a distinct thermal scale, since it transmits energy to other energy scales at a finite rate. The other modes of energy storage, such as Vibrational, Rotational and Translational energies, may be resolved using the arguments presented by Park [11]. Equilibriation between rotational and translational modes are most rapid at all temperature ranges. It is also true that these modes are fully excited at moderate temperatures. The bulk of the vibrational energy is stored in the diatomic nitrogen, since it is the species with the largest mass fraction over an extended temperature range. Equilibriation between the vibrational energy of Nitrogen gas and the electron translational energy has been studied by Lee[5]. In the temperature range of 5,000 to 10,000 K these two energy levels have rather moderate relaxation times and in other words, equilibriate most rapidly. This in essence justifies the use of a two temperature model as described, comprising of T and Tv, as an alternative to a more elaborate multi-temperature model. This reduces stiffness, computational time, required modeling data and still retains a fair level of accuracy in the physical modeling. The exact trade-offs in this assumption will need to be examined after a realistic flow configuration is chosen.

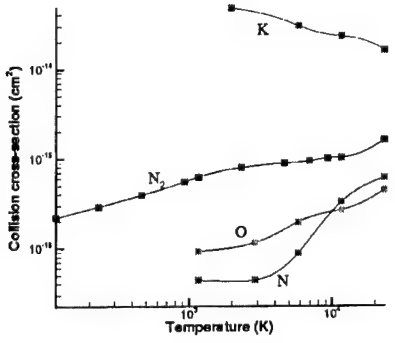

Figure 1: e⁻-collision cross sections

Electric Fields:

In the above formulation, Hall effect has been neglected. The wall conductivity distribution could have significant influence on the flow of Hall currents. This effect will be reintroduced in these governing equations if the need is felt at a later stage. For the present, by rewriting the Ohm's law relation: $j = \sigma (E + V \times B)$, and using Maxwell's equation: $\nabla \times B = \mu_0 j$, we obtain the following expression for the electric field:

$$\vec{E} = \frac{\vec{\nabla} \times \vec{B}}{\mu_0 \sigma} - \vec{V} \times \vec{B}$$

This relation will also be used in applying boundary conditions on the electric field of a conducting wall. In the case of a perfectly conducting wall, j only has a normal component. In an insulator, j has no normal component. If the magnetic field remains steady, the electric field may be expressed in terms of a potential. This would cause large simplifications in the problem, and essentially decouple flow equations from Maxwell equations.

Transport Properties

In the study of high temperature gases, the transport properties such as viscosity, diffusion coefficient, thermal and electrical conductivities are evaluated from the momentum transfer collision cross sections. These cross sections have been tabulated for the collisions between various species in various texts (see for example, [8]). The expressions used to derive some of these quantities are written out below. A sample chart showing the collision cross sections of some important gases with the electron species is shown in Fig.[1].

Using m_s to denote the particle mass in kg of a species s, and $\Delta_{sr}^{(1)}$ and $\Delta_{sr}^{(2)}$ to denote collision integrals between the species s and r and the following definition for the molar concentration:

$$\gamma_s = \frac{\rho_s}{\rho M_s}$$

Coefficient of viscosity is given by:

$$\mu = \sum_{s \neq e^-} \frac{m_s \gamma_s}{\sum_{r \neq e^-} \gamma_r \Delta_{sr}^{(2)}(T) + \gamma_e \Delta_{se}^{(2)}(T_e)} + \frac{m_e \gamma_e}{\sum \gamma_r \Delta_{er}^{(2)}(T_e)}$$

Translational thermal conductivity is given by (using k to denote Boltzmann's constant):

$$\eta_t = \frac{15}{4} k \sum_{s \neq e^-} \frac{\gamma_s}{\sum_{r \neq e^-} a_{sr} \gamma \Delta_{sr}^{(2)}(T) + 3.54 \gamma_e \Delta_{se}^{(2)}(T_e)}$$

Rotational and electronic conductivities are defined in a similar manner, using $\Delta^{(1)}$ in the place of $\Delta^{(2)}$. The vibrational thermal conductivity is assumed to be equal to the rotational conductivity. The species diffusion coefficients are given by:

$$D_s = \frac{\left(\sum \gamma_s\right)^2 M_s (1 - M_s \gamma_s)}{\sum_{r \neq s} \frac{\gamma_r p \Delta_{sr}^{(1)}(T)}{(kT)}}$$

The electrical conductivity of a partially ionized gas is given by the following expression, using n_e, n_i and n_s to denote the number densities of the electrons, ions and unionized species respectively:

$$\sigma = \frac{\frac{n_e \varepsilon^2}{m_e c_e}}{\sum n_s \Delta_{se}^{(2)}(T_e) + 3.9 n_i \left(\frac{e}{8\pi\varepsilon_0 kT}\right)^2 \log\left(\frac{1.24 \times 10^7 T_e^{\frac{3}{2}}}{n_e^{1/2}}\right)}$$

In the above, ε is the electron charge and c_e is the mean thermal velocity of the electrons. The Hall parameter is now be deduced from:

$$\beta = \frac{\omega\tau}{B} = \frac{\sigma}{\varepsilon n_e}$$

Boundary Conditions:

Boundary and initial conditions for this equation set must be specified accurately in order to prevent numerical instabilities and non-physical solution behavior. The flow variables such as velocity, density and pressure can be specified from an equilibrium or perfect gas estimate at the prescribed flight condition. Boundary layer values of species densities, temperature and turbulence energy and intensity must be given as initial conditions. For supersonic and super-alfvenic flows, information propagates only in the downstream direction. The inflow variables are then fixed and outflow variables are copied from within the domain. For subsonic or sub-alfvenic flows, characteristic relations must be used in order to propagate information either into or out of the domain.

The wall (airframe surface) may be set to be a no-slip non-catalytic isothermal boundary. This prescribes a constant wall temperature distribution, zero normal derivatives for species densities and zero velocity at the wall. Electromagnetic boundary conditions may be more involved, depending on the choice of wall material. For a perfect conductor, the normal component of the magnetic field is zero and the jump in the electric field has no tangential component. For a perfect insulator, the gradient of the magnetic field is zero at the surface.

Space/time integration: Numerical Scheme

A first order accurate explicit finite volume scheme to solve the governing equations shown earlier may be written for a cell bearing the index i, volume Ω_i, bounded by $\partial\Omega_i$ with edge lengths Δs as:

$$U_i^{t+\Delta t} = U_i^t - \frac{\Delta t}{\Omega_i} \sum_{\partial\Omega_i} F_n^t + H_n^t \Delta s + \Delta t \, S_n^t$$

The fluxes F and H above must be defined at the cell faces in an appropriate manner in order to be able to capture shock waves accurately. Though the present set of equations has not been solved using such a scheme in any of these references, each reference validates a portion of the complete set of equations presented here. It is anticipated that strong shock waves near blunt body regions, as well as predominantly viscous regions of a flow can cause numerical difficulties with this implementation of Roe's scheme. In order to overcome these difficulties, other flux functions will be built into this

solver. Kinetic flux vector splitting schemes have been successfully tested on ideal fluid MHD problems by Xu[14], Linde [6]. The inclusion of kinetic schemes is computationally simpler. A full description may be found in [6]. However, these schemes are very diffusive and less accurate in comparison with flux difference split strategies, particularly for shear and contact waves. A combination of both, as described in [6] could also yield a viable solution procedure.

Due to inherent limitations, subsonic flow features are heavily damped by upwind schemes. This causes degradation in viscous flow solutions. Wall shear, heat transfer rates and turbulent flow features are affected by this dissipation. Higher order corrections must therefore be made in order to resolve this issue. An alternate numerical procedure to the above, is described by Agarwal and Augustinus [1]. Here, a Runge-Kutta time stepping finite difference scheme with TVD corrections has been used. A second order symmetric TVD model devised by Davis and Yee has been proposed. The advantages of this approach over Roe-type solvers for stiff equations with coupled flow physics is yet unknown. During the course of this study, by controlling the effects of the variables such as Magnetic field intensity, electrical conductivity and so forth, it is possible to compare and converge upon a numerical scheme that will address all of the concerns described above.

Results

Work performed on decoupled Navier-Stokes – Maxwell equations for high temperature seeded and unseeded air has been reported earlier (Munipalli et al. [9,10]). In this paper, we present simple applications of the coupled equation set, the nature of this coupling and some critical issues related to boundary conditions and numerical stability. This paper represents an initial step towards the attainment of a large scale, unstructured grid parallel code capability to simulate MHD problems.

Three schemes are examined here. The first is a Kinetic Flux Vector split scheme as presented by Xu [14] for one-dimensional unsteady cases. The second is the Jameson-Schmidt-Turkel [3] central difference based Runge-Kutta time-stepping scheme, used in two-dimensional problems. Roe's scheme, as presented by Linde [6], is the third scheme used. Finite volume discretizations and dimensional flow quantities are used thoughout.

One-Dimensional Flows

The KFVS scheme has been applied to the 1-D shock tube with finite, zero and infinite electrical conductivity. For the results shown here, a modified Brio and Wu [2] problem has been studied, where the driver and driven conditions are:

Pressure	1.e6	1.e5	(Pa)
Density	10.	1.25	(kg/m^3)
Bx	0.75	0.75	(T)
By	1.	-1.	(T)
γ	2.		
σ	0., 1000., ∞		$(\Omega m)^{-1}$
Δt	4.e-5		(s)
$\Delta t / \Delta x$	4.e-4		(s/m)

400 mesh points were used for the shock tube and the solution was plotted after 200 time steps. The parameter η from Ref. [14] was fixed at 0.5 for all the cases. A CFL number of about 0.8 results from the above selection. Fig.[6] shows a plot of pressure, velocity and Magnetic field for the various situations of interest.

It has been observed that a close correlation exists between the magnitude of the electrical conductivity and the permissible value of Δx. This is due to the presence of a second derivative with respect to x on the right hand side of the governing equations when σ is nonzero. The extra Δx term violates scaling with respect to the conventional CFL number and presents itself as a singular perturbation parameter.

The Neumann stability of this system, therefore follows that of the viscous Burgers' equation, and two parameters must be tracked independently:

$$\nu = \left(u + c_f\right)\frac{\Delta t}{\Delta x}, \quad r = \left(\frac{1}{\mu_0 \sigma}\right)\frac{\Delta t}{\Delta x^2}$$

Where $u+c_f$ is the fastest wave speed at a cell interface. The stability criterion is:

$$\nu^2 \le 2r \qquad r \le \frac{1}{2}$$

Results presented in Fig. [6] show a conductivity of 1000 $(\Omega m)^{-1}$, which was arbitrarily chosen. The scheme however, functions well for this case.

Nature of the NS-Maxwell coupling

Lorentz force and Joule heating terms may be added trivially to most existing Euler or Navier stokes codes in situations where these terms are small and the induced magnetic field is negligible. While this assumption is valid in several cases of engineering importance, a truly coupled solver is important when electrical conductivity increases and the length scales available for MHD interaction are large. In order to

assess the relative importance of coupling vs. decoupling the Navier-Stokes and Maxwell equations, the Brio-Wu test case described above has been simulated with various models.

Firstly, an Euler code based on Roe's scheme (made second order accurate using MUSCL type of upwinding,) was modified to include MHD terms. The simplest manner in which the one dimensionality of the problem may be non-trivially retained is to assume that the velocity is purely uni-directional (x) and the magnetic field is applied in a perpendicular direction (z). In this case, as shown in Fig.[7], the source terms dissipate the velocity profiles and damp out the discontinuities in the pressure profile. When the electrical conductivity is finite, this is indeed the expected effect.

A similar experiment was conducted with the KFVS based code described earlier. Magnetic field, now, is oriented in the x-y plane, and is kept constant through out the channel as Bx = 0.75 T and By = 1 T. Cases were run with and without enabling the update of magnetic field components in the code. As can be seen from Fig. [8], significant departures (upto 100% and more!) may be observed even in cases with a finite conductivity. The case where B was held constant is seen to retain a wave structure similar to perfect gas, while having a distinctly increased distance between the leading shock wave and the contact surface. This aspect will be the subject of a future paper and was discussed briefly in [9],[10].

Two Dimensional Flows

In the 2-D cases, both Roe's approximate Riemann solver, as well as the Jameson-Schmidt-Turkel [3] strategy have been adopted. The latter, primarily due to its simplicity in coding, and available experience with its use in fluid mechanics [3], electromagnetics (Shankar et al. [11]), and recently, in magnetohydrodynamics (Agarwal et al [1]). Second order damping was used in supersonic flow problems, and the MHD pressure:

$$p^* = p + \frac{B^2}{2\mu}$$

has been used to compute the damping coefficient. Normal gradients of this pressure has been set to zero at the wall, and the magnetic field component tangential to the wall has been fixed as zero.

Preliminary results for the case of a supersonic flow past a ramp are presented here. Thin layer Navier Stokes - Maxwell equations have been solved for air (γ = 1.4, R = 277 J/(mol.K)), velocity derivatives along the wall are assumed to not contribute to the shear stress terms. No special treatment for making the magnetic field divergence free has been adopted. Electrical conductivity is assumed to be infinite for the present.

In the Roe solver, however, the source term proposed by Powell [12] has been used to overcome the crisis created by the wave structure. An eight wave system is used in the manner presented by Linde[6]. Central differences have been used to compute Roe averaging. (A more complex density based averaging was also used, but the difference was unnoticeable for the cases studied.) Firstly, the Brio-Wu shock tube problem was simulated using a two-dimensional shock tube with periodic wall conditions. Results, shown in Fig. [9] match closely with 1-D simulations. Magnetic field in the x-direction, which is fixed at 0.75 in the 1-D 7 wave system, is seen to vary about 3% depending on the type of wall boundary conditions used. This fluctuation is sensitive to the Powell-type source terms and can change significantly if they are absent.

Flow past a 5 degree ramp at Mach 6 with applied magnetic field in the y-direction was studied. The presence of fast and slow magneto-acoustic waves are easily seen in these results. Fig. [10] shows the induced field vectors. Near the body surface, the induced field acts in such a way as to annul the tangential magnetic field component. The normal component of the magnetic induction vector H is held continuous across a boundary. Magnetic field B is computed from the relative values of permeability in the two media, which was taken as 14 in the present case. The formation of magnetosonic shocks for various values of applied field is shown in Fig. [11]. The slow shock increases in strength as B increases and is capable of overtaking the fast shock eventually. A comparison with the Jameson-type solver, presented in Fig [12] shows minor oscillations which may be controlled with the appropriate modification of the dissipation terms (which are currently pressure dependent.) Perhaps a eigen vector based limiter would be more appropriate.

Code Development Environment

An existing code environment for Computational Electromagnetics is being modified to incorporate the algorithms proposed here. The code environment is capable of running in a parallel mode using MPI and is being used extensively on PC clusters running LINUX.

Conclusion

The current thinking towards the development of a comprehensive real gas MHD solver on unstructured grids with thermochemical nonequilibrium has been described in this paper. A two temperature nonequilibrium decoupled MHD solver was developed in a prior work, which will be interwoven into a Navier-Stokes – Maxwell coupled solver. Schemes based on approximate Riemann solvers, as well as Jameson-type schemes have been seen to be effective in the solution to the coupled equation set. Some interest also exists in applying the more recently developed Kinetic Flux Vector Splitting scheme to the coupled equation set. Applications to hypersonic inlet mass capture and shear layer stability (Kelvin-Helmholtz type) are being studied currently using these models.

Acknowledgement

This work was supported under the AFOSR contracts F49620-99-C-0015/0070 with Dr. Len Sakell as the program monitor.

References

1. Agarwal, R. K., Augustinus, J., "Numerical simulation of compressible viscous MHD flows for reducing sueprsonic drag of blunt bodies," AIAA 99-0601, Reno, NV, 1999
2. Brio, M., Wu, C. C., "An upwind differencing scheme for the equations of ideal magnetohydrodynamics," Journal of Computational Physics, Vol. 75, pp. 400-422, 1988
3. Jameson, A., Schmidt, W., Turkel, E., "Numerical solutions of the Euler equations by finite volume methods using Runge-Kutta time stepping schemes," AIAA paper 81-1259, Palo Alto, CA, 1981
4. Kerrebrock, J.L., "Nonequilibrium Ionization Due to Electron Heating: I: Theory," AIAA Journal, Vol. 2, No. 6, pg. 1072, June 1964
5. Lee, J.-H., "Electron-Impact vibrational excitation rates in the flowfield of Aeroassisted orbital transfer vehicles," Progress in Aeronautics and Astronautics: Thermophysical aspects of re-entry flows, Vol. 103, ed. J. N. Moss and C. D. Scott, pg. 197, AIAA, NY, 1986
6. Linde, T. J, "A three-dimensional adaptive multifluid MHD model of the heliosphere," Doctoral dissertation, Univ. of Michigan, 1998
7. MacCormack, R. W., "A conservation form method for magneto-fluid dynamics," AIAA 2001-0195, to be presented at the 39th AIAA Aerospace Sciences Meeting, Reno,NV, 2001
8. Mitchner, M., Kruger, C. H., "Partially Ionized Gases," John Wiley & Sons Inc., 1973
9. Munipalli, R., Anderson, D. A., Wilson, D. R., "CFD Evaluation of Seeded and Unseeded Air MHD Accelerators," AIAA 2000-0215, Reno, NV, January 2000
10. Munipalli, R., Anderson D. A., Kim, H.-Y., "Two-temperature computations of ionizing air with MHD effects," AIAA 2000-0450, Reno, NV, January 2000
11. Park, Chul, "Assessment of two-temperature kinetic model for ionizing air," Journal of Thermophysics and Heat Transfer, Vol. 3, No. 3, July 1989
12. Powell, K.G., "An approximate Riemann solver for Magnetohydrodynamics," ICASE Report 94-24, 1994
13. Shankar, V., Hall, W.F., Mohammadian, A.H., "A time domain finite-volume treatment for the Maxwell equations," Electromagnetics, Vol. 10, pg. 127, 1990
14. Xu, Kun, "Gas-Kinetic theory based flux splitting method for ideal magnetohydrodynamics," ICASE report no. 98-53, November 1998

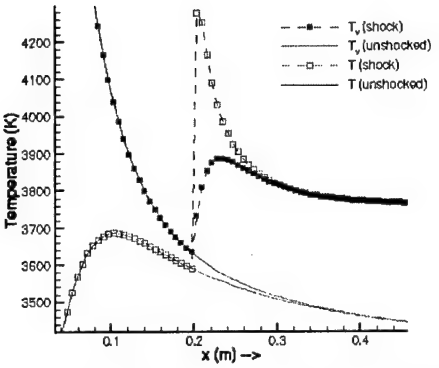

Figure 2 : Thermal relaxation process at T = 3000 K and Tv = 6000 K

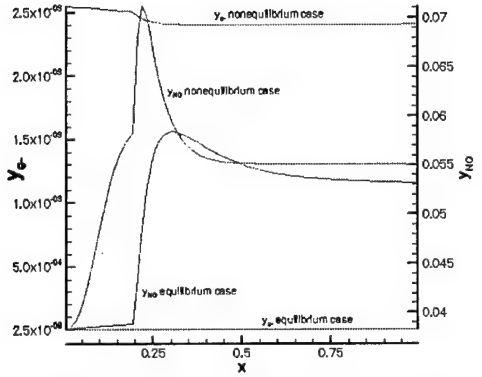

Figure 3: e- and NO distributions for ramp flow with and without thermo-chemical equilibrium

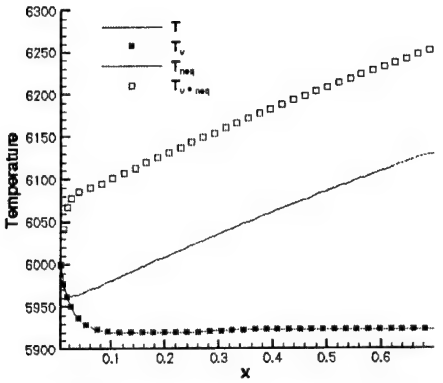

Figure 4 : Nonequilibrium Temperature variation along an unseeded air MHD accelerator with and without the MHD fields

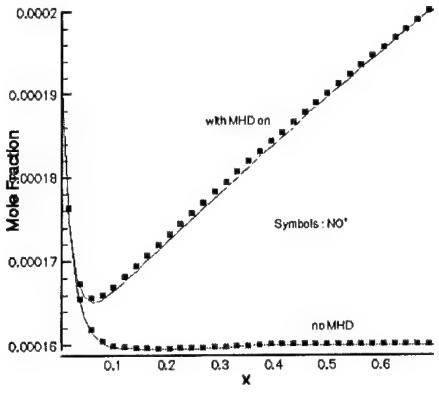

Figure 5: Variation of electron and NO+ mole fractions along a nonequilibrium unseeded air MHD accelerator

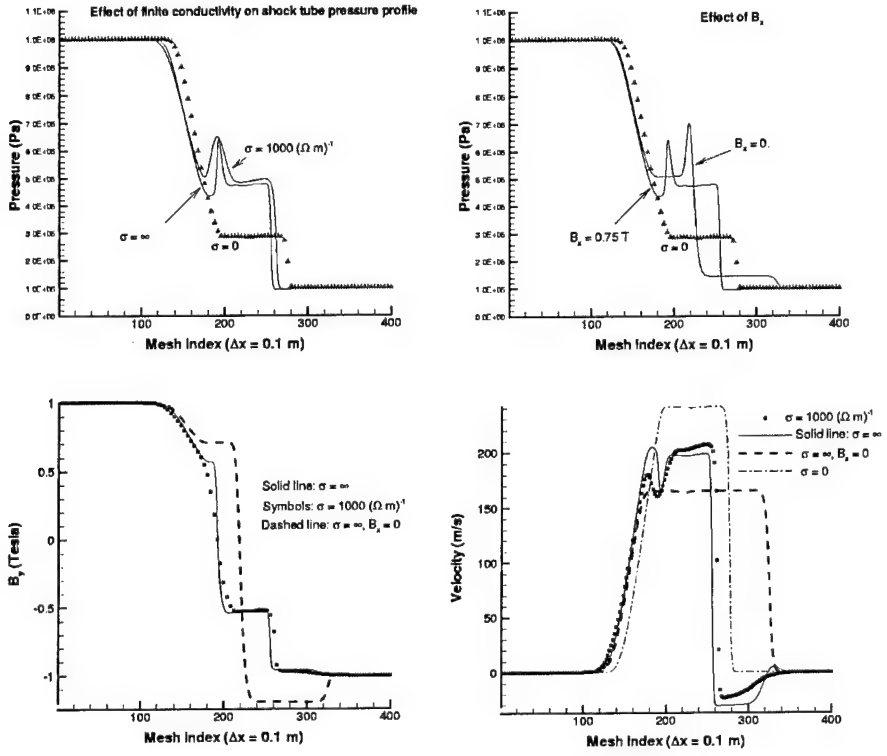

Figure 6: Flow quantities for the modified Brio and Wu problem

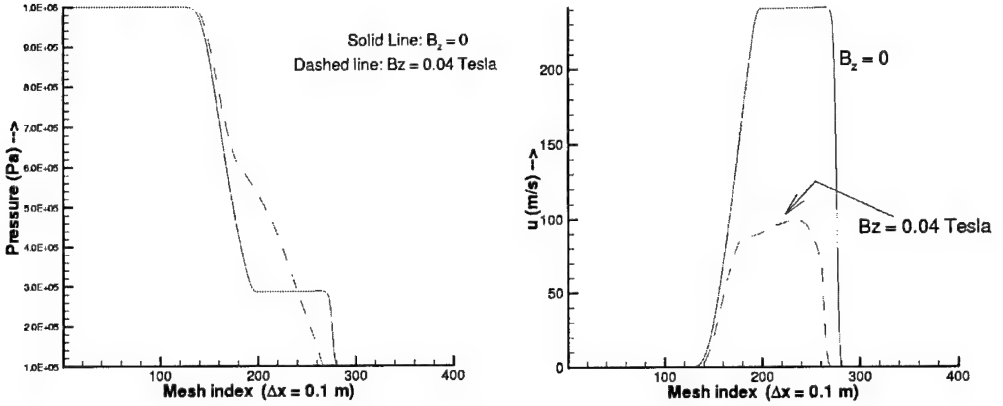

Figure 7: MHD terms included as sources in an Euler equation solver (Brio-Wu shock tube problem)

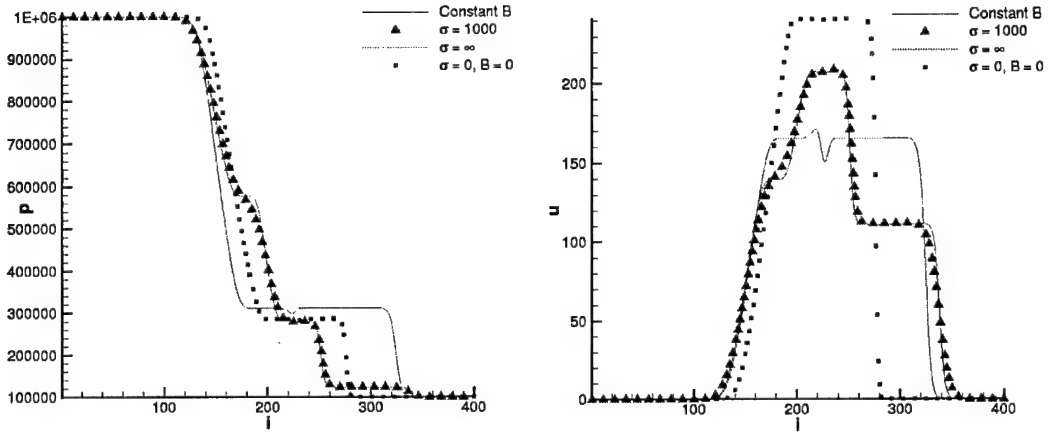

Figure 8: The effect of coupling the NS-Maxwell equations for moderate induced fields (Modified Brio-Wu shock tube problem)

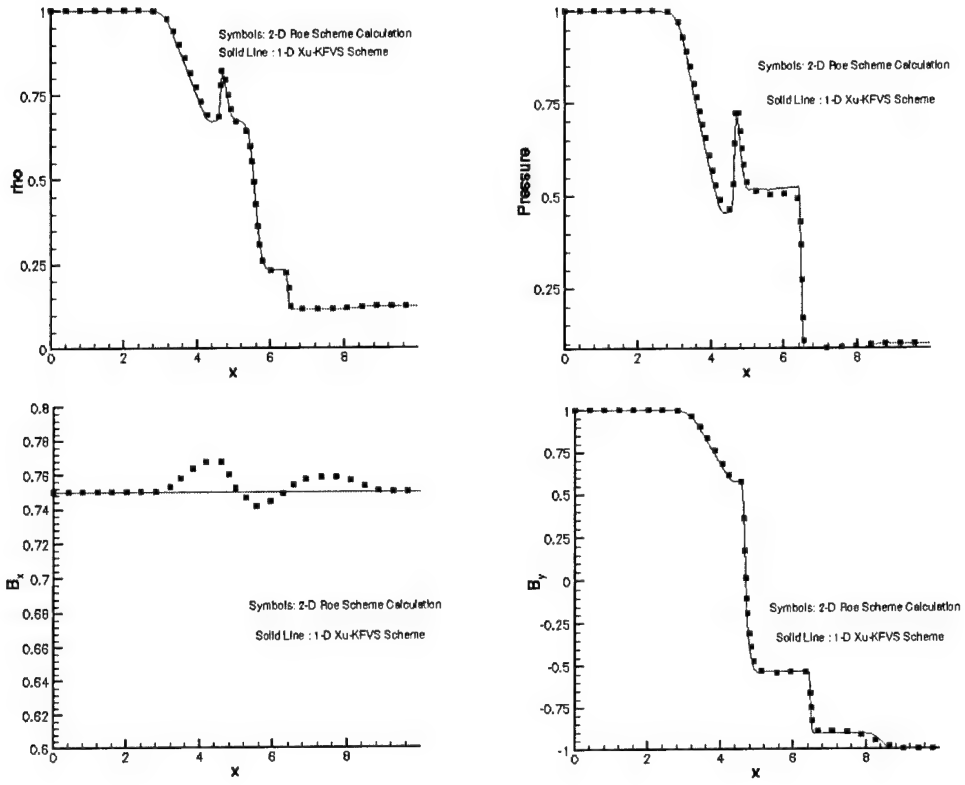

Figure 9 : Comparison of 1-D and 2-D solutions to the Brio-Wu shock tube problem

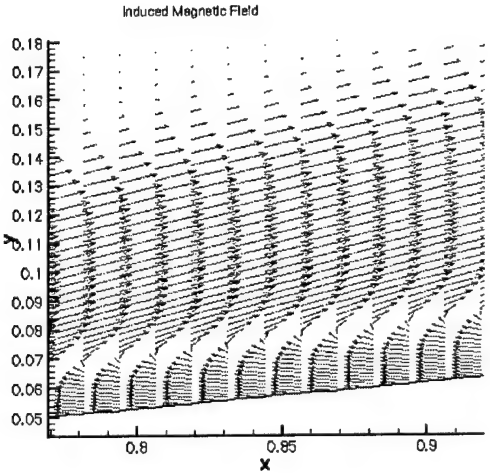

Figure 10 : Induced magnetic field vectors for the ramp flow problem with an imposed vertical field.

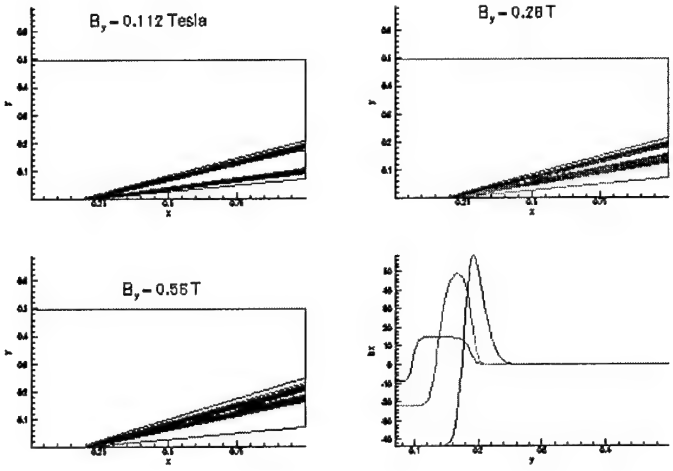

Figure 11 : Formation of fast and slow magnetosonic shocks in 2-D ramp flow problem

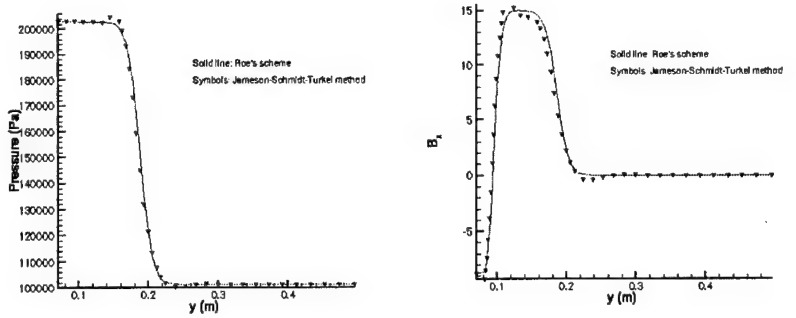

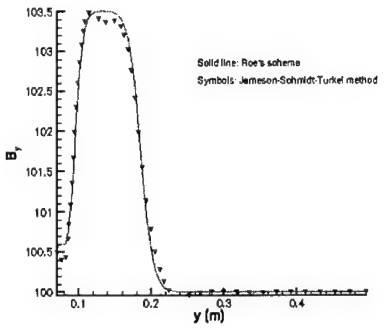

Figure 12: Comparison between Roe's scheme and Jameson-type central difference scheme for an MHD oblique shock wave problem

AIAA 2001-2738

An Unstructured Grid Parallel MHD Solver for Real Gas Simulations

Ramakanth Munipalli*, Vijaya Shankar†, Zhininig Liu*
HyPerComp, Inc., 31255, Cedar Valley Dr., Suite #327,
Westlake Village, CA 91361

Ali Hadid‡
Boeing Rocketdyne Propulsion and Power
Canoga Park, CA 91309

Abstract

In this paper we describe the development strategy for a comprehensive unstructured grid based simulation system for magnetohydrodynamics (MHD) flow over large complex geometries. Earlier work has reported the successful use of modern CFD techniques in simulating MHD based devices ([14],[15]). Here, we focus on hypersonic inlet design augmented with the use of MHD. Boundary layer effects, inlet mass capture, and other flow nonuniformities are discussed. A hierarchical treatment of physics in MHD solvers described here, provides means to both validate numerics and physics in a step-by-step manner, as well as develop confidence estimates for simpler models. Real gas effects include finite conductivity, thermal nonequilibrium, charge separation, chemical reactions, and other diffusive and dissipative effects.

Hierarchical MHD flow physics

Limitations of Source term approach: The most straightforward method in which MHD effects may be introduced into an existing CFD code is by the addition of source terms corresponding to the Lorentz force in the momentum equation, and Joule heating in the energy equation with an initially prescribed distribution of electric and magnetic field. Such an approach is simple to implement in an existing fluid flow code. The applicability of this method is limited by the size of the magnetic field that is induced in the flow by virtue of the currents generated. For large values of induced fields, the magnetic field must be computed simultaneously at each time step. Pressure tends to be underpredicted by such a source term based implementation.

Constant B, no electric field present: For a three dimensional velocity field in which the magnetic field has all the three components, Ohm's law neglecting the Hall effect and electric field, may be written as:

$$\vec{J} = \sigma\left(\vec{V} \times \vec{B}\right) = \sigma\{\left(vB_z - wB_y\right)\mathbf{i} + \left(wB_x - uB_z\right)\mathbf{j} + \left(uB_y - vB_x\right)\mathbf{k}\} \quad [1]$$

where u ,v and w denote velocity components. This relation may be written for simplified 2-D situations where the magnetic field may have components in some preferential directions alone. This is perhaps the simplest manner in which to include the effects of the magnetic field and also the least accurate. For large magnetic Reynolds numbers as well as for cases where electric current and Hall effect are important, this relation cannot be used.

Constant B, with spatially varying electric field: The general Ohm's law including an electric field, is given by $\vec{J} = \sigma\left(\vec{E} + \vec{V} \times \vec{B}\right)$ which, for situations in which the electric field may be deduced from a potential (which always exists when the magnetic field is constant in time,) may be rewritten as:

$$\vec{J} = \sigma\left(-\vec{\nabla}\varphi + \vec{V} \times \vec{B}\right) \quad [2]$$

In order to determine this potential, the divergence of the above equation which is zero, by the law of conservation of charge, is taken, yielding the following equation:

$$\nabla^2\varphi = \nabla \cdot \left(\vec{V} \times \vec{B}\right) \quad [3]$$

Various simplifications may now be applied to this equation. If a space varying magnetic field acting in the z-direction is applied to a two-dimensional velocity field,

$$\nabla^2\varphi = \frac{\partial\left(vB_z\right)}{\partial x} - \frac{\partial\left(uB_z\right)}{\partial y} \quad [4]$$

When the electrical potential is computed, it is readily substituted in eq. [2] to obtain the value of J and thus, the Lorentz force JxB may be deduced. This set of equations must be augmented by the appropriate boundary conditions described in the following section. These equations may be written out trivially for a general three dimensional situation of current interest.

---

* Member Technical Staff, Member AIAA
† Fellow, AIAA; Vice-President, HyPerComp, Inc.,
* Member Technical Staff, Member AIAA
‡ Associate Technical Fellow, Boeing, Member, AIAA

Induced magnetic field in one direction: The situations when the applied magnetic field is oriented along a fixed direction, and the induced field is dominant in one direction have been considered by several authors (e.g., Morley [12], Shishko [18]). Consider the case when the induced field Bx is in the x-direction and the applied field (0,By,Bz) is oriented in the y-z plane. The momentum equation may be rewritten in terms of the induced field, as opposed to the current as used earlier. This and the time advancement of the induced field, are governed by:

$$\frac{\partial \rho u}{\partial t} + \frac{\partial\left(\rho u^2 + P - R_b B_x^2/\mu_m\right)}{\partial x} - R_b\left(B_y\frac{\partial B_x}{\partial y} + B_z\frac{\partial B_x}{\partial z}\right) = \frac{1}{\mathrm{Re}}\nabla^2 u \qquad [5]$$

$$\frac{\partial B_x}{\partial t} - B_y\frac{\partial u}{\partial y} + B_z\frac{\partial u}{\partial z} = \frac{1}{\mathrm{Re}_\sigma \sigma\mu_m}\nabla^2 B_x$$

This equation without the time derivatives and assuming a fully developed channel flow in the x-direction has been applied with insightful results in [12],[18]. Present work provides an opportunity to study time varying induced fields for general cases. The formulation for a general 3-D situation where all the components of the induced field exist, (and the definition of the non-dimensional quantities used above), has been presented in Ref. [14].

Integrated NS-Maxwell equations: A full complement of Navier-Stokes and Maxwell equation set has been solved at HyPerComp for problems of interest in compressible flow (Ref. [14]). The principal difficulty in solving this set of equations is to maintain a divergence free magnetic field (Brackbill and Barnes [1]). Characteristics based techniques exist in compressible flow solvers, designed to avoid this problem. In incompressible flows, one must post-process the magnetic field to remove the effects of non-zero divergence. This typically involves the solution to a Poisson-type equation and may be computationally expensive. However the equation using the electric potential also has this difficulty. The Maxwell equations are written in terms of the magnetic field components.

High temperature effects: Hypersonic MHD is virtually characterized by an abundance of thermochemical nonequilibrium processes. High temperatures encountered in such flows cause significant variations in the gas specific heats, chemical composition, viscosity, thermal and electrical conductivity and the functional dependence of the speed of sound on flow properties. Typical equilibrium and nonequilibrium models have been presented by Munipalli [13], Munipalli et al. [15] for MHD accelerators. Joule heating transfers energy preferentially to the free electron translational modes. By virtue of collisions, this energy is imparted, in order of ease, to the internal electron modes, the vibrational modes (if present), rotational modes and translational modes. While a detailed balancing of energy is needed in high temperature mixture of gases (such as air), we have in the past experimented with the Park two-temperature model with fair comparisons with expected semi-analytical results.

Nonequilibrium treatment near walls: The effects of nonequilibrium in MHD are most pronounced near the electrode region. In the core of the flow, vibrational and electron modes are tightly coupled, and a two temperature model proposed by Park [16], as evidenced form the work of Lee [8] may be adequate. Near an electrode wall, the vibrationally temperature quickly cools to the boundary value, while the electron mode loses temperature much more gradually, well into the sheath region, in the vicinity of a few mean free paths from the wall. This brings up a need for a three temperature model in order to resolve the thermal gradients near an electrode. Three temperature models such as those used by Sleziona et al. [19] are being currently pursued.

Numerical Difficulties

Problem at the research level abound in both physical as well as numerical understanding of MHD processes. Some of these are described here.

Divergence free magnetic fields: Much interest in recent times has led to the evolution of schemes which preserve the divergence free nature of the magnetic field. While a non-zero divergence of magnetic field is a serious error, it is unclear from our current experience, if this problem has as much a bearing in the simulation of hypersonic flows, where the electrical conductivity is rather low as compared to plasmas encountered in nuclear physics or astrophysics.

Accurate modeling of electron temperature: While numerical stiffness dominates the simulation of finite rate chemistry processes and thermal relaxation, the near-electrode region presents a numerical challenge of a different nature. The length scales in which important transport processes occur near an electrode are several orders of magnitude smaller than all other scales present in the flow. In ref. [3] a solution matching procedure has been developed, by which the wall processes may be analytically reconstructed. This has been successfully applied to the case of an arc-heater, and it is believed that a similar approach may be brought to bear in hypersonic MHD.

Hartmann number limitations: Large Hartmann numbers are encountered routinely in the flows of liquid metals in nuclear fusion and many modern metal casting processes. In such situations, flow velocity gradients near the wall become several times enhanced, and frequently lead to numerical instability. This problem remains intractable to a large extent to date. Leboucher [7] presents an approach by which wall functions and a staggered mesh treatment may alleviate this concern in incompressible flows. Fortunately, this does not seem to be a major issue in aerodynamics due to the low values of electrical conductivity.

Treatment of wall boundary conditions

Fluid Quantities: The wall (airframe surface) may be set to be a no-slip non-catalytic isothermal boundary. This prescribes a constant wall temperature distribution, zero normal derivatives for species densities and zero velocity at the wall.

Electrode surface: At high voltages in weakly ionized gases, a sheath layer exists close to electrode surfaces. This is a free-molecular region in which charge separation can exist and accounts for a potential drop, as well as two-dimensional nonuniformities in the current distribution. The length scale of the sheath layer is often several orders of magnitude smaller than the boundary layer thickness, and therefore, one must take recourse to analytical corrections for the electromagnetic effects occurring in the sheath. The sheath comprises of electron-ion recombination processes which cease when no further net mass influx of electrons is possible due to the effective potential drop. This results in (recombination) energy release, which is applied to the energy equation:

$$\dot{q} = I_s \frac{N_s}{4}\left(\frac{8kT}{\pi m_s}\right)^{1/2} \qquad [6]$$

where the index s refers to ionized particles, and I refers to the ionization energy. Electron, Ion and wall temperatures are identical in the sheath. The difference in the mass of electrons and ions entering the sheath layer causes a potential drop given by:

$$\Delta\varphi = \frac{kT}{2e}\log\left[\frac{m_+}{m_e}\right] \qquad [7]$$

These processes take place in a layer whose thickness is of the order of the Debye length, which is somewhat smaller than the mean free path of electrons in the situations being considered. Since this distance is too small to be resolved in a computational mesh, this relation is applied as a boundary condition.

Effect of segmentation of electrodes: In applying current boundary conditions on a wall comprising of segmented electrodes, certain simplifications must be made. If the computational mesh can resolve each electrode sufficiently (which is extremely difficult to accomplish in real problems,) one would set the normal component of current to zero in the insulating region and the tangential gradient of the electric potential to zero on a conducting surface. However, if an infinitely segmented electrode arrangement is assumed, it is possible to deduce the following condition on the wall (Munipalli [29]):

$$\frac{\partial\varphi}{\partial y} = -\beta\frac{\partial\varphi}{\partial x} \qquad [8]$$

where y denotes the direction normal to the wall and x along the wall, φ is the electric potential and β is the Hall parameter. This expression seems adequate for practical applications. As an example the potential distribution in a slightly expanding channel from AEDC experiments in the 1960s has been computed and seen to match almost exactly with test data. Results are shown in Fig.[1]. 117 electrode pairs are installed on parallel walls and a magnetic field is applied in a perpendicular direction. While the potential difference in each electrode pair is fixed by connecting a battery across it, the potential difference along the channel is derived by using this condition in conjunction with a flow solver.

Magnetic Field: At a perfectly conducting wall, normal component of the magnetic induction H is continuous across the wall. Frequently in computations, the tangential component of this field is set to zero, which is an approximation for slender bodies. The magnetic field strength inside the solid body would be obtained by scaling the gas magnetic field strength by the ratio of the magnetic permeability in the two media. The induced magnetic field vectors in a supersonic conducting flow past a ramp is shown in Fig. [3]. Here, a vertical magnetic field is applied, which is nearly cancelled tangential to the wall by a tangential induced field in the opposite direction.

Four principal methods in which MHD boundary conditions are being implemented in our work, are explained below.

(a) *No induced field, insulating walls:* This is the simplest situation among the cases of interest. No BC is needed on the magnetic field, while a Neumann condition is applied to the electric potential.

(b) *Induced field with insulating walls:* Here, the normal component of the induced magnetic field strength vector H is often assumed to be continuous across a solid wall. The boundary condition on the

normal component of the magnetic field is written as (where μ denotes the magnetic permeability):

$$\frac{B_{n,wall}}{B_{n,fluid}} = \frac{\mu_{m,wall}}{\mu_{m,fluid}} \qquad [9]$$

(c) *Thin conducting walls:* This boundary condition may be formulated with respect to either an electric potential, if there is no induced field, or an induced magnetic field, if present. In the first case, when the wall is conducting, if the magnetic field is assumed to be oriented along the z-direction, and the wall in the x-y plane, if the number c denotes the ratio of the electrical conductivity of the wall to that of the fluid medium, the following boundary relation applies:

$$\bar{J} \cdot \mathbf{k} = -\nabla\varphi \cdot \mathbf{k} = -\nabla_{xy} \cdot \left(c\,t\,\nabla_{xy}\varphi\right) \qquad [10]$$

where t denotes the non-dimensional thickness of the wall. The gradient operators above are evaluated in the x-y plane. This equation provides for the continuity for the flow of currents, and provides a wall potential distribution matching the electric field in the flow. A similar condition may be evolved for the case of induced fields, and for the case described earlier (induced field in the x-direction, applied field in the y-z plane,) the following relation may be written on a wall placed in the x-y plane:

$$c\,t\frac{\partial B_x}{\partial z} + B_x = 0 \qquad [11]$$

In reality, all of the above are vector relations, and may be written out for an arbitrarily oriented mesh structure.

The formation of Hartmann layers perpendicular to the applied magnetic field near the wall regions distinguishes MHD flows from traditional fluid boundary layers. Hartmann layers provide a path for current lines from the core flow to close. The thickness of the Hartmann layer, δ, is set equal to the reciprocal of the Hartmann number. For large Ha, the Hartmann layers are so thin that it is difficult to resolve them numerically. Leboucher [47] reported success in an integral treatment of the Hartmann layers and obtained stabilized solutions for Hartmann numbers up to 1000. This involved adding δ to the effective thickness of the conducting boundary:

$$-\nabla\varphi \cdot \mathbf{k} = -\nabla_{\mathbf{xy}} \cdot \left(\left(c\,t + \delta\right)\nabla_{xy}\varphi\right) \qquad [12]$$

This is coupled with an exponential decay of the wall tangential velocity with respect to the core flow. Using the divergence free condition, it is possible to deduce all velocity components thus, if desired. Without this integral treatment, the numerics were found to be unstable for large Hartmann numbers. Good comparisons were obtained with respect to analytical solutions.

(d) *Thick walls:* This would be the most general situation, and requires the solution to the electric potential or the magnetic field inside of the solid wall region. While the outer boundary of the walls may be assumed to be insulating and the conditions in (a), (b) be applied there, the interface between the walls and the fluid require the continuity of normal current. For an electric potential, this may be written simply in terms of normal derivatives, as:

$$\left.\frac{\partial\varphi}{\partial n}\right|_{fluid} = c\left.\frac{\partial\varphi}{\partial n}\right|_{wall} \qquad [13]$$

The electric potential may then be solved inside the wall from these conditions. In the case of induced magnetic fields, the normal component of the curl of the magnetic field vector is held constant across the wall.

Code Architecture and Attributes

The proposed development of a CFD/MHD coupled solver will be based on the code architecture of an existing unstructured grid-based CEM solver called UPRCS. This finite-element CEM algorithm has been implemented for massively parallel and scalar computer architectures. Along with the CEM solver, a complete suite of user interface utilities are provided in the computational environment to go from a CAD model to the final solution. These tools are shown in Figure [8], arranged as they are used in the simulation cycle.

The tools include:

- The Rockwell Science Center developed grid generator UNISG for performing unstructured grid generation.
- A 3-D GUI (graphical user interface) for pre and post-processing called UNSPREP. This tool aids the user in setting up grid-related solver parameters.
- A help sensitive run control parameter input page GUI.
- Domain decompositioning tools for parallel simulations.
- The solver, which has been ported to many parallel and scalar computer architectures.
- A collection of graphically driven post-processing tools for performing results visualization and solver performance analysis.

The software written by HyPerComp, is implemented in a combination of C++, C, and Fortran and includes C++

class libraries for common re-usable functions. It should be noted that all of the software in the solver suite is either freely available or developed in-house.

Numerical Schemes: A variety of numerical schemes have been implemented first on structured meshes and are being ported to the unstructured mesh framework. Schemes tested so far include the Kinetic Flux Vector Splitting method of Xu [20], Roe's scheme, as presented by Linde [9], Runge-Kutta based schemes with artificial dissipation as presented by Jameson et al [5], with success. Cases involving finite rate processes were made implicit with respect to the stiff source terms and used with a Roe scheme. Details are presented in [15].

Validation

Due to the inherently un-intuitive nature of general MHD flows, validation poses a formidable problem in code development activities. Some of the earlier formal numerical work such as that of Brio and Wu [2] performed a rigorous validation based upon Riemann invariants and Rankine-Hugoniot relations, and has since been used for validating other numerical schemes. Munipalli et al. [15] have validated nonequilibrium gas models with MHD using analytical relations and power balance estimates from Kerrebrock [6].

An acute need exists for developing a systematic validation procedure for MHD flows with various levels of physics. A procedure based on the method of characteristics is being developed and will be presented in a future paper. Electrode surface phenomena, electron collisional processes, ionization and recombination rates for general methods of flow ionization all need to be well established before introducing into modern code environments, and this is seen as a task for the CFD community at large for the future. A bulk of technical literature from the 1950s and 1960s containing analytical and experimental results remains to be brought to bear in the current context. A couple of recent papers have shows a firm and positive interest in this direction [4], [17].

Sample Results

Treatment of electric field and current: As described earlier, the electric field may be computed from a Poisson-type equation, assumed to be zero, or backed out from the magnetic field. Fig. [2] shows a viscous channel flow with a spatial distribution of magnetic field normal to the plane of the paper, varying from 0 to 1 and then back to zero. Current lines may be shown to lie in the plane of the paper in this case, and therefore, must form closed loops or extend to infinity, in order for conservation to hold. Contours of electric potential and current lines are shown here, Poisson solutions are obtained at each computational step.

Induced magnetic field vectors are shown in Fig. [3] for a supersonic flow past a ramp, where the wall normal field (on an insulated wall) was assumed continuous, thereby making the induced field purely tangential to the wall.

Contours of current density (computed from the curl of the magnetic field) are plotted in Fig. [4] for a Mach 4 flow past a ramp. The magnetic field is inclined along the x-axis, and current lines extend to infinity in the z-direction. Jumps in the current density occur across shocks and expansion waves. A systematic validation procedure by which these jumps may be verified is being developed.

Inlet flow fields: Flow fields in various inlets designed to operate at Mach numbers between 6 to 10 have been studied. Sample results in Figure [5] show a strong dependence of the induced magnetic field on the flow structure. An induced magnetic field about 10 times larger than the applied field in the x-direction has been observed for a perfectly conducting gas. When finite values of electrical conductivity is used, the induced field is diminished greatly, and a more complete correlation using the Rankine-Hugoniot relations is being currently derived.

Figure [6] shows the increase in the shock angle with increased applied magnetic field in the x-direction. A small discontinuity developing close to the wall is the second magnetosonic shock whose angle increases with applied field. A peak pressure value near the wall corresponding to this second shock is seen to increase with applied field. Figure [7] shows an implementation of MHD as a source term in an Euler solver for the flow past a ramp. Pressure profile along the exit plane shows a linear increase in pressure (corresponding to the pressure gradient term,) balanced by the Lorentz force. The numerical value of this gradient may readily be validated.

An unstructured grid implementation of these concepts has been initiated. Figure [11] shows a 3-D unstructured flow in a Mach 8 inlet with and without an applied field. A weak Mach wave along the side of the inlet was seen to intensify to a shock upon application of a magnetic field. The shock angle at the inlet is also altered, and a greater compression is achieved for the same flow turning angle.

Viscous effects: Hypersonic flows on slender fore-bodies often involve the development of thick boundary layers, which interact with the shock waves to form

extremely complex shock layer dynamics. Sample results from these with and without MHD effects are shown in Figs. [9],[10]. A more detailed study of viscous effects with induced fields is underway.

Acknowledgement

This work is being supported by the Air Force Office of Scientific Research, under the supervision of Maj. William Hilbun, and was initiated by Dr. Len Sakell.

References

1. Brackbill, J.U., Barnes, D.C., "The effect of nonzero $\nabla.B = 0$ on the numerical solution of the magnetohydrodynamic equations," J. Comp. Phys., Vol. 35, pg. 426, 1980
2. Brio, M., Wu, C. C., "An upwind differencing scheme for the equations of ideal magnetohydrodynamics," Journal of Computational Physics, Vol. 75, pp. 400-422, 1988
3. Felderman, E.J., and MacDermott, W.N., "Near-Electrode Model with Nonequilibrium Ionization (at 100 atm,) AIAA 95-1993, June 1995
4. Hoffmann, K.A., Damevin, H.-M., Dietiker, J.-F., "Numerical simulation of hypersonic magnetohydrodynamic flows," AIAA 2000-2259
5. Jameson, A., Schmidt, W., Turkel, E., "Numerical solutions of the Euler equations by finite volume methods using Runge-Kutta time stepping schemes," AIAA paper 81-1259, Palo Alto, CA, 1981
6. Kerrebrock, J.L., "Nonequilibrium Ionization due to electron heating, (2 parts)," AIAA Journal Vol. 2, No. 6, pg. 1072, June 1964
7. Leboucher, L., "Monotone Scheme and boundary conditions for finite volume simulation of magnetohydrodynamic internal flows at high Hartmann number," J. Comp. Phys., Vol. 150, pg. 181, 1999
8. Lee, J.-H., "Electron-Impact vibrational excitation rates in the flowfield of Aeroassisted orbital transfer vehicles," Progress in Aeronautics and Astronautics: Thermophysical aspects of re-entry flows, Vol. 103, ed. J. N. Moss and C. D. Scott, pg. 197, AIAA, NY, 1986
9. Linde, T. J, "A three-dimensional adaptive multifluid MHD model of the heliosphere," Doctoral dissertation, Univ. of Michigan, 1998
10. MacCormack, R. W., "An upwind conservation form method for the ideal magnetohydrodynamics equations," AIAA 99-3609, Norfolk, VA, June 1999
11. Mitchner, M., Kruger, C. H., "Partially Ionized Gases," John Wiley & Sons Inc., 1973
12. Morley, N.B., Abdou, M.A., "Modeling of fully developed, liquid metal thin film flows for fusion divertor applications," Fusion Engineering and Design, Vol. 30, pg. 339-356, 1995
13. Munipalli R., "Numerical investigation of unsteady real gas flowfields with MHD effects," Ph.D. Dissertation, Univ. of Texas at Arlington, 1998
14. Munipalli, R., Anderson, D. A., Wilson, D. R., "Development of Computational Capabilities in Real Gas MHD," presented at the 39th AIAA Aerospace Sciences Meeting, Reno, NV, Jan. 2001
15. Munipalli, R., Anderson D. A., Kim, H.-Y., "Two-temperature computations of ionizing air with MHD effects," AIAA 2000-0450, Reno, NV, Jan. 2000
16. Park, Chul, "Assessment of two-temperature kinetic model for ionizing air," Journal of Thermophysics and Heat Transfer, Vol. 3, No. 3, July 1989
17. Poggie, J., Gaitonde, D.V., "Computational studies of magnetic control in hypersonic flow," AIAA paper 2001-0196, January 2001
18. Shishko, A.Ya., "A theoretical investigation of steady-state film flows in a coplanar magnetic field," Magnetohydrodynamics, Vol. 28, pg. 170, 1992
19. Sleziona, P.C., Auweter-Kurtz, M., Messerschmidt, E.W., "Evaluation of an air-driven plasma wind tunnel source," AIAA paper 96-1854, 1996
20. Xu, Kun, "Gas-Kinetic theory based flux splitting method for ideal magnetohydrodynamics," ICASE report no. 98-53, November 1998

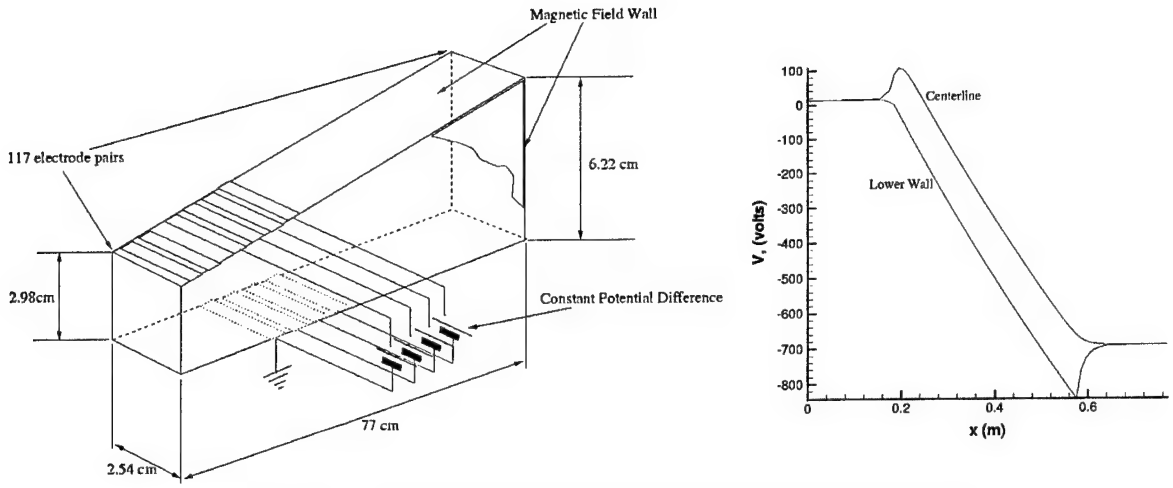

Figure 1 : Electric field in a channel with segmented electrodes

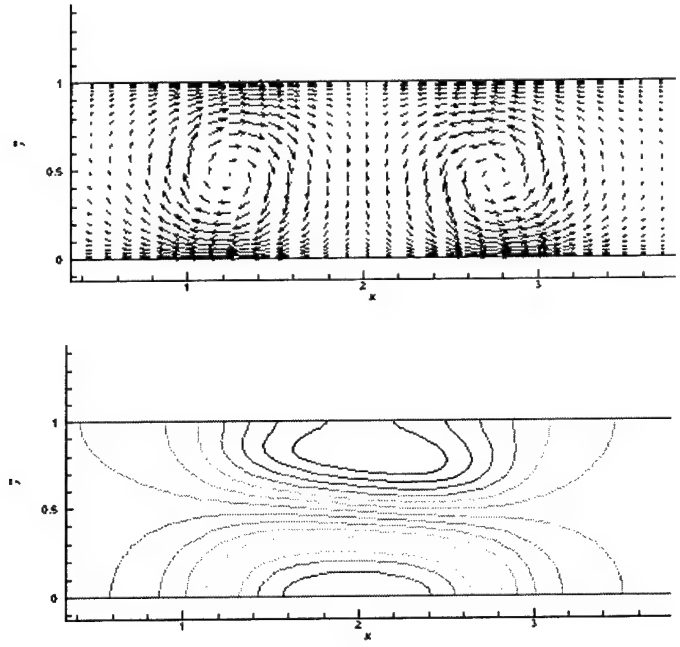

Figure 2 : Electric current vectors (above) and electric potential contours(below) for MHD flow in a channel where an out of plane magnetic field is applied, ramping up between x=1,1.5 and down between 2.5,3.

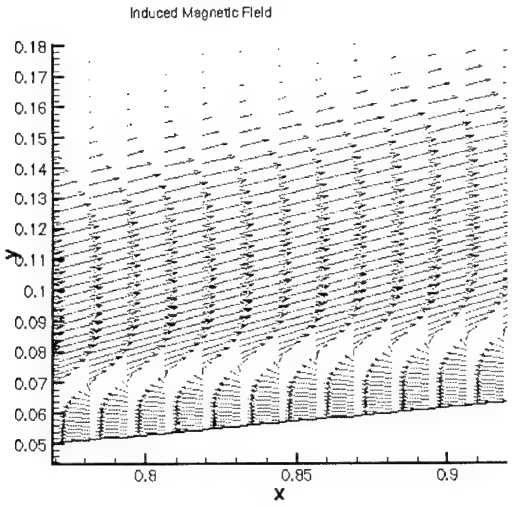

Figure 3 : Induced magnetic field vectors for ramp flow problem with an imposed vertical field.

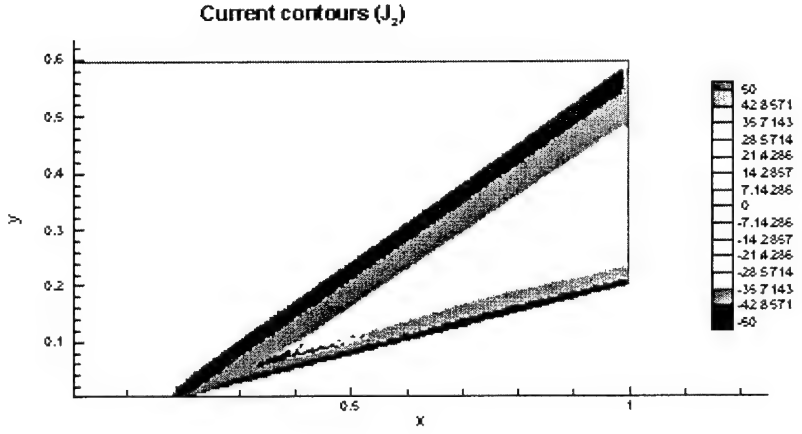

Figure 4: Contours of electric current derived from curl (B) for Mach 4 flow past a ramp. Current travels in the z-direction to ∞.

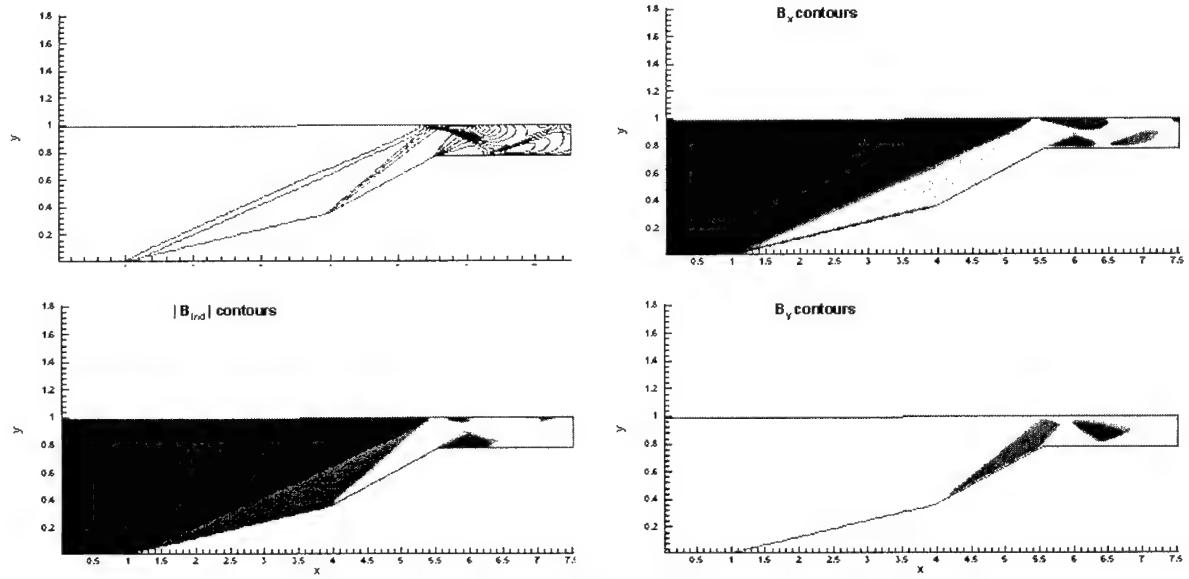

Figure 5: Mach 8 inlet. Clockwise from top-left: (a) Density contours with B = 0; (b),(c) x,y components of the magnetic field; (d) Magnitude of the induced field (-0.3 to 10 * B_x applied)

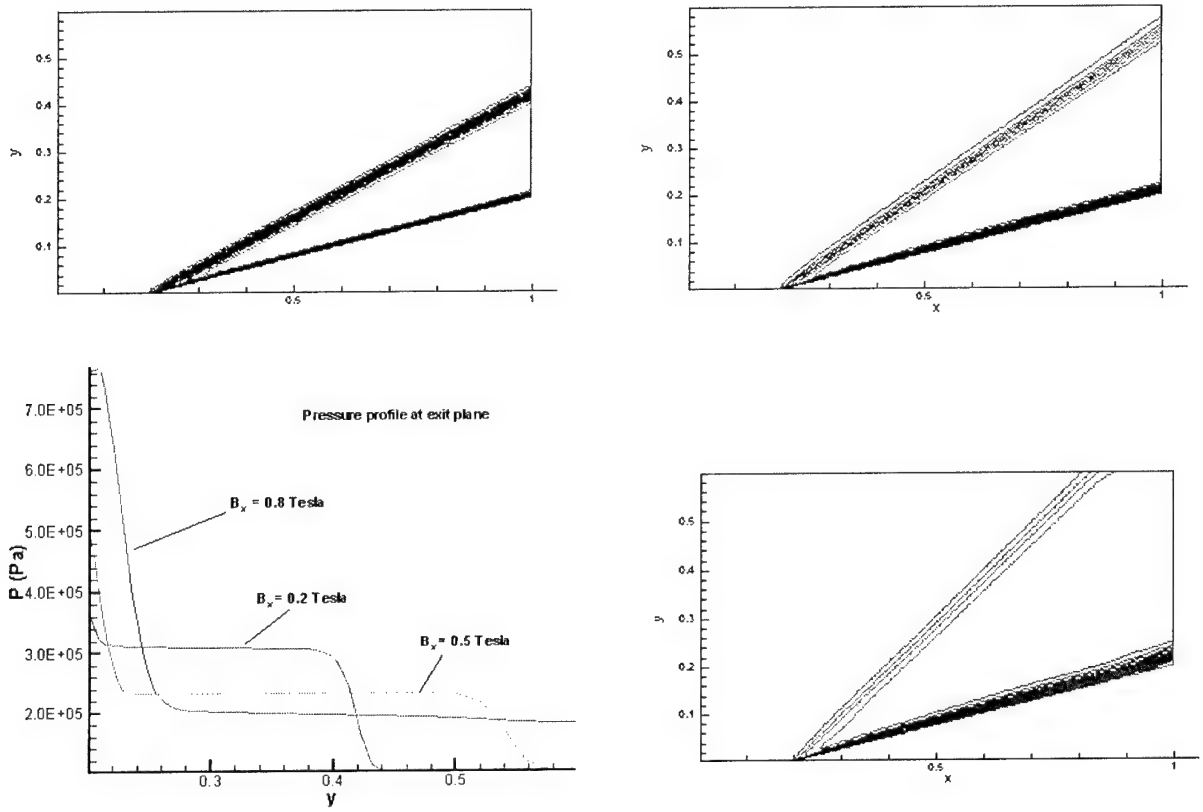

Figure 6: Increasing magnetic field strength (0.02 to 0.08 Tesla) on a Mach 4 flow (ideal MHD) solution.

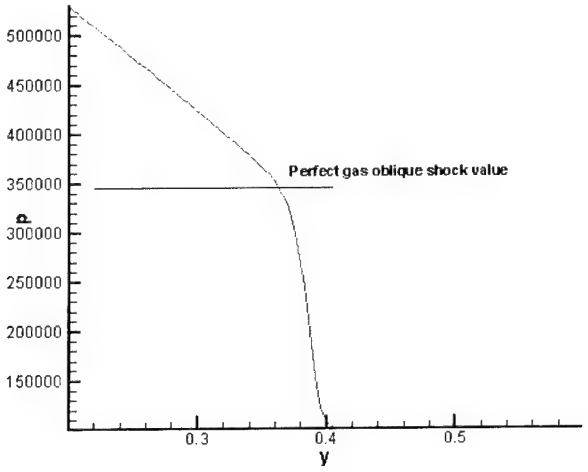

Figure 7: Pressure along the exit plane of a Mach 4 flow past a ramp with MHD added as source terms. Perfect gas post-shock pressure has been marked

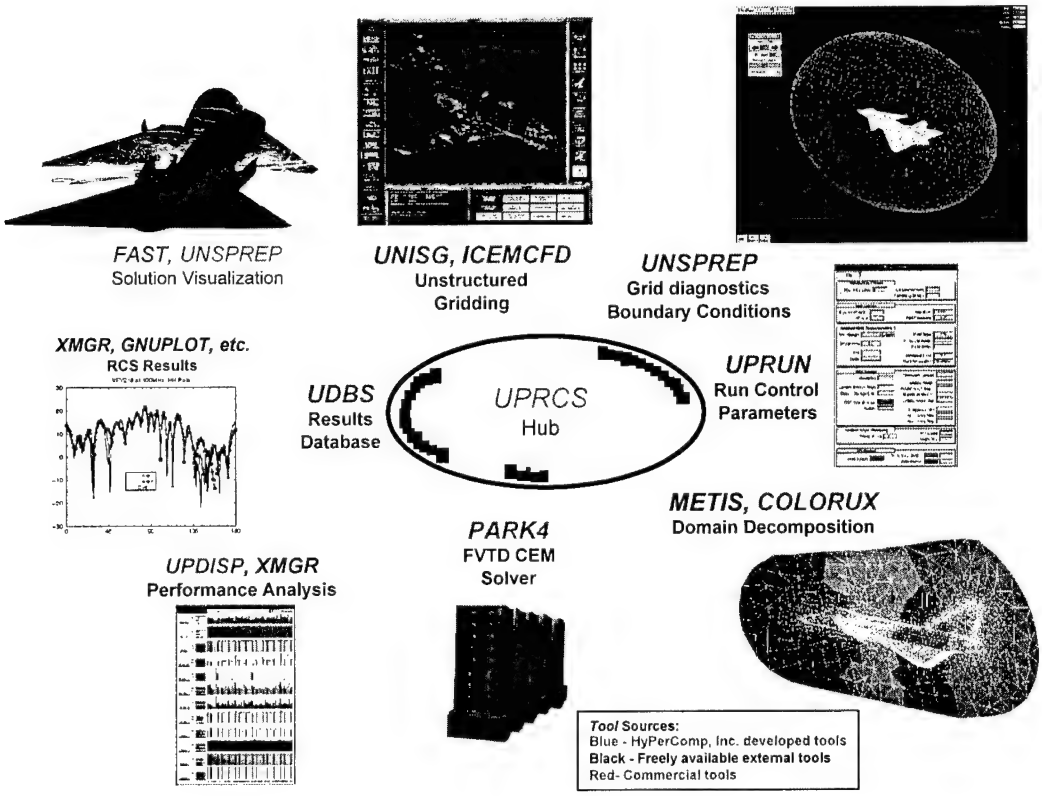

Figure 8: UPRCS solver code suite developed by HyPerComp, Inc.

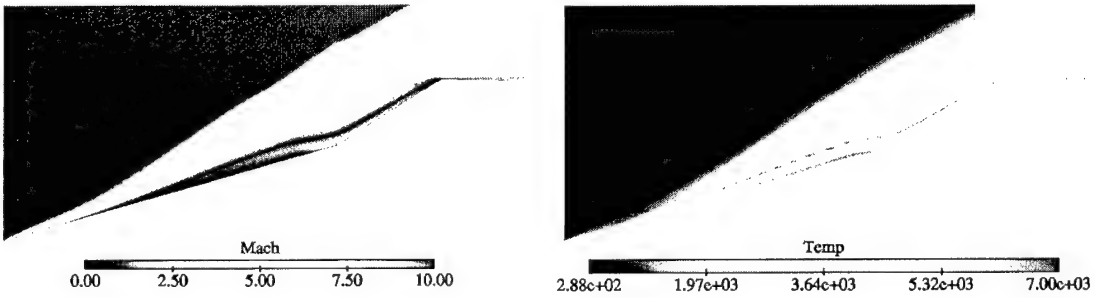

Figure 9: Mach 10 inlet (from inviscid design) with viscous effects and large mass spillage

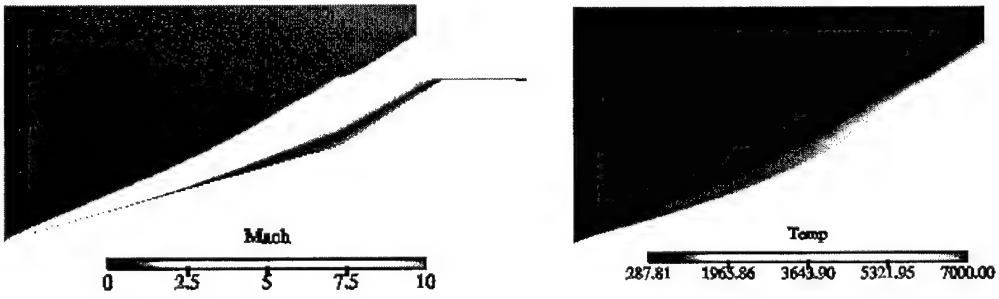

Figure 10 : Inlet from Fig. [9] with applied magnetic field

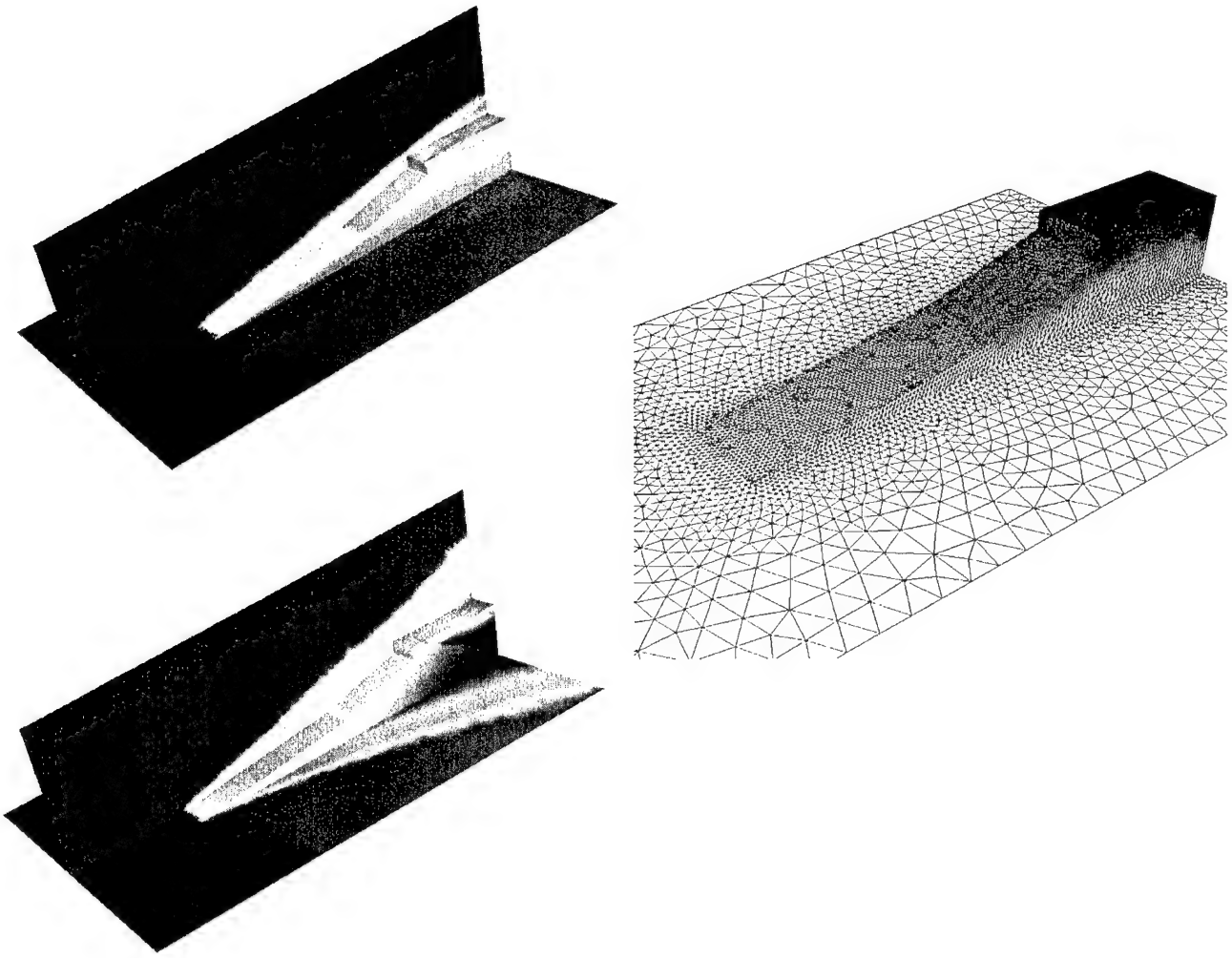

Figure 11 : Preliminary unstructured mesh simulations of hypersonic inlet with MHD interactions. Above left: B = 0, below left: Bx = 1 Tesla, σ = 40 /Ω/m in a Mach 8 inlet. Electrical conductivity a simple temperature dependant function.

A Design Environment for Plasma and Magneto-Aerodynamics

Shashi Aithal[+], Ramakanth Munipalli[*] and Vijaya Shankar[†]
HyPerComp, Inc., 31255, Cedar Valley Dr., Suite #327,
Westlake Village, CA 91361

Abstract

A numerical platform based on detailed physics for the simulation of plasma/MHD aerodynamic flows is under development at HyPerComp, Inc. In our earlier papers on the subject ([1]-[4]), we have addressed the treatment of seeded and unseeded air using a variety of models to describe the electromagnetic field. These studies have been migrated to an unstructured mesh based parallel code structure, which is being currently used to study MHD effects on hypersonic inlets.

We present in this paper, our ongoing studies of ionization mechanisms induced by e-beams. The principal difference here will be the formation of ions at low temperature caused by the electron beams, as opposed to the high temperature formation of NO and its ions (or the equilibrium ionization of alkali salts) in our previous studies. Computations were performed on a typical 3-D supersonic inlet geometry. E-beam induced plasma kinetics were coupled with MHD equations and 3D inviscid flow equations. A two-temperature (T, Tv/Te) gas model is used to include effects of thermal non-equilibrium. Effects of e-beam induced ionization and MHD forces on supersonic flow deceleration were investigated.

Introduction

Weakly ionized gases have a variety of aerospace applications. MHD inlet control, supersonic drag reduction, plasma-enhanced combustion (in scramjets) are some of the notable examples. Simulation of such flows requires the solution of Navier-Stokes equations, finite-rate chemical kinetics and Maxwell's equations. Frequently, these flows occur in complex 3D geometries and hence can be very computationally intensive. Higher order numerical schemes are required in order to accurately capture the shock formation and reflection phenomena. Hence a design tool to simulate such flows would have to use high-performance computational methods with robust higher order numerical schemes to obtain solutions in a reasonable amount of time.

High Speed Inlet control using MHD and plasma-assisted combustion of complex hydrocarbon fuels in scramjets are applications where such a design tool would be invaluable. A key issue in these applications is ionizing the incoming air stream. The requirements for producing this ionized air stream are very stringent. Large volumes (~ 1 m^3), low gas temperatures (1000 - 2000 K), high electron density (~ 10^{13} /cm^3), long residence times (≥ 10 msec), low power budget (1 – 10 MW/m^3), strong magnetic fields (~ 10 Tesla) are the main requirements for these air plasmas. Several techniques have been proposed in recent literature, to achieve these conditions. Some of these techniques are, high-energy electron beams (10 < E < 100 KeV), high voltage nanosecond pulses, DC & RF discharges, E-beams in vibrationally excited gases and seeding of the incoming gas stream. High-energy electron beams are most efficient in terms of ionization efficiency [5] and hence have been used in several studies to model air plasmas.

Electron beams produce directed ionization in gases. They provide a convenient means to generate locally high electrical conductivity at relatively low temperatures. The energy of the e-beams can be varied in the range of 10 to 100 keV, to provide high enough electrical conductivity at moderate flow static pressures. The efficiency of electron beams diminishes with increasing pressure due to the inherent

---

[+] Member, Technical Staff
[*] Member, Technical Staff, Member, AIAA
[†] Fellow, AIAA; Vice-President, HyPerComp, Inc.

nature of the electrons to be lost with greater ease in such situations (largely due to attachment with O_2). The e-beam chemistry model used in this work has been used by several authors [6-8] and has been validated by experiment [8]. The reactions and rate constants are those used in [8] and are shown in Table 1 in the Appendix.

The tools being developed here fill the need for a high-performance, numerically robust design capability to accurately predict flow fields of weakly ionized gases. Such a design tool would include real gas effects such as variable transport properties, finite electrical conductivity, finite-rate chemical kinetics, thermal non-equilibrium and effects of electromagnetic fields.

Numerical formulations and perspectives

Maxwell – Navier-Stokes coupled equation set

The conservation equations governing the flow of weakly ionized gases may be written in the following form:

$$\frac{\partial U}{\partial t} + \vec{\nabla} \cdot (Fx, Fy, Fz) + \vec{\nabla} \cdot (Hx, Hy, Hz) = S$$

in which the fluxes F are inviscid or convective, while H are viscous or dissipative. The source term S comprises of the production of, and interaction between the various flow quantities. This equation may be expressed in the integral conservation form in a control volume Ω bounded by $\partial\Omega$, as follows:

$$\int_{\Omega} \frac{\partial U}{\partial t} d\Omega + \oint_{\partial\Omega} [F_n ds + H_n ds] = \int_{\Omega} S d\Omega$$

F_n and H_n in the above equation are face normal flux components. The vector used in this equation are expanded below. An index s is used for the various gaseous species that are considered. The gas model used in this work comprises of the following components: N_2, O_2, N_2^+, O_2^+, O_2^-, e^-. We currently employ a two temperature model of ionizing air, similar to that of Park [9]. Energy addition by MHD at high temperatures can bring about a departure from equilibrium between the various energy modes. There are two energy equations, one for the total energy conservation and the other describing the vibrational-electronic energy. The following matrices describe the conservation laws:

$$U = \begin{bmatrix} \rho_s \\ \rho \vec{V}^T \\ \rho E \\ \rho e_v \end{bmatrix} \quad \text{, with } \rho_s = \begin{bmatrix} \rho_{O_2^+} \\ \rho_{N_2^+} \\ \rho_{O_2^-} \\ \rho_{O_2} \\ \rho_{N_2} \\ \rho_{e^-} \end{bmatrix},$$

$$\vec{V} = [u, v, w]$$

$$F_n = \begin{bmatrix} \rho_s U_n \\ \rho U_n \vec{V}^T + p\vec{n} \\ \rho U_n H \\ \rho U_n e_v \end{bmatrix},$$

$$H_n = \begin{bmatrix} -\rho D_s \vec{\nabla} y_s \cdot \vec{n} \\ -\vec{\tau}_n \\ -\vec{V} \cdot \vec{\tau}_n - \eta \vec{\nabla} T \cdot \vec{n} - \eta_v \vec{\nabla} T_v \cdot \vec{n} - \rho \sum_s h_s D_s \vec{\nabla} y_s \cdot \vec{n} \\ -\eta \vec{\nabla} T_v \cdot n - \rho \sum_s h_{v,s} D_s \vec{\nabla} y_s \cdot \vec{n} \end{bmatrix}$$

$$S = \begin{bmatrix} \dot{\omega}_s \\ (\vec{j} \times \vec{B}) \\ \vec{J} \cdot \vec{E} + \dot{Q}_{rad} \\ \vec{J}_e \cdot \vec{E}' + \dot{\omega}_v + \dot{Q}_{e,rad} \end{bmatrix}$$

The transfer of energy across the various energy levels is contained in the nonequilibrium energy production rate $\dot{\omega}_v$. This term contains the energy transfer to the electronic and vibrational modes via collisions, electron pressure gradient, Landau-Teller type of relaxation of these modes with the translational and rotational modes, and release in vibrational and electronic energy caused by ionization or the change in the number densities of polyatomic molecules. The expressions used to model these features may be found in various references (e.g.: Munipalli [1-4]).

Radiative energy addition by means of microwave and other beams can possibly be used to cause an increase in the electron energy and ionization. This is modeled by the terms Q_{rad}. Fluxes F_n and H_n are written at the cell

face in each control volume. In the results presented in this paper effects of dissipative fluxes (i.e. viscosity, thermal conductivity, species diffusivity and mobility effects) are not included.

MHD Model:

In the calculations presented in this paper, the magnetic Reynolds number is assumed to be small. This implies that the induced magnetic field is negligible and that the electric field may be derived from a scalar potential: $\vec{E} = -\vec{\nabla}\varphi$. Ohm's law may then be used to relate this potential to the current density:

$$\vec{J} = \sigma\left(-\vec{\nabla}\varphi + \vec{V}\times\vec{B}\right) - \frac{\omega\tau}{B}\left(\vec{J}\times\vec{B}\right)$$

Where σ denotes the electrical conductivity, $\omega\tau/B$ is the Hall parameter, J is the electric current density and B is the applied magnetic field vector. Since the induced magnetic field is neglected, the only electromagnetic field quantity that needs to be computed numerically at each time step is the electric potential.

When the divergence of the above expression is set to zero and is re-written in terms of the electric potential, a Poisson type equation is obtained, which must be solved at each computational time step. In the results presented in this paper, the Hall-effect terms are neglected in the generalized Ohm's law given above.

Setting the divergence of the current density (without the Hall terms) to zero leads to the following expression:

$$\nabla\cdot\left[\sigma\left(-\nabla\varphi + \vec{V}\times\vec{B}\right)\right] = 0$$

Solution of the above Poisson equation yields the electric potential φ and electric current density j. The joule heating term and Lorentz forces in the energy and momentum equations can thus be obtained. In this work, Bx = Bz = 1 T, By = 0.

Chemistry model:

The chemistry model used in this work is based on Ref [8]. This model has been validated with experimental data and hence has been chosen in this work. The electron production rate by the e-beam (S_o) is chosen to be constant and set equal to 1.5E24 $m^{-3}s^{-1}$. The spatial extent of the e-beam is set by assuming (see Figure 1)

$$S = S_o, \text{ for } X_0 < X < X_1$$

$$S = 0, \text{ for } X < X_0 \text{ or } X > X_1$$

The electrical conductivity of the ionized air is computed using the expression for partially ionized gas given by Rosa [10]

$$\sigma = \frac{n_e e^2}{m_e c_e}\left[\frac{1}{\sum_k n_k Q_k + 3.9 n_i\left(\frac{e^2}{8\pi\varepsilon_o kT}\right)^2 \log\Lambda}\right]$$

$$\text{where } \Lambda = \left(\frac{1.24*10^7 T^{1.5}}{n_e^{0.5}}\right)$$

In a mixture of gases, n_i denotes the number density of ions and Q_k is the neutral-neutral collision cross-section.

Boundary Conditions:

Boundary and initial conditions for the governing equations described above must be specified accurately in order to prevent numerical instabilities and non-physical behavior of the solution. For supersonic and super-alfvenic flows, information propagates only in the downstream direction. The inflow variables are then fixed and outflow variables are obtained by extrapolation. For subsonic or sub-alfvenic flows, characteristic relations must be used in order to propagate information either into or out of the domain.

No slip boundary conditions are applied to the velocity along the wall for viscous flows. In the present work, the flow is considered to be inviscid, hence the gradient of the tangential component of velocity is set equal to zero at the walls. Normal derivatives for species densities are set equal to zero on the walls. The gradient of the gas temperature and vibrational temperature is set equal to zero at the walls. Electromagnetic boundary conditions may be more involved, depending on the choice of wall

material. In the present work, the electric current density normal to all boundaries is set equal to zero, i.e.

$$J_n = \vec{J} \cdot \vec{n} = 0$$

Space/time integration: Numerical Scheme

A point-implicit finite volume scheme is used to solve the governing equations shown earlier. For a cell bearing the index *i*, volume Ω_i, the time advancement scheme is written as:

$$U_i^{t+\Delta t} = U_i^t + C_L^{-1} r_i^t$$

where,

$$C_L = \left[I + \frac{\delta t}{\Omega_i} M_L^{'} \right]$$

and

$$M_L^{'} = M_{inv}^{'} + M_{visc}^{'} - \Omega_i M_{src}^{'}$$

The right hand side vector r is the flux summation based on quantities at time level t. Inviscid fluxes are computed from a Roe-type procedure, in which a density based averaging is performed similar to the perfect gas equivalent. Viscous and dissipative fluxes are computed from central differences. Details of this implementation may be found in Refs. [4,12].

In the above equation, ***I*** is an *n* x *n* (n is the total number of dependent variables in the vector U) identity matrix and M_L' is the combined Jacobian including inviscid, viscous and source term contributions.

Reacting and plasma flow equations are characterized by widely varying spatial and time-scales. The point-implicit formulation is necessary in order to obtain stable solutions for a stiff system of governing equations. As mentioned earlier, M_{visc} = 0 in the results presented in this paper.

The formal order of accuracy of this numerical procedure is enhanced by using the TVD approach, as described by Barth [11], using local gradients computed from a Gaussian summation. Work is underway to develop this environment into a higher order multi-physics solver using the Discontinuous Galerkin technique.

Results

Figure 1 shows the geometry used in the present work. The e-beam chemistry model was validated by conducting a simulation with free stream conditions of 1 atm, 300 K (as in Ref [8]). For the purpose of validation, the electron-ion formation by means of the e-beam is simulated in the region 3.46 < x < 4.56m. The production rate for electron-ion pairs by the e-beam is assumed to be 1.5E24 m^{-3}/s as in [8]. The magnitude of the electron concentration is compared with results reported in Fig. 9 in ref. [8]. Figure 2 shows the axial variation of electron number density for the above conditions. It is see that the peak electron number density is close to that predicted by experiments (1.8E16 #/m3-s) in Ref 8.

We use a base inlet geometry designed for Mach 8 operation from inviscid considerations, earlier studied by Sheikin et al [13]. A flight Mach number of 6 at an altitude of 30 km was chosen as an off-design condition in our study. Corresponding to this altitude, the ambient density, pressure and temperature are 1.84E-2 Kg/m3, 1.2E3 N/m2 and 226.5 K, respectively. With an intent to improving the performance of this inlet at the lower than design Mach number, the following case-studies were made.

Flow Without MHD

Figure 3(a), (b) show contours of axial velocity, and temperature. The velocity and temperature contours show the formation of shocks due to the two ramps. Shock reflection from the top boundary (inviscid wall) is also seen. Figure 4 show the axial variation of gas temperature and vibrational temperature along the ramp surface. It is seen that there is very little change in the vibrational temperature of the gas along the length of the ramp channel. At the pressure/temperature conditions being considered here, the V-T relaxation time is rather large (a few milli-seconds,) and Tv lags far behind the translational temperature T. When Joule heating and other forms of energy addition

preferentially excite the vibrational/electronic modes, the vibrational temperature can grow to be in excess of the translational temperature, and energy is exchanged across these modes by relaxation. This may be seen in the subsequent results in this section.

Constant conductivity with Bx = Bz = 1:

A parametric study of the effect of electrical conductivity and extent of the ionized region was also performed. These simulations were made on a coarse mesh. Figure 5 shows the effect of the MHD forces on the flow field. For this case the electrical conductivity is maintained at 20 mho/m in a region between 1.0 < x < 5.5 m. Figure 5(a) and (b) show the velocity contours with and without MHD effects. It is seen that there is a noticeable change in shock angle and flow deceleration due to the MHD forces.

Constant conductivity with Bx = 0, Bz = 1:

Figure 6 shows the current lines for a case with a constant conductivity of 20 mho/m but with a constant magnetic field of Bz = 1. The absence of an X-component of the magnetic field and the insulating boundary conditions give rise to current lines that close on themselves in the XY plane.

MHD with variable σ and e-beam ionization

MHD forces generated in ionized air depend primarily on the electrical conductivity and the applied magnetic field. The electrical conductivity of air is governed by the number density of mobile charge carriers in the flow (see expression for electrical conductivity described earlier). Hence, it is instructive to estimate the conductivity of e-beam ionized air as a function of S_o (e-beam induced ionization).

A few parametric cases were run to study the effect of beam-induced electron production rate (S_o) on the maximum electrical conductivity. These values are reported in Table 2 in the appendix. It is known that the peak electron density is proportional to the square root of the e-beam induced electron production rate [7]) and this is seen in Table 2. The electron production rate S_o is determined by the e-beam characteristics and is given by the following expression [7]:

$$S_o = \frac{\left(j_b / e\right)\rho Y E_b}{W_i}$$

where, W_i is the ionization energy to produce an electron-ion pair (34 eV), E_b is the energy of the e-beam (typically ~ 100 KeV), ρ is the gas density (and Y is the electron stopping power in (MeV m^2/kg). At higher altitudes, the gas density is lower, hence for a given e-beam energy, a proportionally higher beam current density is required to produce the required e-beam induced electron-ion production rate. The electron production rate of E24 m^{-3}/s in Ref [8] is based on a beam current density of approximately 5 mA/cm^2 and beam energy of about 30 KeV. Column II in Table 2 shows the current density scaled with gas density for the various beam induced production rates shown in column I. It is seen that to produce an electrical conductivity around 20 mho/m, a very high value of beam current is required and hence could present practical engineering problems in implementation. For the beam strength of S_o = 1.5E24 m^{-3}/s used in this work, the maximum value of sigma is about 5 mho/m.

Figure 7 (a), (b), (c) show contours of axial velocity, temperature and electron number density, respectively. The free-stream Mach number is 6, and the e-beam is applied in the region from 4.0 < x < 4.75 m. The strength of the e-beam induced ionization (S_o) was equal to 1.5E24 m^{-3}/s. A uniform magnetic field of B_x = B_z = 1T was used in these simulations. The velocity and temperature profiles look similar to the case where there was no MHD present. It is seen in Fig 7(c) that in the region with the e-beam the electron density is high but close to zero everywhere else in the domain. Figure 8 (a) shows the current vectors in a cross-section at x = 4.37 (center of the e-beam region). Figure 8 (b) shows the current lines with contours of σ. The current traces are spiraling due to the presence of a magnetic field in the X-direction.

Figures 9 (a) and 9 (b) show the variation of axial velocity and vibrational temperature near the ramp surface, respectively. Figure 9 (a) show the reduction in the axial velocity due to the presence of the JXB terms. It is seen in Fig. 9 (b) that addition of the Ohmic heating terms (J.E) quickly increases the vibrational temperature as compared to the case with no MHD.

Variable σ, S_o = 1.5E26 m^{-3}/s and e-beam applied over $3.5 < x < 5.5$

Figure 10 (a) shows variation of T, Tv and electron number density with S_o = 1.5E26 m^{-3}/s. Figure 10 (b) shows variation of T, Tv and electrical conductivity. The higher value of beam induced ionization gives rise to a higher value of electrical conductivity and electron number density. Since the contribution of the Ohmic heating term to the vibrational mode is high, the vibrational temperature is high as pointed out above.

Conclusion

This paper presents the results of our ongoing investigations in the inclusion of real gas effects in a practical flow solver to simulate plasma and MHD effects in hypersonic flow. The cold incoming supersonic stream is ionized by the use of e-beams. A plasma kinetic model describing the ionization of cold air is coupled with a Poisson solver and 3-D MHD equations. It is seen that large volume E-beam generated ionization is required to bring about reasonable amounts of shock displacement. Inviscid flow simulations show that high beam current densities are required to generate the ionization levels needed for shock displacement. Real gas effects such as species diffusion, mobility and viscosity will be included in future simulations.

Acknowledgement

This work was supported under the AFOSR contracts F49620-99-C-0015/0070 with Maj. William Hilbun as the program monitor. The authors also express their thanks to Dr. Sergey Macheret from Princeton University for valuable discussions and Mr. Touraj Sahely of HyPerComp, for generating the 3-D meshes used in this paper.

References

1. Munipalli R., V. Shankar, A Hadid, "Shock waves in hypersonic inlets with MHD," 23rd International Symposium on Shock Waves, Fort Worth, TX, July 2001
2. Munipalli R., V. Shankar, Z. Liu, A. Hadid, "An Unstructured Grid parallel MHD Solver for Real gas MHD simulations," AIAA 2001-2738, 32nd Plasmadynamics and Lasers Conference, Anaheim, CA, June 2001
3. Munipalli, R., Anderson, D. A., Wilson, D. R., "CFD Evaluation of Seeded and Unseeded Air MHD Accelerators," AIAA 2000-0215, Reno, NV, January 2000
4. Munipalli, R., Anderson D. A., Kim, H.-Y., "Two-temperature computations of ionizing air with MHD effects," AIAA 2000-0450, Reno, NV, January 2000
5. "Physical and chemical processes in gas dynamics: cross sections and rate constants – Vol. 1," Eds. G.G.Chernyi, S.A. Losev, S.O. Macheret, B.V. Potapkin, AIAA Progress in Aeronautics and Astronautics Series, Vol. 196, 2002
6. S. O. Macheret, M. N. Shneider, R. B. Miles, "External Supersonic flow and scramjet inlet control by MHD with electron beam ionizer", AIAA paper, 2001-0492, 39th AIAA Aerospace Sciences Meeting and Exhibit, 8-11 January 2001, Reno, NV
7. A. L. Kuranov, E. G. Sheikin, " MHD control on Hypersonic Aircraft under "AJAX" concept. Possibilities of MHD Generator", 40th AIAA Aerospace Sciences Meeting January 2002/ Reno, NV.
8. P. Palm, E. Ploenjes, I. V. Adamovich, J. W. Rich,'E- Beam Sustained Low-power Budget Air Plasmas', AIAA Paper 2002-0637, 40th AIAA Aerospace Sciences Meeting & Exhibit 14-17 January 2002/ Reno, NV.

9. Park, Chul, "Assessment of two-temperature kinetic model for ionizing air," Journal of Thermophysics and Heat Transfer, Vol. 3, No. 3, July 1989
10. Rosa, R. J. "Magnetohydrodynamic Energy Conversion", McGraw Hill Book Company, 1968.
11. Barth, T.J., "Aspects of unstructured grids and finite volume solvers for the Euler and Navier-Stokes equations," VKI Lecture series, 1994-05
12. Gnoffo, P.A., Gupta, R.N., Shinn, J.L., "Conservation equations and physical models for hypersonic air flows in thermal and chemical nonequilibrium," NASA TP-2867, 1989
13. Brickin, D. I., Kuranov, A. L, Sheikin, E. G.: 'Scramjet with MHD control under "AJAX" concept. Physical Limitations', AIAA paper 2001-0381 (2001)

Appendix

Table 1: E-beam chemistry model with reaction rates constants

No.	Reactions	A	n	Ea/R
1	$e^- + 2O_2 = O_2^- + O_2$	2.5E-42 (m^6/s)	0	0
2	$e^- + O_2 + N_2 = O_2^- + N_2$	1.6E-43 (m^6/s)	0	0
3	$e^- + O_2^+ = O_2$	2.0E-12 (m^3/s)	0	0
4	$e^- + N_2^+ = N_2$	2.0E-12 (m^3/s)	0	0
5	$O_2^- + O_2 = 2O_2 + e^-$	2.2E-24 (m^3/s)	0	0
6	$O_2^- + N_2 = O_2 + N_2 + e^-$	1.8e-26 (m^3/s)	0	0
7	$O_2^- + O_2^+ + O_2 = 3\ O_2$	1.55E-37 (m^6/s)	0	0
8	$O_2^- + O_2^+ + N_2 = 2\ O_2 + N_2$	1.55E-37 (m^6/s)	0	0
9	$O_2^- + N_2^+ + O_2 = 2\ O_2 + N_2$	1.55E-37 (m^6/s)	0	0
10	$O_2^- + O_2^+ + N_2 = O_2 + 2N_2$	1.55E-37 (m^6/s)	0	0

Table 2: Variation of Electrical conductivity with pressure and S_o

S_o (#/m3/s)	J_b (mA/cm2)	ρ(kg/m3)	Pressure (N/m2)	N_e (#/m3)	σ (mho/m)
1.5E24	5	1.22	1.01E5	1.8E16	0.0002
1.5E24	3.32E2	1.84E-2	1.2E3	7.9E17	5.5
1.5E25	3.32E3	1.84E-2	1.2E3	2.64E18	11.7
1.5E26	3.32E4	1.84E-2	1.2E3	8.53E18	19.56
1.5E23	3.32E1	1.84E-2	1.2E3	2.6E17	2.5
1.5E22	3.32	1.84E-2	1.2E3	7.7E16	0.8

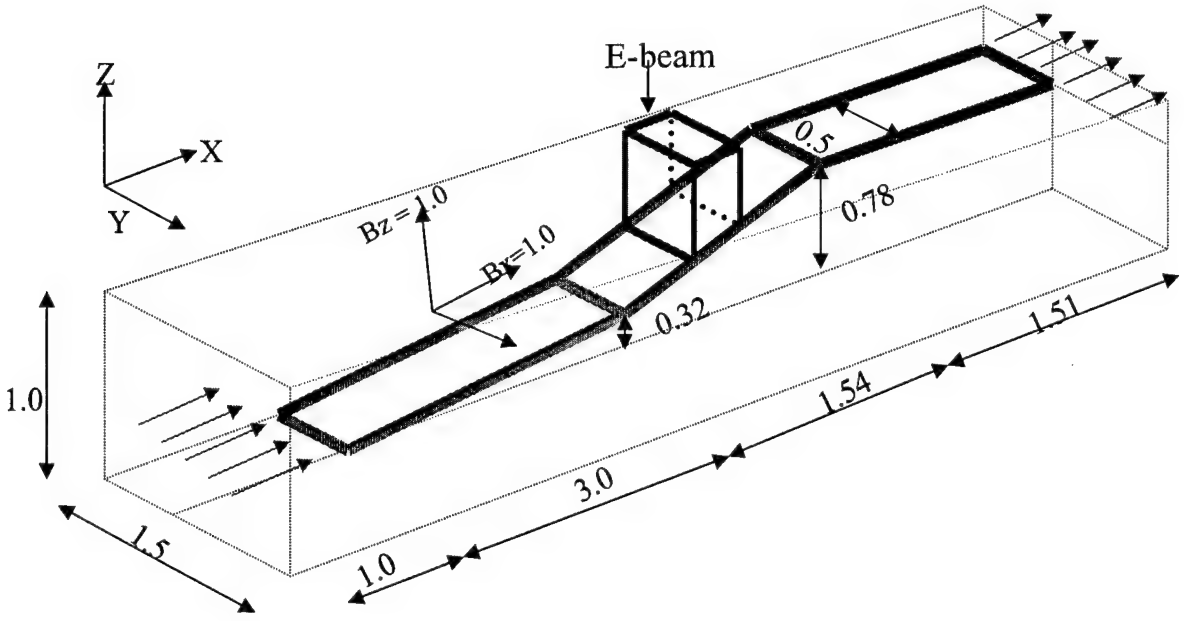

Figure 1: Schematics of the geometry (all dimensions in meters)

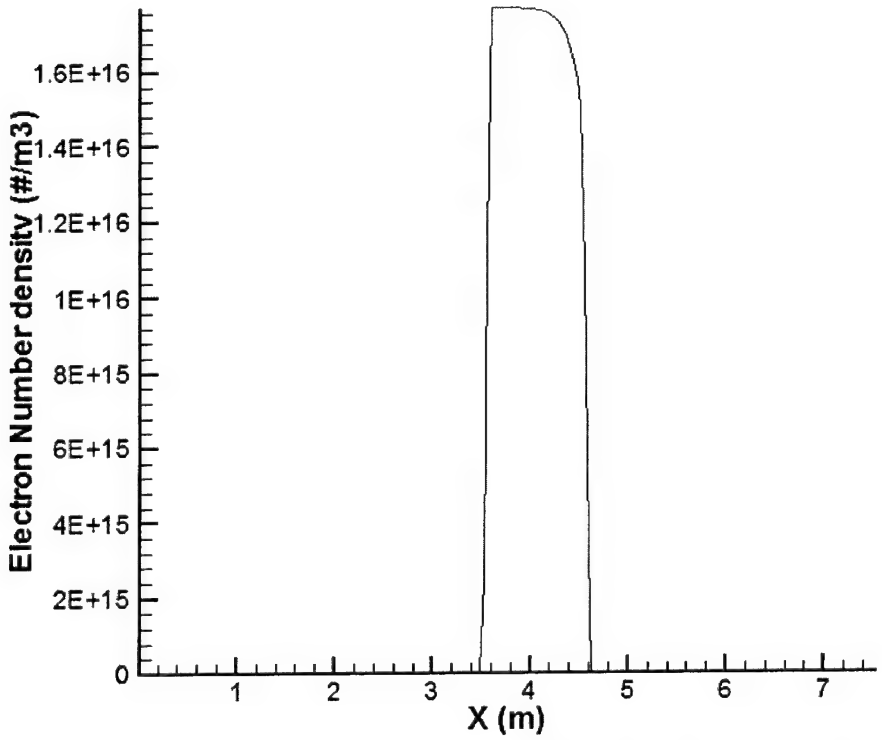

Figure 2: Variation of electron number density S_o = 1.5E24 m^{-3}/s at Po =1 atm and To = 300K.

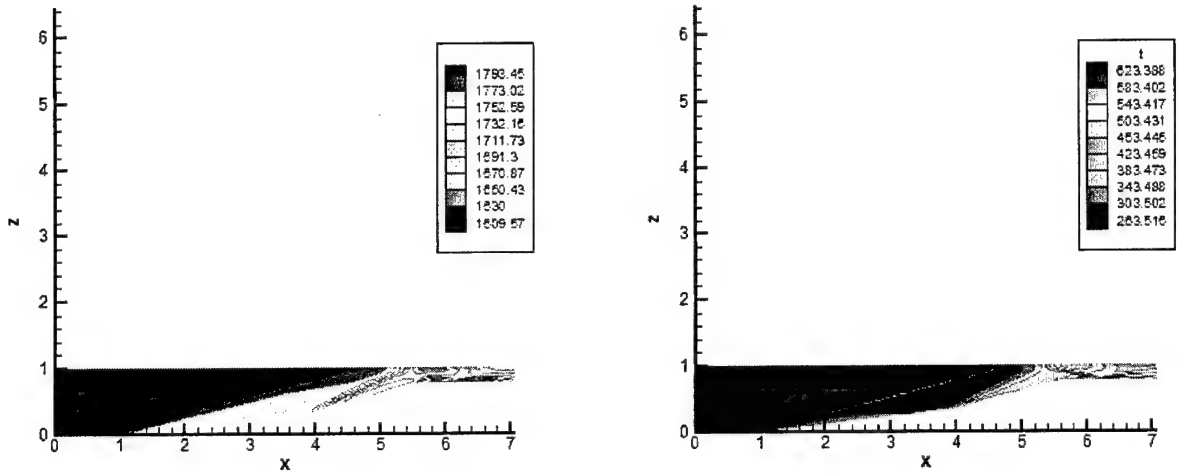

(a) (b)

Fig 3:Contours of velocity (a) and temperature (b) with no MHD effects.

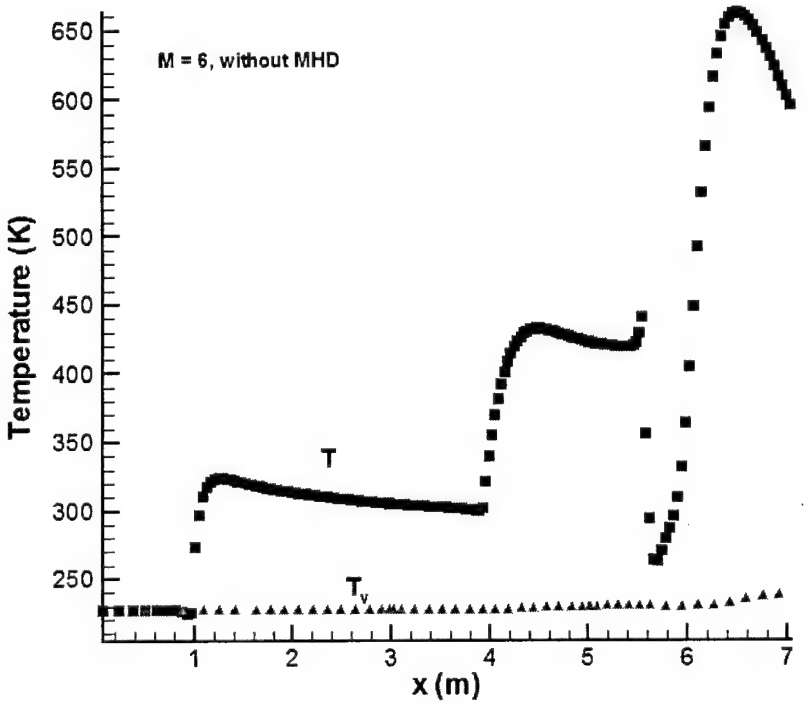

Figure 4: Axial variation of gas temperature and vibrational temperature with no MHD

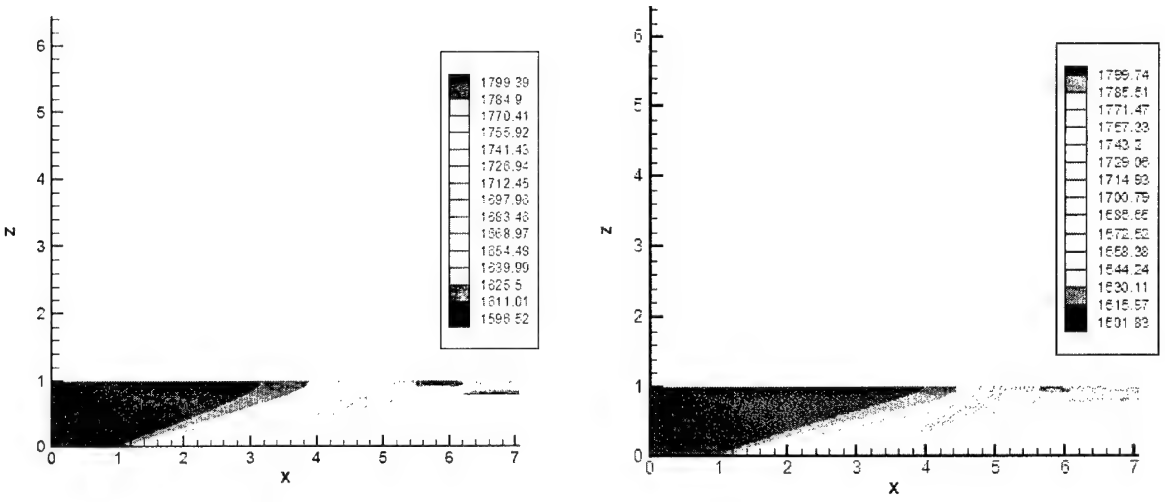

(a) (b)

Figure 5: Velocity contours with (a) and without MHD (b) for a constant electrical conductivity of 20 with E-beam applied over $1.0 < x < 5.5$ m

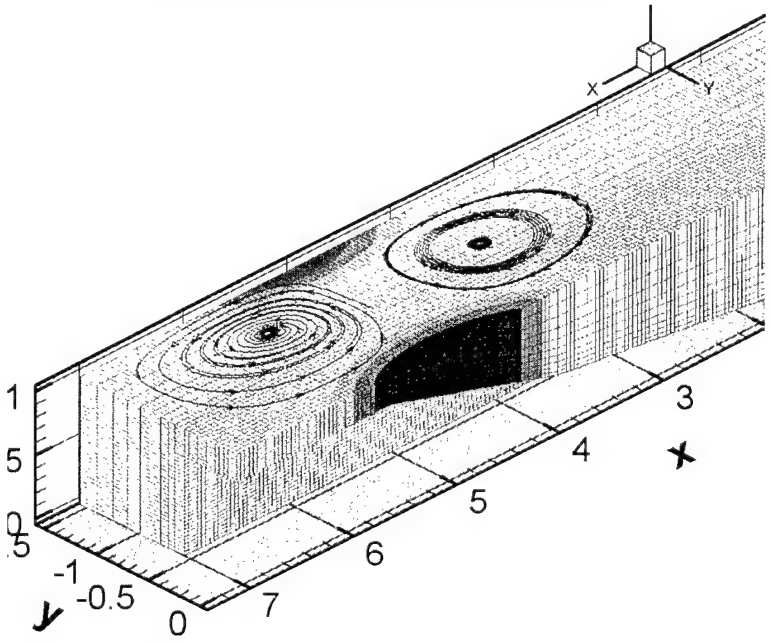

Figure 6: Current lines for $\sigma = 20$, $B_x = 0$, $B_z = 1$

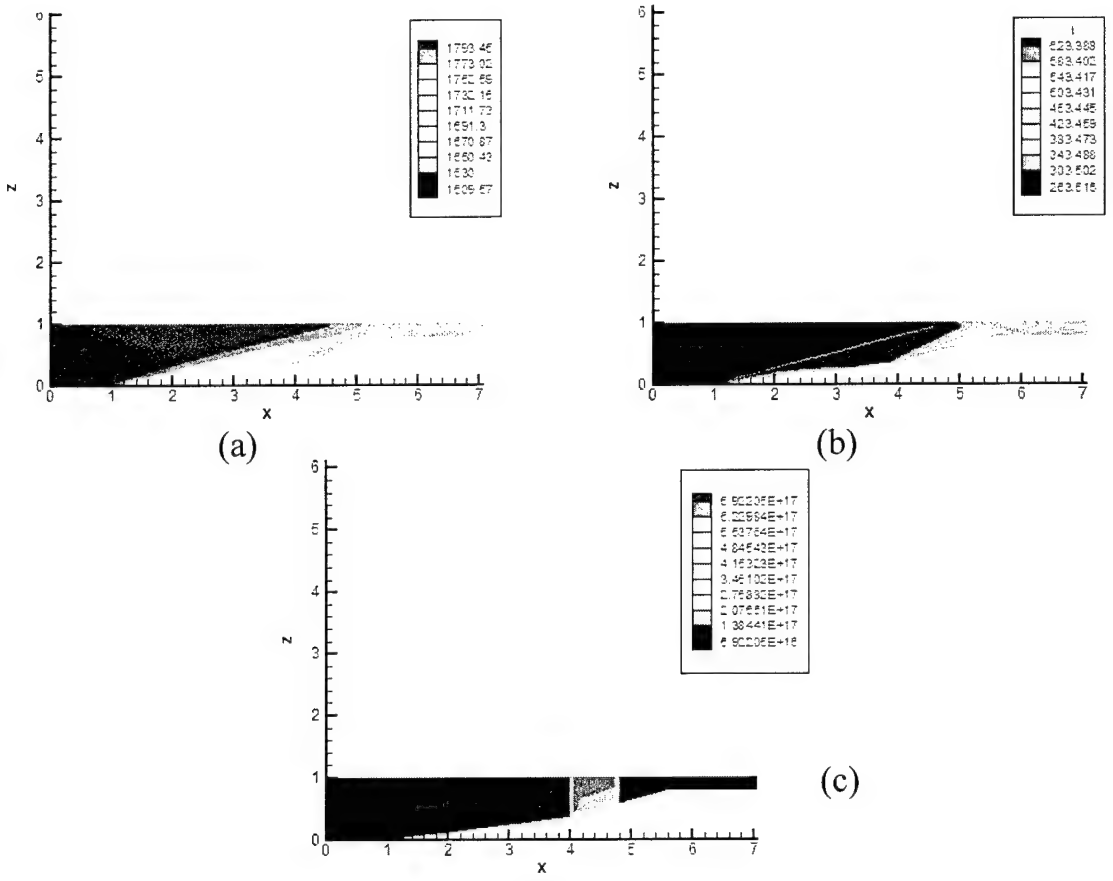

Fig 7: Axial velocity (a), temperature (b) and electron number density (c) with MHD

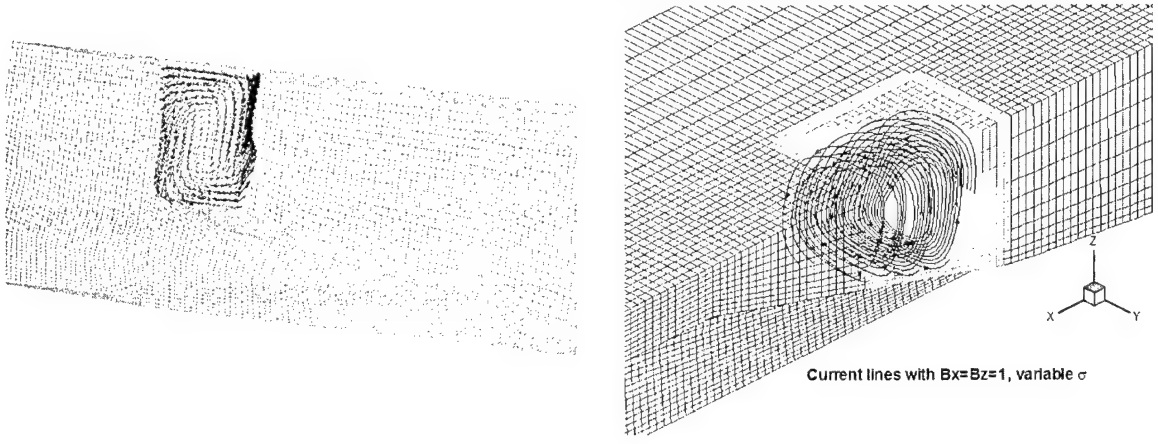

(a) (b)

Figure 8: Current vectors (a) and current lines (b) in the e-beam region

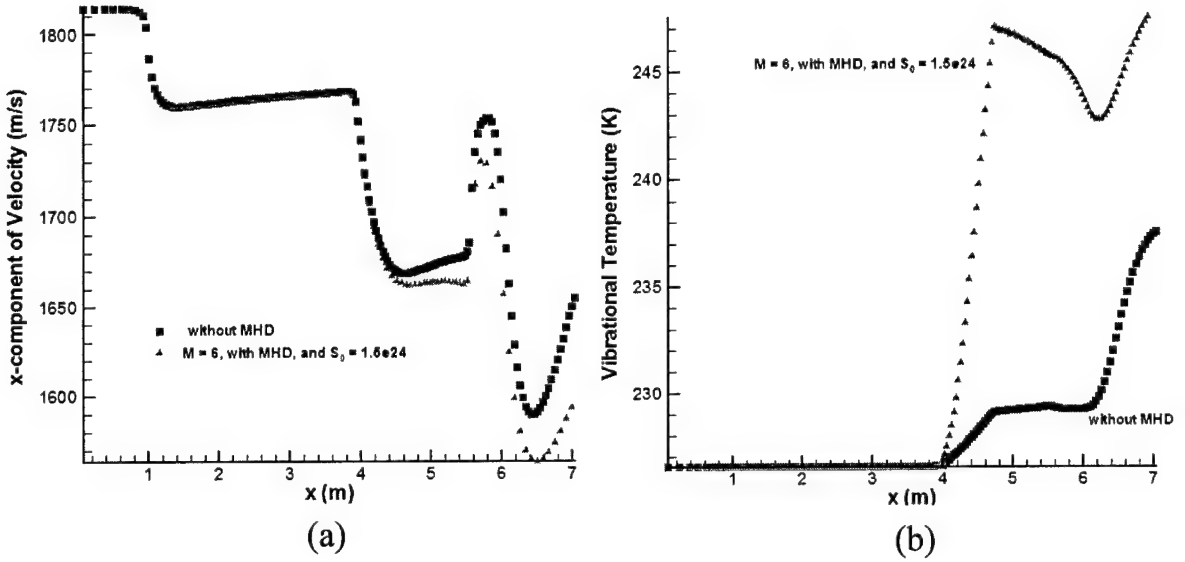

Figure 9:Axial variation of velocity (a) and vibrational temperature (b) with MHD

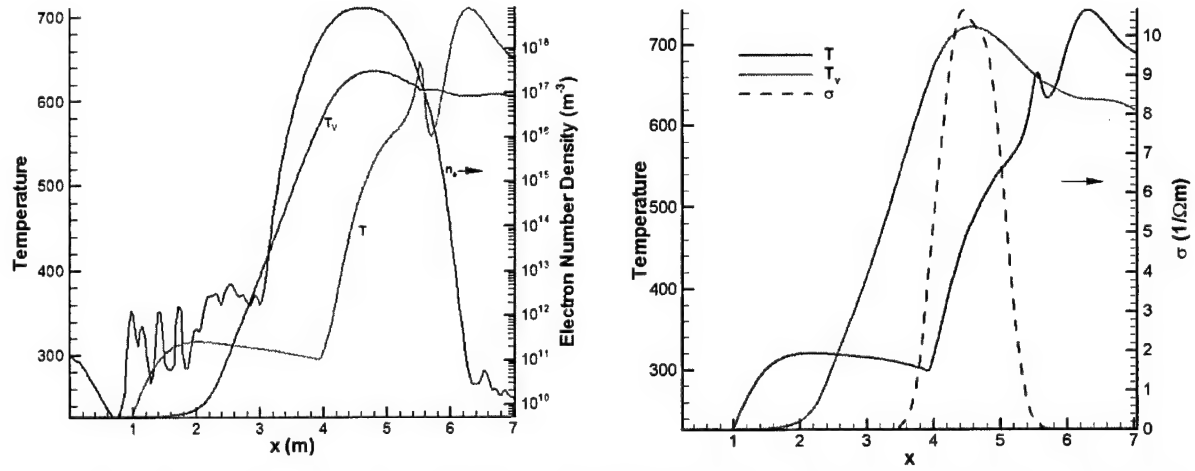

Figure 10: Axial variation of T, Tv and electron number density (a), and T, Tv and σ (b) for a case with S_o = 1.5E26 m^{-3}/s

Effect of wall conduction in proposed MHD enhanced hypersonic vehicles

Ramakanth Munipalli[+], Shashi Aithal[*] and Vijaya Shankar[†]
HyPerComp, Inc., 31255, Cedar Valley Dr., Suite #327,
Westlake Village, CA 91362

Abstract

In AJAX-type vehicle design concepts (e.g., ref. [7]), the flow of a conducting medium in the presence of a magnetic field produces currents that must form closed loops or extend indefinitely, in the absence of charge sources. While the solid walls of the airframe are normally assumed to be insulating in CFD estimates of AJAX performance, even mildly conducting airframe materials cause currents to leak away from the flow (considering the very low achievable values of electrical conductivity of air in flight,) and may potentially cause major changes in flow compression and shock structures on this account. Here, we present the effect of conducting walls in hypersonic inlet flow computations. Even small cracks in insulations (4-5 orders of magnitude smaller than the flow length scale,) have large scale effects on the flow, and the influence of MHD on flow control aspects. Conducting wall physics is superposed on our previous work in this area (refs. [2],[13]-[17]).

Introduction

Recent years have witnessed a great surge in simulation capabilities pertaining to ionizing air flows and MHD (e.g., ref. [20]). This has been coupled with experiments demonstrating physical phenomena of interest in such flows, and analytical estimates of performance enhancements in hypersonic vehicle design caused by these techniques.

Effect of wall conductivity

Existing literature in the area of hypersonic flows with MHD frequently relies on the assumption that the walls bounding air flows are insulating, or have some pre-set potential distribution that determines the current within the fluid medium. When the walls are fully conducting, or comprise of insulation in which imperfections may occur (albeit minute,) literature has shown numerous situations in which the computed pressure is vastly different (by more than an order of magnitude,) from the insulating wall assumption. (See, e.g., Refs [4],[11]). In airframes, a metallic structure is more of a norm than an exception, and this seems to call for a major revision of MHD performance estimates obtained from insulating wall approximations.

Figure [1] shows a situation in which current is generated in a flow by virtue of conducting gas moving in the presence of a magnetic field. This current does not penetrate insulating walls (shown in thick black,) but seeks out the high conduction path through cracks in insulation or solid metallic elements in order to close loops. In this paper, we attempt to assess the MHD effects of conducting walls and quantify them for cases of interest. The pressure gradient is accentuated (10s of times) when more current flows in the fluid, typically, when conducting walls are present. Indeed, any MHD effect that is felt upon a flow is dependent on the electrical conductivity of the gas. A practical realization of these concepts in a flight vehicle will depend critically on enhanced electrical conductivity and the ability to carry high strength magnets on-board.

Ionization and electrical conductivity of gases

The electrical conductivity of a gaseous medium such as air may be enhanced by various forms of ionization. Weakly ionized gases have a variety of aerospace applications. MHD inlet control, supersonic drag reduction, plasma-enhanced combustion (in scramjets), are some of the notable examples. A key issue in these

[+] Member, Technical Staff, Member, AIAA: e-mail: mrk@hypercomp.net
[*] Member, Technical Staff
[†] Fellow, AIAA; Vice-President, HyPerComp, Inc.

applications is ionizing the incoming air stream. The requirements for producing this ionized air stream are very stringent. Large volumes (~ 1 m^3), low gas temperatures (~ 2000 K), high electron density (~ 10^{13} /cm^3), long residence times (≥ 10 msec), low power budget (1 – 10 MW/m^3), strong magnetic fields (~ 10 Tesla) are the main requirements for these air plasmas.

Several techniques have been proposed in recent literature, to achieve these conditions. Some of these techniques are: high-energy electron beams (E ≥ 100 KeV), high voltage nanosecond pulses, DC & RF discharges, E-beams in vibrationally excited gases and seeding of the incoming gas stream. We consider high energy electron-beams to produce ionization in air in this paper. Some recent studies have indicated their superiority to other methods of ionization (ref. [9]).

Electron beams produce directed ionization in gases. They provide convenient means to generate locally high electrical conductivity at relatively low flow temperatures. Ref[2] presents our implementation of the electron beam models in a thermochemical nonequilibrium MHD solver.

Problem Formulation

Flow Equations

Over the years, we have developed models of varying complexity to describe MHD effects on air. These models range from ideal gas, to equilibrium air with seeding, nonequilibrium ionizing air with multiple temperatures, and have recently extended these to include the effects of electron beams. The reader is referred to Munipalli et al. [13-17] for a description of the electromagnetic and gas models and our previous experience with MHD modeling in hypersonic flow acceleration and inlet studies.

Electromagnetics – the inductionless approach

In our earlier work (refs. [13]-[17]), we considered the differences between various electromagnetics models for use in magneto-aerodynamics, ranging from fully coupled NS-Maxwell equations to various forms of inductionless models using the electric potential (refs, [14], [16]). Electrical conductivity of air, with most practical ionization techniques being investigated in the present day, does not exceed 10-100 mho/m, resulting in a magnetic Reynolds number that is extremely small. In the calculations presented in this paper, the magnetic Reynolds number is assumed to be small. This implies that the induced magnetic field is negligible and that the electric field may be derived from a scalar potential: $\vec{E} = -\vec{\nabla}\varphi$. Ohm's law may then be used to relate this potential to the current density:

$$\vec{J} = \sigma\left(-\vec{\nabla}\varphi + \vec{V}\times\vec{B}\right) - \frac{\omega\tau}{B}\left(\vec{J}\times\vec{B}\right)$$

Where σ denotes the electrical conductivity, ωτ/B is the Hall parameter, J is the electric current density and B is the applied magnetic field vector. Since the induced magnetic field is neglected, the only electromagnetic field quantity that needs to be computed numerically at each time step is the electric potential. The current density may be recast in terms of the effective electric field $E' = -\nabla\varphi + \vec{V}\times\vec{B}$. For simplicity, this expression is shown here for a magnetic field applied in the z-direction alone:

$$\boldsymbol{J} = \frac{\sigma}{1+(\omega\tau)^2}\begin{bmatrix} 1 & \omega\tau & 0 \\ -\omega\tau & 1 & 0 \\ 0 & 0 & 1+(\omega\tau)^2 \end{bmatrix}\vec{E}'$$

When the divergence of the above expression is set to zero and it is re-written in terms of the electric potential, a Poisson type equation is obtained, which must be solved at each computational time step. This equation is easily derived. A full version of this equation including property gradients, is being omitted here due to space constraints. Due corrections to electron-beam current and electron pressure gradient will be presented in the final version of the paper. At interfaces (solid as well as liquid,) where the electrical conductivity has a gradient, this equation must be written in a weak form, since the gradient of the conductivity is infinite. Virtually, the component normal to the interface, of the following equation must be satisfied in order for the solution to be unique:

$$\nabla\varphi = \boldsymbol{V}\times\boldsymbol{B}$$

Electrical conductivity and the Hall parameter are transport parameters, that are evaluated using appropriate numerical expressions, as described in Refs. [2],[15].

Boundary Conditions:

Boundary and initial conditions for the equations described must be specified accurately in order to prevent numerical instabilities and non-physical solution behavior. For supersonic and super-alfvenic flows, information propagates only in the downstream direction. The inflow variables are then fixed and outflow variables are obtained by extrapolation. For subsonic or sub-alfvenic flows, characteristic relations must be used in order to propagate information either into or out of the domain.

No slip boundary conditions are applied to the velocity along the wall for viscous flows. In the present abstract, the flow is considered to be inviscid, hence the gradient of the tangential component of velocity is set equal to zero at the walls. Normal derivatives for species densities are set equal to zero on the walls. The gradient of the gas temperature and vibrational temperature is set equal to zero at the walls. Electromagnetic boundary conditions may be more involved, depending on the choice of material conditions at the wall. In the case of an insulating wall, the gradient of the electric potential normal to the wall is zero, and when the wall does conduct, an extended domain is used to depict solid boundaries. A thin conducting wall option is also available, wherein a fraction of the incoming current is distributed tangentially along the wall, governed by a component of the Poisson equation for the electric potential.

Numerical Scheme:

The governing equations are integrated using a point-wise implicit scheme described in Munipalli et al. [14]. Upwind fluxes based on Roe-type linearization are used in a finite volume format on general unstructured meshes. The formal order of accuracy of this numerical procedure is extended by using the TVD approach, as described by Barth [3]. Work is underway to develop this environment into a higher order multi-physics solver using the Discontinuous Galerkin technique.

Conducting walls

When the walls are thick, computations must be carried out within the wall region for electromagnetic and thermal quantities but not for fluid momentum and density. This involves blocking out of these regions from the flow solver. An index array denotes the material type in each cell. Boundary conditions are applied at this interface rather than the edges of the computational domain, for the flow solver. A far field or Boundary Element Method (BEM) boundary condition may be applied at the outer edge of the solid walls. However, since solution process must be carried out internal to these walls, it does involve a sizeable computational expense. It is believed that the BEM will reduce this burden significantly, and this method is described below. The inclusion of a BEM model in our MHD codes is presently ongoing.

It is convenient to think of the flow of current in MHD flows in terms of an equivalent static electric circuit, as sketched in Fig. [2]. Current generated by the flow of a conducting medium in a magnetic field, flows in parallel in various pathways. These include: (a) the conduction path through the working medium-air, (b) radiative transmission at high power, charge separation and cascade ionization of flow, and, (c) conduction through solid walls and other such external circuits. As a first cut estimate, these resistances may be used to estimate the flow of current and the approximate Lorentz force that may be generated. Considering momentum and energy balance across the flow path, we may estimate the pressure force, and from there, control moments that are produced.

There are three instances in which the effects of wall conduction become important in MHD:

(a) Mesh-resolved conducting walls, where a computational mesh is used to resolve the currents penetrating the wall region. Fig. [5] shows a jet flow case where current enters the rectangular walls of a channel where a transverse magnetic field is applied. Fig. [3] shows a case of a channel wall with a very

minute crack in insulation. Computation shows a significant amount of current leaking through this crack, causing a pressure gradient enhanced by about 100 times from the fully insulated case. These results will differ for different flow geometries and MHD interaction parameters. Hypersonic flow cases will be presented in the final paper.

(b) Infinitely segmented walls, where an assumption is used that the current tangential to the surface is small, and that the electric potential gradient in the tangential direction may be specified analytically. Figure [4] shows a case of an MHD accelerator with segmented electrodes, where prohibitively large mesh sizes are needed to resolve individual electrodes. Analytical BCs provide a simple means to compute the flow.

(c) Thin conducting walls, where a continuity equation for current (in terms of the electric potential) is written in a wall-tangential direction. This model has been developed for incompressible flow applications at HyPerComp (Refs. [16],[17]), and is presently being added to the hypersonic flow solver.

Coupled Boundary Element Method

The Boundary Element Method (BEM) is an attractive choice for some of the coupled solid-fluid problems encountered in MHD. Simply put, this method reduces a volume problem to a surface problem, thereby reducing its dimensionality by one, and thus avoiding the need to generate a volume mesh in semi-infinite or completely enclosed regions. Examples could be the air enclosing the outer walls of MHD chambers, metallic or insulating penetrations in liquid metal flow, the far field in a two fluid flow and so forth. The importance of BEM has been recognized by various authors. Masse et al. [10] and related codes at http://www.simulog.fr/eis/flux1.htm, Tezer-Sezgin et al. [21] and Guermond et al. [5] present a flavor of the potential of this method. A possible application of this method is presented here, that can be used for both MHD as well as heat transfer applications in much the same manner.

The most significant use of BEM is seen in computational regions where there is no flow (Ref.[21] uses the BEM for the flow itself, but with certain simplifying assumptions.) In a steady state situation, both heat conduction, the diffusion of magnetic field as well as the electrical potential, all obey Laplace's equation, which can be quickly written in a discrete boundary dependent manner: For an arbitrary quantity u, we have:

$$\nabla^2 u = 0 \rightarrow \frac{1}{2}u_P + \int_{\partial\Omega} u \frac{\partial u^*}{\partial n} d\Omega = \int_{\partial\Omega} u^* \frac{\partial u}{\partial n} d\Omega$$

The starred quantity u* represents a Green's function for Laplace's equation, that is analytically known. Boundary conditions may prescribe u or the normal derivative of u or a linear combination of both.

Results

In this paper, we present results obtained by solving for the electromagnetic fields within the solid walls, in this case, using the electric potential formulation. Some frequently used non-dimensional quantities in this type of study are:

Wall conductance: $c = \frac{\sigma_w t_w}{\sigma_0 L}$ the ratio of the wall conductivity to the mean flow conductivity, multiplied by ratio of the wall thickness to the characteristic flow length.

Hartmann number: $Ha = BL\sqrt{\frac{\sigma}{\mu}}$, where B is the mean magnetic field applied.

Interaction parameter: $N = \frac{BL\sigma}{\rho V}$, which scales the effect of the MHD interaction with flow momentum.

Using the estimates for the resistances of the various parts of the flow described in Figure [2], Tillack [21] derived a method to evaluate pressure drop across an MHD channel with fully developed flow and conducting walls. Figure [] uses this analysis to estimate pressure gradient in a fully developed flow at various Hartmann numbers for various values of wall conductance,

at a Reynolds number of 10^6. Figure [] shows a sample computation along these lines of a developing flow with conducting walls. It is rather apparent that the effect of wall conductivity on flow pressure gradient is sizeable. It must be noted that these estimates are based on incompressible flow assumption. However, the situation is not vastly different for compressible flows.

We present now, a different look at this situation by considering external flow past a cylinder. In ideal fluid dynamics, viscous flow past a cylinder produces the Karman vortex street downstream, and an oscillatory pressure field in the aft side of the cylinder. When mean flow quantities are considered, statistical averages of the recirculation length behind the cylinder, and other such global effects may be discerned. Figure [7] shows the mean pressure field in the evolution of the flow past a cylinder with and without MHD and conducting walls. A cursory glance reveals that the pressure drop, thereby drag, across the cylinder is reduced with MHD, due to the relative uniformity of pressure in the close vicinity of the object. An additional feature of interest, is that this effect is more prevalent in the insulating wall case rather than the conducting wall case, because of the manner in which current is distributed in the flow field in both cases. The current lines are shown in Figure [6].

We present two cases of supersonic flow in a channel with conducting walls. In the first case, the walls are flat, and the flow is smooth inside the channel. The MHD effect is weak, the interaction parameter being rather small. The main reason for this is that the conductivity is rather small, and the three dimensional nature of MHD has not been used to advantage. Indeed, the magnetic field is applied in the direction normal to the plane, and currents there fore must flow within the plane of the flow. First, we study the amount of current that is generated within the flow for conducting as well as insulating walls. Figure [8a] shows the case when the flow conductivity is about 100 mho/m, while the wall conductivity is 1.e-6 mho/m. Figure [8b] shows the roles reversed, when the wall conductivity is 1.e3 mho/m, and the flow conductivity is about 10 mho/m. The difference in the magnitude of the current that is flowing through the channel is phenomenal, being a few orders of magnitude higher for the case with conducting walls, on average. If the interaction parameter is increased for this calculation, no stable solution was observed numerically. This is attributed to the electron heating model currently used in the code, that seems to cause rather violent shock disturbances caused by Joule heating. A more gradual relaxation model between electron energy and flow energy is being incorporated. Current lines are sketched in Figure [9] for both these cases.

Figure [10] shows the flow in a supersonic compression channel with conducting walls at a Mach number of 3. Again, the interaction parameter was held deliberately low, just to get a feel for the flow currents that are produced. We same feature was again seen, namely, that the conducting wall case has about 10 times higher current in the flow on an average than the insulating wall case. Figure [11] shows the shock pattern in this channel.

We are currently attempting to integrate these models with other advanced physical models for ionizing air for realistic hypersonic flight conditions. Figure [12] shows sample plots of current lines from our recent study in hypersonic inlets with insulating walls. The same case will be applied to conducting walls in the near future.

Conclusion

This paper presents the results of our ongoing investigations in the development of realistic physical and numerical models in plasma and MHD flows. We have seen the effects of wall conductivity to be crucial to pressure variations in both internal and external flows, and have an impact on drag, mass capture and other such parameters affecting hypersonic flow systems. In the future, we intend to demonstrate these effects on a full scale hypersonic NASP type inlet configuration.

Acknowledgements

This work was supported under the AFOSR contracts F49620-99-C-0015/0070 with Maj.

William Hilbun as the program monitor. An inter-disciplinary MHD simulation capability was developed under DOE Phase-II SBIR contract # 03-00ER83018 with Mr. Sam Berk as program monitor.

References

1. Agarwal, R. K., Augustinus, J., "Numerical simulation of compressible viscous MHD flows for reducing supersonic drag of blunt bodies," AIAA 99-0601, Reno, NV, 1999
2. Aithal S.M., Munipalli R., Shankar V., "A Design Environment for Plasma and Magneto-Aerodynamics," to be presented at 34th AIAA Plasma dynamics and Lasers conference, Orlando, FL, June 2003
3. Barth, T.J., "Aspects of unstructured grids and finite volume solvers for the Euler and Navier-Stokes equations," VKI Lecture series, 1994-05
4. Buhler, L., "The influence of small cracks in insulating coatings on the flow structure and pressure drop in MHD channel flows," *Fusion Engineering and Design*, Vol. 27, pg. 650-658, 1995
5. Guermond, J.L., Minev, P.D., "Mixed finite element approximation of an MHD problem involving conducting and insulating regions: 2-D and 3-D cases," *TICAM report 02-11*, UT-Austin, April 2002
6. Kerrebrock, J.L., "Nonequilibrium Ionization Due to Electron Heating: I: Theory," AIAA Journal, Vol. 2, No. 6, pg. 1072, June 1964
7. A. L. Kuranov, E. G. Sheikin, " MHD control on Hypersonic Aircraft under "AJAX" concept. Possibilities of MHD Generator", 40th AIAA Aerospace Sciences Meeting January 2002/ Reno, NV.
8. "Physical and chemical processes in gas dynamics: cross sections and rate constants – Vol. 1," Eds. G.G.Chernyi, S.A. Losev, S.O. Macheret, B.V. Potapkin, *AIAA Progress in Aeronautics and Astronautics Series*, Vol. 196, 2002
9. S. O. Macheret, M. N. Shneider, R. B. Miles, "External Supersonic flow and scramjet inlet control by MHD with electron beam ionizer", AIAA paper, 2001-0492, 39th AIAA Aerospace Sciences Meeting and Exhibit, 8-11 January 2001, Reno, NV
10. Masse Ph., Fautrelle, Y., Gagnoud, A., "Coupled methods for 3-D coupled problems: 10 years of experiments in MHD," *IEEE Trans. Magnetics*, vol. 28, no. 2, 1992
11. K. Messadek, L. Buhler, R. Stieglitz, " MHD flows in Thick-Walled Pipes of Ferromagnetic and non-ferromagnetic material ," 5th International PAMIR conference on Fundamental and Applied MHD, September 2002
12. Mitchner, M., Kruger, C. H., "Partially Ionized Gases," John Wiley & Sons Inc., 1973
13. Munipalli R., V. Shankar, A Hadid, "Shock waves in hypersonic inlets with MHD," 23rd International Symposium on Shock Waves, Fort Worth, TX, July 2001
14. Munipalli R., V. Shankar, Z. Liu, A. Hadid, "An Unstructured Grid parallel MHD Solver for Real gas MHD simulations," AIAA 2001-2738, 32nd Plasmadynamics and Lasers Conference, Anaheim, CA, June 2001
15. Munipalli, R., Anderson, D. A., Wilson, D. R., "CFD Evaluation of Seeded and Unseeded Air MHD Accelerators," AIAA 2000-0215, Reno, NV, January 2000
16. Munipalli R., with the APEX task-2 group, "A review of computational modeling efforts in liquid metal MHD," to appear in Fusion Engineering & Design, 2003
17. Munipalli R., et al., "Development of a simulation environment for incompressible MHD flows on arbitrary grids: HIMAG," DOE SBIR Phase-II final report, June 2003
18. P. Palm, E. Ploenjes, I. V. Adamovich, J. W. Rich,'E- Beam Sustained Low-power Budget Air Plasmas', AIAA Paper 2002-0637, 40th AIAA Aerospace Sciences Meeting & Exhibit 14-17 January 2002/ Reno, NV.

19. Park, Chul, "Assessment of two-temperature kinetic model for ionizing air," Journal of Thermophysics and Heat Transfer, Vol. 3, No. 3, July 1989

20. Shang, J.S., "Recent research in Magneto-aerodynamics," *Progress in Aerospace Sciences*, Vol. 37, pg. 1-20 (2001)

21. Tezer-Sezgin, M., Dost, S., "Boundary element method for MHD channel flow with arbitrary wall conductivity," *Appl. Math. Modeling*, Vol. 18, pg. 429, 1994

22. Tillack, M.S., "MHD flow in rectangular ducts," UCLA Fusion Engineering Report, UCLA-FNT-41, July 1990

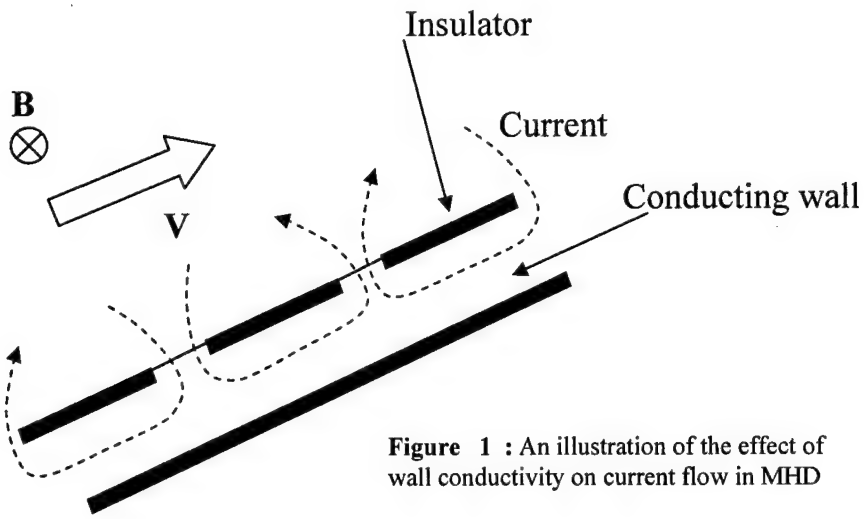

Figure 1 : An illustration of the effect of wall conductivity on current flow in MHD

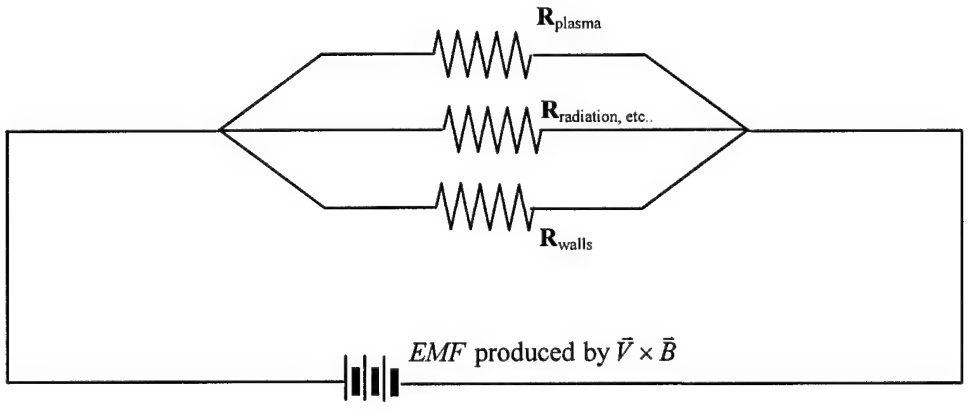

Figure -2 : A circuit diagram for current flow in MHD

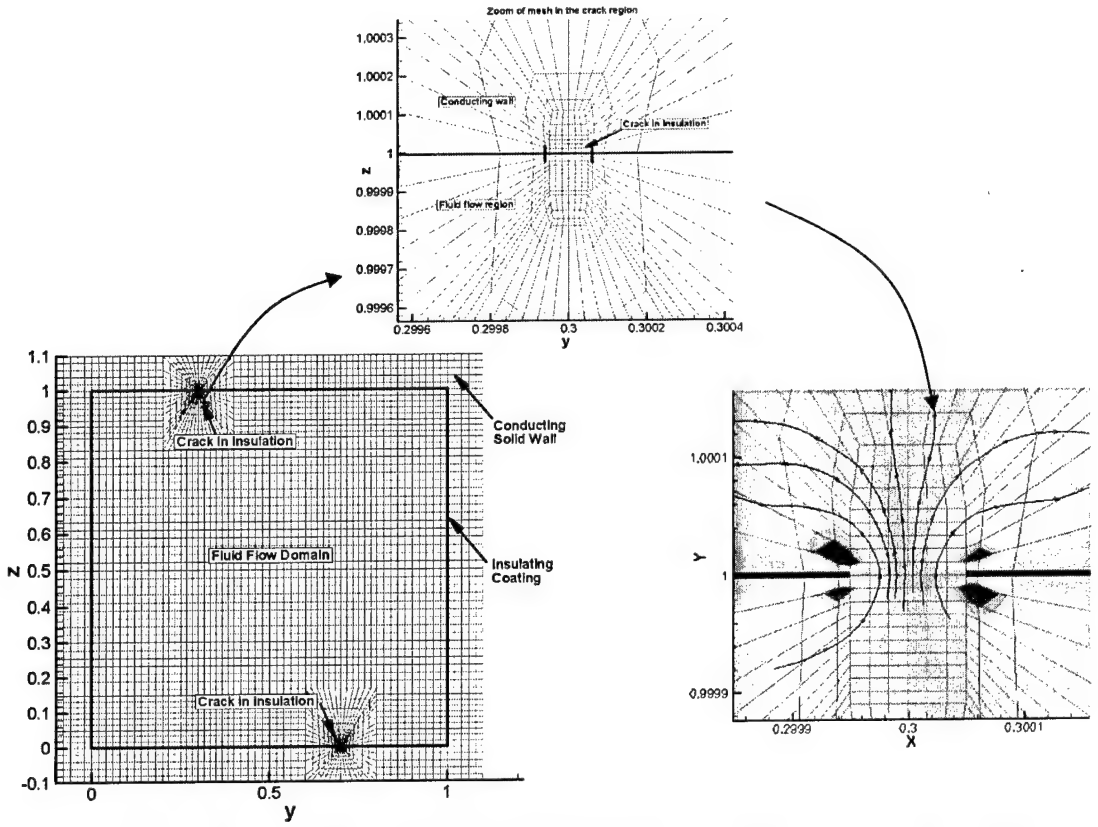

Figure 3: Section of a channel flow with fine (10^{-5} of channel dimension) crack, resolved using an unstrctured hexahedral mesh. Sample contour plot of x-current density and current lines are shown.

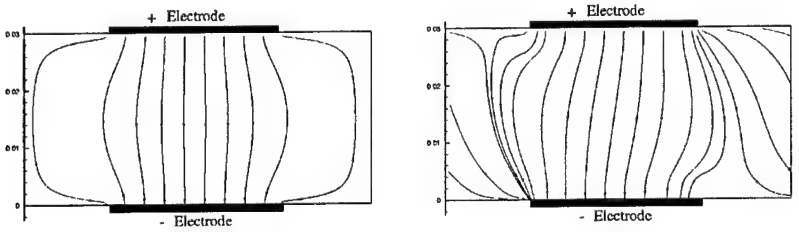

Figure 4 : Current lines in the vicinity of a pair of powered electrodes (above,) and Potential distribution along an MHD accelerator channel powered by segmented electrodes

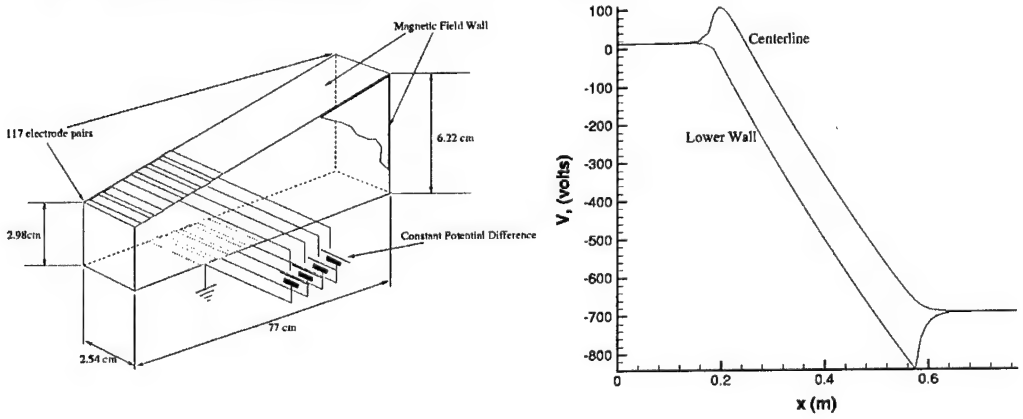

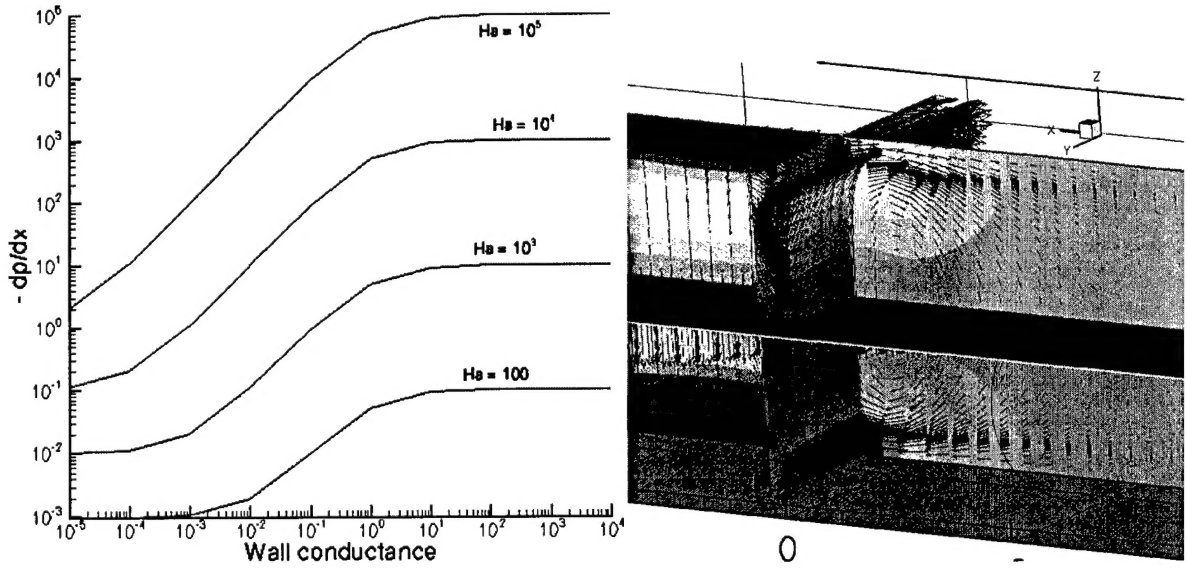

Figure 5: Closed channels with conducting walls at Re = 10^6, showing pressure drop and current vectors

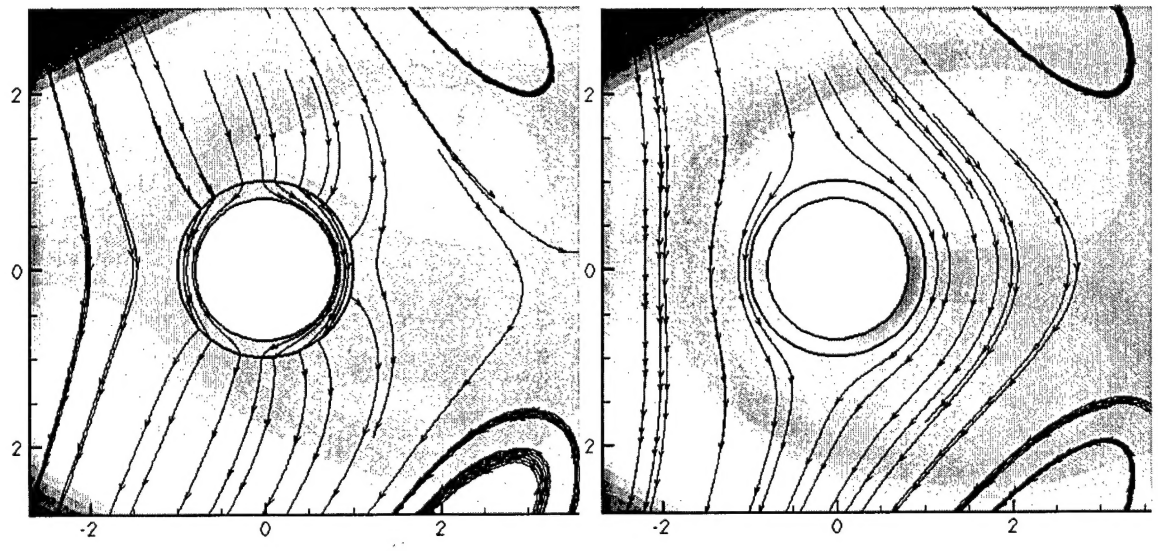

Figure 6: Cylinder flow with and without conducting walls
Ha = 10, c = 20 (left), c = 0.002 (right)

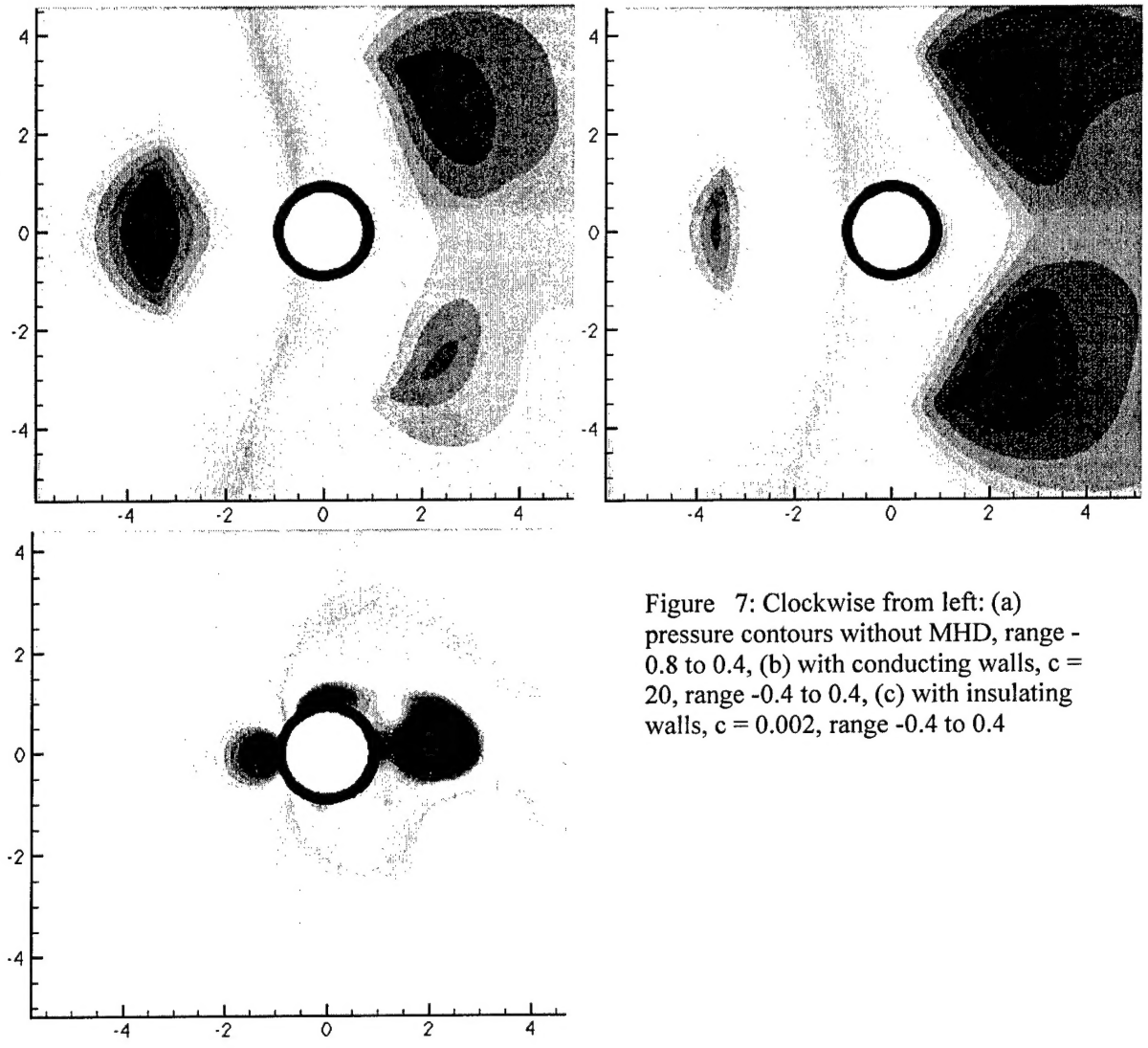

Figure 7: Clockwise from left: (a) pressure contours without MHD, range -0.8 to 0.4, (b) with conducting walls, c = 20, range -0.4 to 0.4, (c) with insulating walls, c = 0.002, range -0.4 to 0.4

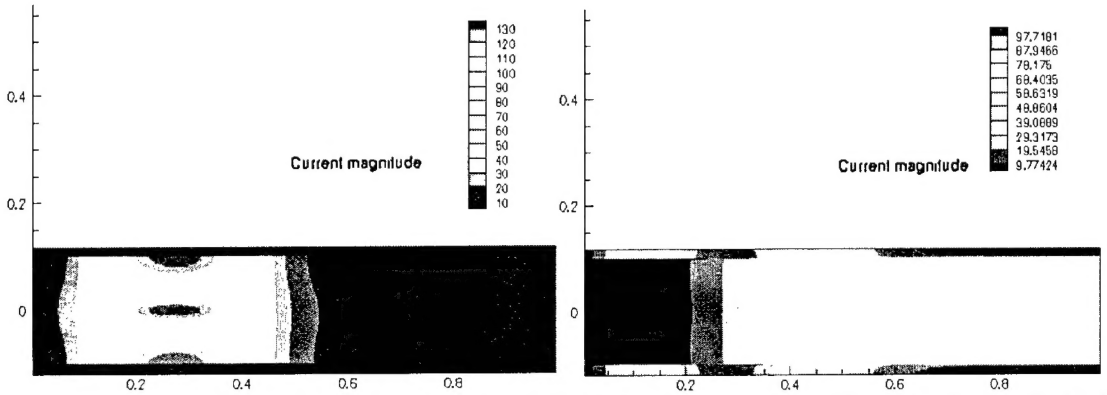

Figure 8: Supersonic channel flow with a fringing B-field, insulating walls (left) conducting walls (right)

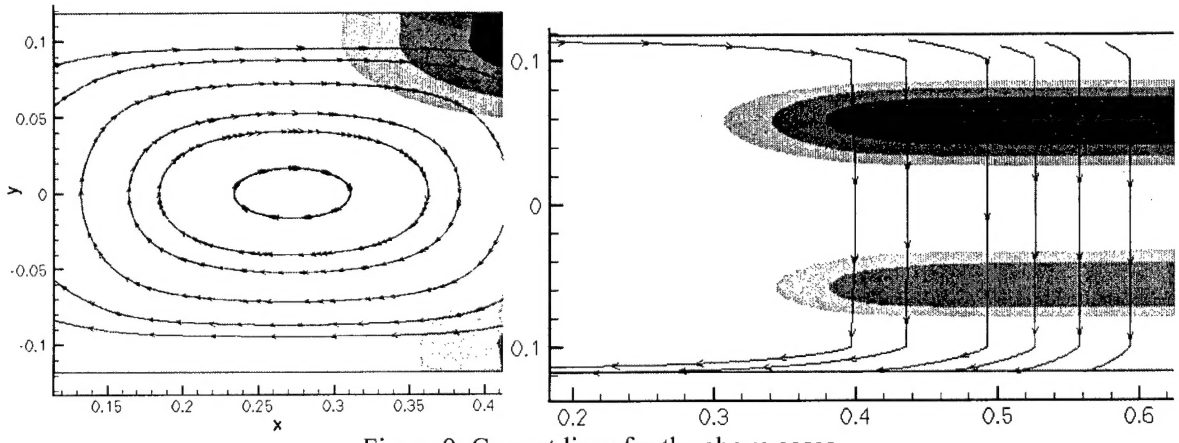

Figure 9: Current lines for the above cases

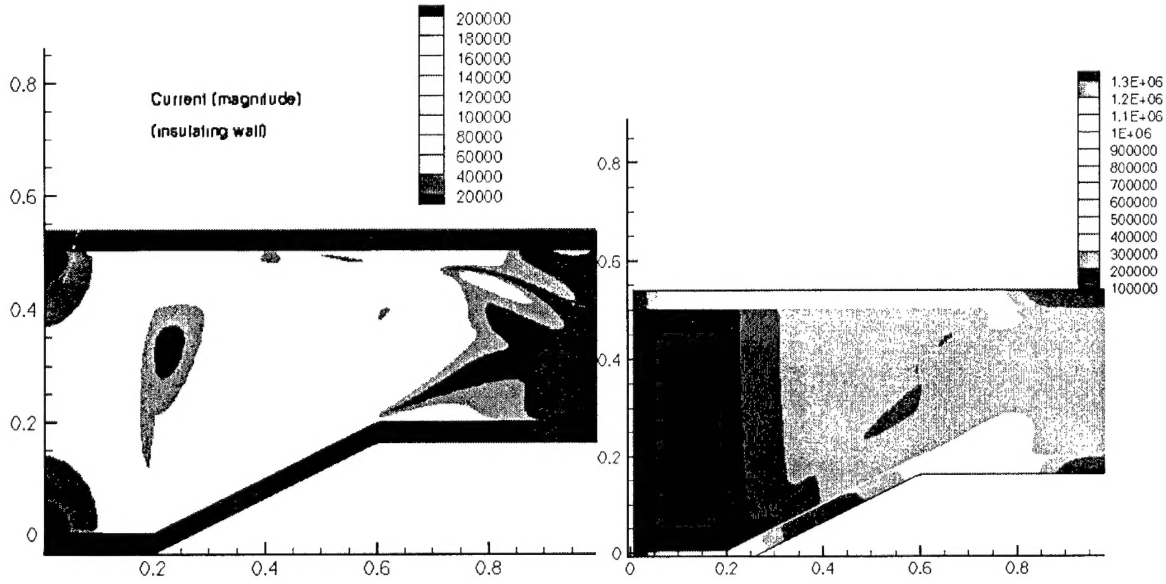

Figure 10: Current magnitude for a channel flow in an inlet type configuration with insulating walls (left) and conducting walls (right)

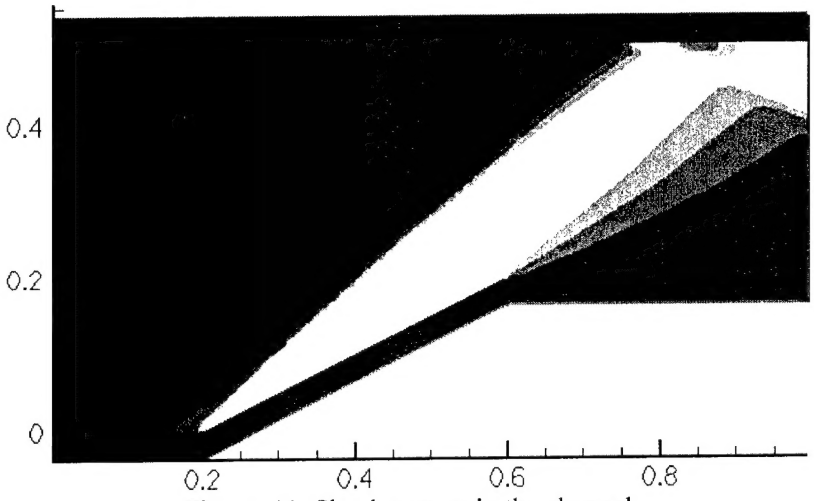

Figure 11: Shock pattern in the channel

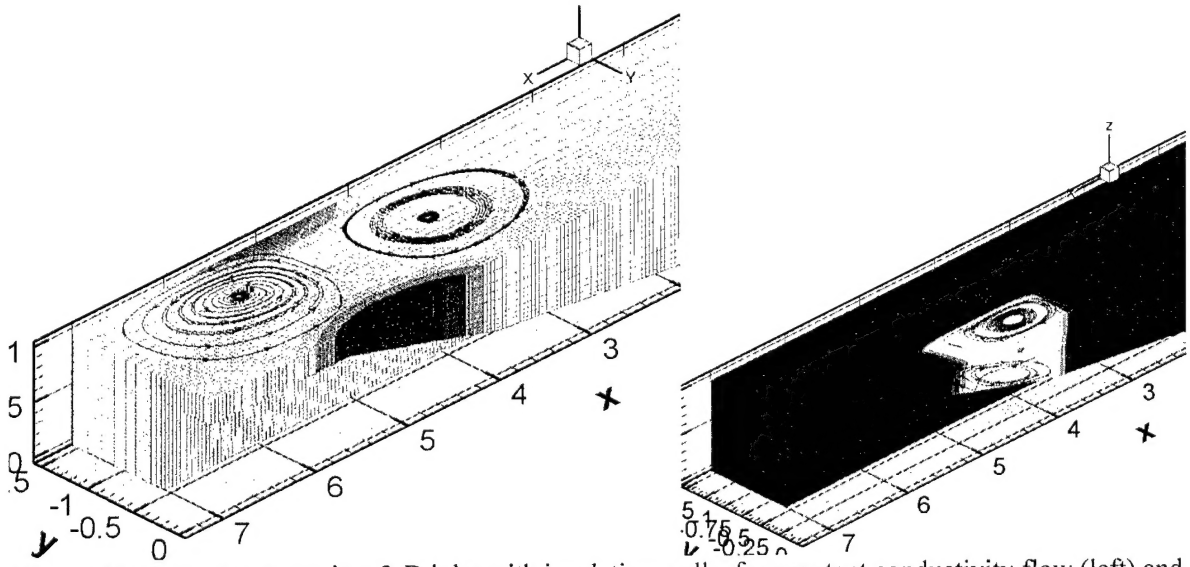

Figure 12: Current patterns in a 3-D inlet with insulating walls, for constant conductivity flow (left) and flow enhanced by local e-beam ionization (right)